1989

Thiolato-bridged, early/late heterobimetallic complexes.

Teresa Anne. Wark
University of Windsor

NOTICE

The quality of this microform is heavily dependent upon the quality of the original thesis submitted for microfilming. Every effort has been made to ensure the highest quality of reproduction possible.

If pages are missing, contact the university which granted the degree.

Some pages may have indistinct print especially if the original pages were typed with a poor typewriter ribbon or if the university sent us an inferior photocopy.

Reproduction in full or in part of this microform is governed by the Canadian Copyright Act, R.S.C. 1970, c. C-30, and subsequent amendments.

AVIS

La qualité de cette microforme dépend grandement de la qualité de la thèse soumise au microfilmage. Nous avons tout fait pour assurer une qualité supérieure de reproduction.

S'il manque des pages, veuillez communiquer avec l'université qui a conféré le grade.

La qualité d'impression de certaines pages peut laisser à désirer, surtout si les pages originales ont été dactylographiées à l'aide d'un ruban usé ou si l'université nous a fait parvenir une photocopie de qualité inférieure.

La reproduction, même partielle, de cette microforme est soumise à la Loi canadienne sur le droit d'auteur, SRC 1970, c. C-30, et ses amendements subséquents.

THIOLATO-BRIDGED, EARLY/LATE HETEROBIMETALLIC COMPLEXES

by

© Teresa Anne Wark

A Dissertation
Submitted to the
Faculty of Graduate Studies and Research
through the Department of Chemistry
and Biochemistry in Partial Fulfillment
of the Requirements for the Degree
of Doctor of Philosophy at
The University of Windsor

Windsor, Ontario, Canada

September, 1989

ISBN 0-315-54527-5

ABSTRACT

A number of early/late, transition metal complexes using titaniurn and vanadium alkylthiolates as metalloligands. These species were studied by various spectroscopic methods and single crystal X-ray diffraction.

Reaction of $Cp_2Ti(\mu\text{-}SEt)_2$ (**2**) with $[(MeCN)_4Cu]PF_6$ and trisubstituted phosphines or pyridine gives complexes with one coordinated ancillary ligand, of the form $[Cp_2Ti(\mu\text{-}SEt)_2CuL]PF_6$ (**3-8**). Spectroscopic data showed the species to be fluxional in solution with the cis disposition of the ethyl groups favoured thermodynamically. Complex **3** (L = PPh_3) crystallizes in the monoclinic space group $P2_1/c$, with a = 15.157(4) Å, b = 15.809(6) Å, c = 18.527(7), β = 100.86(3)°, Z = 4, and vol = 4359(3) Å^3, while **4** (L = PCy_3) crystallizes in the monoclinic space group $P2_1/n$, with a = 9.389(2) Å, b = 36.333(6) Å, c = 11.584(3) Å, β = 107.81(2)°, Z = 4, and vol = 3762(1) Å^3.

Reaction of $Cp_2Ti(SMe)_2$ (**10**) or **2** with $[(MeCN)_4Cu]PF_6$ in MeCN gives complexes **12** and **13**, respectively, of the form $[Cp_2Ti(\mu\text{-}SR)_2Cu(NCMe)_2]PF_6$. The metalloligand **10** crystallizes in the tetragonal space group $P4_12_12$, with a = 9.288(5) Å, c = 14.487(5) Å, Z = 4, and vol = 1249(1) Å^3. Complex **12** crystallizes in the triclinic space group $P\bar{1}$, with a = 8.038 Å, b = 13.169(3), c = 11.732(3) Å, α = 8.038(2)°, β = 109.31(2), γ = 89.29(2), Z = 2, and vol = 1122(1) Å^3. Complex **10** reacts with two equivalents of $[(MeCN)_4Cu]PF_6$ in THF to give $[(Cp_2Ti(\mu\text{-}SMe)_2)_2Cu]PF_6$ (**14**).

The vanadium methanethiolate ligand $Cp_2V(SMe)_2$ (**15**) crystallizes in the tetragonal space group $P4_12_12$, with a = 9.276(4) Å, c = 14.164(4) Å, Z = 4, and vol = 1218(1) Å^3. Vanadium alkylthiolates were used to prepare both three- (**17-18**) and four-coordinate copper complexes (**19-20**) in order to obtain paramagnetic species with an early metal isoelectronic with Ti(III).

Reaction of **10** with $(COD)_2Ni$ and PCy_3 gives species **21** which is analogous to **3**. When two equivalents of **10** are added to $(COD)_2Ni$, a trimetallic species

$(Cp_2Ti(\mu\text{-}SMe)_2)_2Ni$ (**22**) results. Complex **22** crystallizes in the tetragonal space group $I\bar{4}$, with a = 8.100(2) Å, c = 20.021(6), Z = 2, and vol = 1317(1) $Å^3$. Reaction of $Cp_2V(SMe)_2$ with $(COD)_2Ni$ leads to a nickel(II) hexamer (**23**) with two bridging thiolates per nickel centre. Complex **23** crystallizes in the monoclinic space group $P2_1/n$, with a = 11.393(3) Å, b = 11.483(3) Å, c = 11.821(4) Å, β = 90.08(2)°, Z = 2, and vol = 1547(1) $Å^3$.

Reaction of **10** or $(Cp_2Ti(\mu\text{-}SMe))_2$ (**24**) with several Rh(I) reagents led to the rhodium thiolato-bridged dimer $((COD)Rh(\mu\text{-}SMe))_2$ (**26**) via thiolate abstraction. Complex **26** crystallizes in the monoclinic space group $P2_1/n$, with a = 8.551(2), b = 10.058(3), c = 22.187(4), β = 92.54(1)°, Z = 4, and vol = 1906(1) $Å^3$. Reaction of $Cp_2V(SCH_2CH_2CH_2PPh_2)_2$ (**27**) with $[(COD)Rh]BF_4$ led to thiolate abstraction.

The interaction between the constituent metals in the bi- and trimetallic species is best described as electron donation from the electron-rich, late metal to the electron-deficient, early metal. This type of communication may be the mechanism occurring in heterogeneous systems exhibiting strong metal-support interactions.

To My Family

I think I can - I think I can - I think I can
Watty Piper
(The Little Engine that Could)

ACKNOWLEDGEMENTS

I would like to take this opportunity to express my gratitude to those people in the Department of Chemistry and Biochemistry who have made my stay here enjoyable, productive and enlightening. First, I would like to acknowledge the former and present members of the D-Team for being great people with whom to work and for being great friends. They are Graham S. White, Lucio Gelmini, David G. Dick, Christine Rogers-Goulin, Hilde P. Berends, T. Timothy Nadasdi, and Robert T. Toth. I would especially like to thank Christine Rogers-Goulin and David G. Dick for their continued support and friendship throughout the trials and tribulations of graduate school. I don't know that I would have made it this far without them.

I must also thank the technical staff for helping to make my research and teaching run smoothly. Mr. Jerry Vriesacker is thanked for his enormous help in operating the inorganic teaching laboratory. I would like to express my gratitude to Mr. Mike Fuerth and Mr. Jim Olsen for keeping the NMR spectrometers and the X-ray Diffractometer in fine working order. In addition, considering the amount of glassware that I have broken over the years, I would be remiss in my duties if I did not thank Mr. Alvan Ditchburn for piecing things back together.

My final note of thanks is to Dr. D. W. Stephan for his guidance, enthusiasm and encouragement throughout the course of this work.

TABLE OF CONTENTS

LIST OF TABLES

LIST OF FIGURES

LIST OF SCHEMES

LIST OF ABBREVIATIONS

a	hyperfine coupling constant
Å	Angstrom
AES	Auger electron spectroscopy
br	broad
Bu	butyl
Bz	benzyl
COD	cyclooctadiene
Cp	cyclopentadienyl anion
Cp'	methylcyclopentadienyl anion
Cy	cyclohexyl
CV	cyclic voltammetry
d	doublet
dec	decomposes
dmpe	dimethylphosphinoethane
dppe	diphenylphosphinoethane
δ	chemical shift
ϵ	molar absorbtivity, $M^{-1}cm^{-1}$
EPR	electron paramagnetic resonance
ESCA	electron spectroscopy for chemical analysis
Et	ethyl
EXAFS	extended X-ray absorption and fine structure
F	structure factor
Fc	calculated structure factor
Fo	observed structure factor
G	Gauss

g	grams
g	Lande g factor
h	hour
Hz	Hertz
IR	infrared
J	coupling constant
kJ/mol	kilojoule mole^{-1}
L	ligand
L-L	bidentate ligand
λ	wavelength
m	multiplet
Me	methyl
MHz	megahertz
min	minutes
mL	millilitre
mm	millimetre
mmoles	millimoles
MO	molecular orbital
mp	melting point
mV	millivolts
MULTAN	multiple tangent; direct methods program for X-ray crystallographic structure solution
NBD	norbornadiene
n-Bu	*normal*-butyl
nm	nanometre
NMR	nuclear magnetic resonance
n-Pr	*normal*-propyl

ORTEP	Oak Ridge Thermal Ellipsoid Program
Ph	phenyl
ppm	parts per million
Pr	propyl
py	pyridine
q	quartet
R	agreement factor, $\Sigma\|\|Fo\|-\|Fc\|\|/\Sigma\|Fo\|$
R	organic substituent
Redox	reduction-oxidation
Rw	weighted agreement factor, $(\Sigma w(\|Fo\|-\|Fc\|)^2/\Sigma wFo^2)^{1/2}$
s	singlet
σ	estimated standard deviation
SCE	saturated calomel electrode
SHELX-76	program package for X-ray crystallographic structure solution by George Sheldrick
SMSI	strong metal-support interactions
sol	solvated
t	triplet
t-Bu	*tert*-butyl
THF	tetrahydrofuran
TTU	1,4,8,11-tetrathiaundecane
UV-Vis	ultra violet-visible
V	volts
w	weighting factor, $4Fo^2/\sigma^2Fo^2$
X	halide

CHAPTER ONE

INTRODUCTION

1.1 Introduction

Understanding catalytic processes is a major thrust in organometallic chemistry.[1,2] Of particular interest are those catalysts which consist of electron-rich, late metals supported on electron-deficient, early metal oxides. Recent experiments have shown that the support, which was previously believed to be inert, participates in the catalysis via electronic communication with the dispersed metal.[3-5] With a view to modelling this interaction, the synthesis and study of discrete, transition metal complexes which incorporate both an early and a late transition metal in close proximity comprise the foci of this research. Understanding the metal-metal interactions and subsequently, the reaction pathways of these heterogeneous systems, may lead to development of new homogeneous catalysts. These new catalysts have the potential to cooperatively activate small molecules by exploiting the different chemistry exhibited by the constituent metals.

1.2 Heterogeneous Catalysis

1.2(i) Industrial Processes

Most industrial chemicals, produced on a large scale, are prepared using heterogeneous, transition metal catalysts.[1] In these systems, small metal particles are dispersed on supports made, for example, of silica or titania. The interaction of the substrate takes place at a metal surface, in a two-phase process. Recovery of the catalyst and separation of the product from the catalyst are much easier for the heterogeneous systems compared to homogeneous catalysts. However, the two-phase process requires higher temperatures and pressures than its soluble counterpart.

A large number of industrially important processes involve the use of carbon

monoxide. One such process is the reaction of carbon monoxide and water, termed the water gas shift reaction, in order to prepare hydrogen. (Scheme 1.1). The most widely

$$CO + H_2O \rightleftharpoons CO_2 + H_2$$

Scheme 1.1: Water Gas Shift Reaction

used heterogeneous process involving CO is the Fischer-Tropsch synthesis. This reductive polymerization of carbon monoxide yields linear hydrocarbons, olefins and alcohols (Scheme 1.2), employing iron, cobalt, ruthenium, or rhodium catalysts. Many

$$CO + H_2 \xrightarrow{\text{catalyst}}$$

$$CH_3(CH_2)_nCH_2OH + CH_3(CH_2)_nCH{=}CH_2$$

$$+ CH_3(CH_2)_nCH_3 + H_2O$$

Scheme 1.2: Fischer-Tropsch Synthesis

reviews of the Fischer-Tropsch synthesis have appeared in the literature.[6-9]

Although there is a great deal of debate over the mechanism of this catalysis, the one which has gained widespread acceptance was proposed originally by Fischer and Tropsch and more recently supported with work by Brady and Pettit.[10,11] The initial step in this mechanism is the dissociation of carbon monoxide on the catalyst surface to form carbides. A carbide then inserts into a surface hydride to form a methyl group. This methyl group then inserts another CH_2 group to propagate the chain. Homogeneous species have not been able to reductively couple carbon monoxide, which supports the idea that the dissociation of CO is a critical step in the mechanism.

There are many factors which affect the product distribution for this process. Variables such as CO/H_2 ratios, pressure, temperature and the catalyst are important factors contributing to the wide range of products. This lack of selectivity is a drawback of the Fischer-Tropsch synthesis, as is the large amount of CO_2 produced during the water-gas shift reaction used to prepare hydrogen.

1.2(ii) Strong Metal-Support Interactions

It was first reported in 1978, by Tauster et al., that the chemisorption ability of transition metals in heterogeneous catalysis was altered depending on the type of support material.[3,12] The adsorption of dihydrogen and carbon monoxide is different for those systems which have titania, vanadia or niobia supports compared to those systems employing silica or alumina. Different catalytic behaviour, with respect to selectivity and activity, is a consequence of the metal-support interaction.

Previously, it was thought that the support was inert and only served to maintain a high surface area of metal particles, such as Ni, Pd, Pt, Rh or Cu; however, it is now clear that the early metal support plays a chemically significant role as well. The reason for this behaviour is not clear, although electronic communication between the metal particles and the support or geometric constraints imposed by the support material on the metal particles have been suggested.[4,5] This phenomenon has been termed Strong Metal-Support Interactions (SMSI), and has received much attention from surface scientists.[4,5,12,13] There is still a great deal of speculation as to the mode of interaction between the early and late metals and the mechanism by which adsorption is decreased.

The initial report of SMSI involved use of titania as the support material.[3] Titania supports were impregnated with metal salts of Ru, Rh, Pd, Os, Ir, or Pt and subjected to reducing conditions at both high (500 °C) and low (200 °C) temperatures for one hour. It was found that after high temperature reduction, the system had a markedly reduced ability to adsorb hydrogen and carbon monoxide. Impurities, such as sulfur, were

considered as a possible explanation for the observation. However, one would expect the same type of impurities in silica or alumina supports as found in the titania species. Also, the percentage of sulfur compared to the amount of titanium dioxide was found to be very small, therefore unlikely to cause such a drastic change in absorption behaviour. Another proposal used to explain the experimental results was encapsulation of the metal particles by the support material, thus reducing the number of available sites for substrate binding. However, the metal surfaces subjected to high or low temperature reduction appeared to be similar after reduction. In addition, the loss of chemisorption ability can be restored by oxidation at 400 °C. It was suggested that if the support system was collapsing and encapsulating the metal particles, the process would not be reversible. Tauster proposed that there was a previously unreported phenomenon occurring in which the titanium metal atoms of the support were interacting with the dispersed, late metal centres.[3]

In order to investigate the generality of the reported metal-support interaction, a series of oxide supports with dispersed iridium was tested.[14] It was found that oxides of titanium, niobium, manganese, vanadium and tantalum are able to suppress the adsorption of hydrogen after high temperature reduction. Conversely, the oxides of silicon, aluminum, scandium, hafnium, zirconium and yttrium did not show the diminished ability to adsorb hydrogen. These results can be correlated to the ease of reducibility of the support material. For the species exhibiting SMSI, there are lower oxides known, while for the other species this is not true. For example, Nb_2O_5 was one of the starting oxides and the lower valent oxide, NbO_2, is known. These results suggest that a metal-support interaction occurs between early transition metals comprising the support and late transition metal particles dispersed on the support which is not unique to titanium.

The manner by which the support metals migrate to the surface is not well understood. The dispersed metal particles are not affected by support metals more than a few atomic units away due to screening effects within the metal. Therefore, the support metal must migrate into the dispersed metal or the SMSI effect would not be seen with

dispersed metals of large particle size. Several experiments have shown that titania can migrate quickly into nickel and rhodium films.[4,5] Due to the speed with which the titania migrates, it is thought that migration occurs along imperfections or grain boundaries, as opposed to diffusion. Systems have been investigated in which a thin film of Pt, Pd, or Rh is used to cover the titania surface. The SMSI phenomenon is seen in these cases, leading to the conclusion that the effect is short range.

The oxide layer, which forms on the dispersed metal, is thought to be of a reduced form. In the titania system, it is proposed to be a Ti(III) species which is present after reduction. One method to determine the oxidation state of the support metal is to expose a surface containing Ti(III) atoms to a flux of metal atoms and then examine the change in signal due to disappearance of Ti(III). Many techniques have been used for investigation of the early metal component of the system,[4,5] these include EXAFS,[15,16] AES,[17-22] XPS,[17,19,23] and ESCA.[24] Electron paramagnetic resonance has also been used to examine Pt/Ti species in order to identify Ti(III).[19]

Systems comprised of rhodium and titanium have been studied by EXAFS in order to determine the structure around the rhodium atom.[15,16] Two studies have appeared in the literature in which the Ti-Rh distance was reported to be 2.71 and 3.42 Å. While the latter value is too long to be significant, the former is short enough to allow an interaction. These studies also show the rhodium coordination sphere to include 2.4 oxygen atoms. These oxygens are from the oxide comprising the support.

Electron microscopy studies on a platinum/titania system showed morphological changes upon reduction or oxidation.[25] When platinum is dispersed on silica or alumina and reduced at high temperature the Pt particles appear as hemispherical aggregates. However, with titania, after reduction at 875 K, the platinum forms flat 'pillboxes' a few atoms thick. Treatment with oxygen at 875 K destroys the SMSI state and causes the pillboxes to form larger hemispherical aggregates. When the system is again reduced, the pillboxes return. This process shows the relative strength of the interaction between the

early and late metal, since it must be stronger than the cohesive forces in the metal aggregates.

Theoretical calculations have been performed on a Pt/Ti system in order to describe the types of bonding possible.[26] One contribution to the interaction is a weak covalent contribution due to overlap of the dispersed metal and support metal d orbitals. However, a stronger interaction was found to be an ionic attraction between the support metal and the dispersed metal due to charge transfer from the reduced cation to the dispersed metal. Therefore, the support must be reduced in order to possess an electron to donate to the late metal.

The reasons for altered adsorption behaviour, selectivity and activity of the systems exhibiting the SMSI effect are areas of speculation. One explanation for the suppression of CO or H_2 adsorption invokes the idea of electronic communication between the dispersed and support metals. If there is a transfer of electron density from the oxide layer to the metal, the strength of the bond between the adsorbate and the metal would be weakened.[4] This would cause a reduction in the chemisorption of carbon monoxide or hydrogen. Depending on the type of catalysis undertaken, the selectivities and activities are altered. Processes such as hydrogenolysis of ethane, hydrogenation of ethene and dehydrogenation of cyclohexane are much slower when the catalyst used has been reduced at high temperature.[1] However, for processes such as methanation, the rate is increased ten-fold for similar systems.[4] A proposal for this, depicted in Figure 1.1,

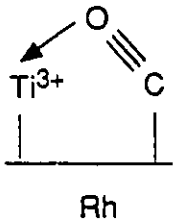

Figure 1.1: Interaction of CO with Rhodium and Titanium

involves interaction of the oxophilic, Ti(III) centre with the oxygen end of the carbon monoxide whose carbon is bound to rhodium.[27] Dissociation of CO should be enhanced by acid-base interaction with the Ti(III) centre. The idea of a CO moiety bound through carbon to a late metal and to an early metal through oxygen has led to vigorous research in the area of carbon monoxide reduction chemistry.[28-35]

This area of surface science has received, and continues to receive, a great deal of attention. Much debate is still occurring over the mechanism of migration of the support material, as well as, the manner by which the support-metal interaction affects catalysis. However, it is known that the early and late transition metals are in close proximity and that the oxide support undergoes reduction. Investigation of electronic communication between the two metals centres is central to understanding SMSI.

1.3 Thiolato-Bridged Complexes

A requirement for discrete molecular models of the systems exhibiting SMSI is the close proximity of the disparate transition metals. This can be accomplished by having metals which are bonded or linked to one another by ligand bridges. One approach used to link two transition metals has been to functionalize one of the metals, then use this functionality to bridge to another centre. Thiolates are well-known for their ability to bridge between transition metals, making use of the lone pair of electrons on the sulfur atom. This method of preparing either homometallic or mixed metal complexes is the focus of this discussion.

There are other ways, in addition to the metalloligand method, of incorporating bridging thiolate ligands into transition metal complexes. One such technique is to displace halide ions from already existing bimetallic complexes.[36-43] Early work by Chatt and Hart used this method to prepare thiolato-bridged platinum complexes.[36] It is also possible to prepare di- and trinuclear complexes by reacting a metal salt with a mono- or multidentate thiolate ligands such as 2,2'-dimercaptodiethylsulfide.[44-54] Recently,

homometallic complexes containing thiolate ligands have been prepared by reacting a metal carbonyl, a metal carbonyl hydride or other carbonyl-metal fragments with thiols or thiolate salts.[55-61] Cotton[62-65] and Alper[66-68] have reported several species prepared by oxidative addition of disulfides or diesters across metal-metal multiple bonds. Cluster and cage complexes, reported by Holm[69-73] and others[74-81] have been prepared by spontaneous self-assembly. These various techniques are included in a recent review,[82] as well as, complexes containing cyclopentadienyl ligands with bridging sulfides.[83]

The focus of this discussion are those complexes which have been prepared by reaction of thiolate metalloligands with other metal species, such as metal carbonyls or metal salts. The complexes are categorized as those containing two of the same metal (homometallic), two metals which appear close together in the periodic table (adjacent or near-neighbour), or two metals which are located far apart in the periodic table (early/late).

1.3(i) Homometallic and Adjacent Metal Thiolato-Bridged Complexes

There has been a tremendous amount of research involving the synthesis, characterization and reactivity of homometallic thiolate complexes. Complexes containing metals from the chromium triad form one of the largest groups of thiolato-bridged transition metal species. The first mixed metal complexes prepared by the metalloligand method were reported by Dias and Green.[84-86] Reaction of $Cp_2M(SR)_2$ with $M'X_2$ (M = Mo or W, M' = Co, R = Me or *n*-Bu, and X = Cl, Br, I, or SCN; M = Mo, M' = Fe, R = Me or *n*-Bu, and X = Cl) in ethanol or tetrahydrofuran gave complexes of the type shown in Figure 1.2. Reaction of $Cp_2M(SPh)_2$ (M = Mo or W) with $M'(CO)_6$ (M' = Cr, Mo, or W) led to bimetallics postulated to be of the form $Cp_2M(\mu\text{-}SPh)_2M'(CO)_3$. However, a subsequent X-ray study in 1974,[87] of the species where M = W, revealed four coordinated carbonyl groups, as seen in Figure 1.3. Dahl and Wei examined the species $[Fe(CO)_3(\mu\text{-}SEt)]_2$ with a view to determining the extent of

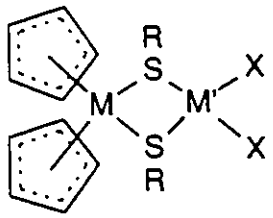

R = n-Bu or Me; X = Cl, Br, I, or SCN

M = Mo or W; M' = Fe or Co

Figure 1.2: Schematic Drawing of $Cp_2M(\mu\text{-}SR)_2M'X_2$

metal-metal interaction.[88] They found that the Fe_2S_2 core is puckered in order to facilitate interaction of the metals and that this accounts for the acute angles at the bridging sulfur atoms (ca. 68.3°), thereby indicating Fe-Fe bonds. These features have been used by other workers as criteria for identifying metal-metal interactions. In complexes of the type $Cp_2M(\mu\text{-}SPh)_2M'(CO)_4$ there are no metal-metal bonds, since the angles seen in the core are not consistent with the proposed requirements. The phenyl groups are cis with a bent MS_2M' core caused by steric repulsion between the substituents on the sulfur atoms.

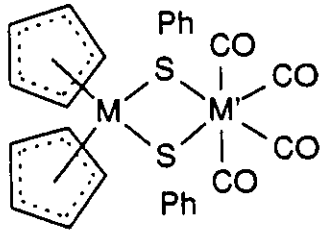

M = Mo, W; M' = Cr, Mo, or W

Figure 1.3: Schematic Drawing of $Cp_2M(\mu\text{-}SPh_2)M'(CO)_4$

Molybdenum or tungsten methanethiolate ligands have also been reacted with metal species from the nickel triad. When $Cp_2M(SMe)_2$ is reacted with $(R_3P)_2M'Cl_2$ (M'

= Pt, R = Et or Ph, M' = Ni, $(R_3P)_2$ = dmpe) dinuclear species result, while reaction with $NiCl_2$ or $(PhCN)_2M'Cl_2$ (M' = Ni, Pd, or Pt) yields trinuclear cations (Figure 1.4).[86] The

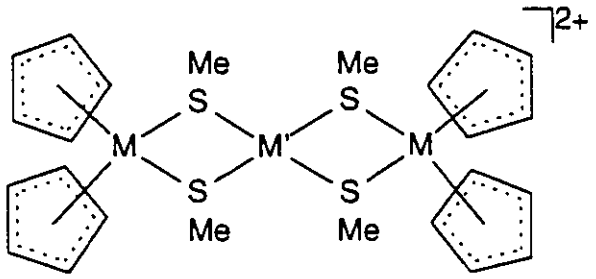

M = Mo or W; M' = Ni, Pd, or Pt

Figure 1.4: Schematic Drawing of $[(Cp_2M(\mu\text{-}SMe)_2)_2M']^{2+}$

related nickel complex, $[(Cp_2Mo(\mu\text{-}SMe)_2)_2Ni][BF_4]_2{:}2H_2O$, was characterized by X-ray crystallography,[89] thus confirming the proposed structure which was based on proton NMR, analytical and molar conductance data.

Werner et al. have reported another route to Mo-Ni complexes.[90] These species were prepared by the reaction of $Cp_2Mo(SR)_2$ (R = Me, Ph, or *t*-Bu) with $(Cp_3Ni_2)BF_4$, to give $[Cp_2Mo(\mu\text{-}SR)_2NiCp]BF_4$, as shown in Figure 1.5. The products were studied by ^1H

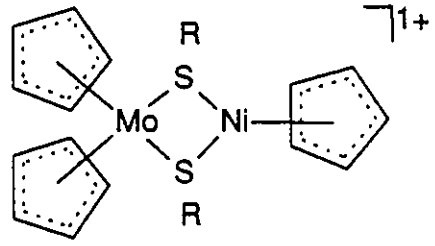

R = Me, n-Bu, or Ph

Figure 1.5: Schematic Drawing of $[Cp_2Mo(\mu\text{-}SR)_2NiCp]^{1+}$

and ^{13}C NMR spectroscopy. An X-ray crystallographic study of the *t*-butyl species

showed the core to be puckered.

Reaction of $Cp_2M(SMe)_2$ with $(RhCl(allyl)_2)_2$ or $((COD)RhCl)_2$, yields bimetallic species, as the hexafluorophosphate salts (M = Mo or W) shown in Figure 1.6.[86] A crystal study of the allyl complex was reported in 1974 by Prout and Rees and showed the methyl groups to be in a trans disposition.[91] A distance of 3.813(3) Å was found between the Mo and the Rh, too long to be a metal-metal bond. Also, the angles at the bridging sulfur atoms are large (101.3(3)° and 102.2(3)°) and the metal angles are acute (S1-Mo-S2 75.4(5)° and S1-Rh-S2 80.2(5)°).

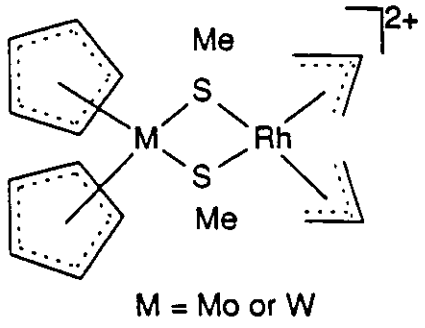

Figure 1.6: Schematic Drawing of $[Cp_2M(\mu\text{-}SMe)_2Rh(allyl)_2]^{2+}$

Another type of metalloligand was prepared by derivatization of the cyclopentadienyl groups of $Cp_2Mo(SR)_2$. Green and coworkers synthesized $(C_5H_4(CH_2)_2SR)_2Mo(SR)_2$ (R = *n*-Pr or Ph) in order to use it as a tetradentate ligand to coordinate Pd, Rh, or Pt.[92] Reaction of the metalloligand with $(PhCN)_2PtCl_2$, $(PhCN)_2PdCl_2$, or $RhCl_3$ led to species assigned as $(C_5H_4CH_2CH_2S\text{-}n\text{-}Pr)_2Mo(\mu\text{-}S\text{-}n\text{-}Pr)_2(MCl_n)_2$ (n = 2, M = Pt or Pd; n = 3, M = Rh). As these species have limited solubilities, they were not fully characterized. Reaction of the molybdenum-thiolate with $[(dppe)Rh(acetone)]BF_4$, $((COD)RhCl)_2$, or $[(Ph_3P)_2Pt][PF_6]_2$ yielded complexes of the form $(C_5H_4CH_2CH_2S\text{-}n\text{-}Pr)_2Mo(\mu\text{-}S\text{-}n\text{-}Pr)_2ML_n$ (M = Rh, n = 1, L = dppe or COD; M = Pt, n = 2, L = PPh_3). In these complexes, the metalloligand is bidentate, coordinating through the thiolates bound directly to molybdenum. Variable temperature ^1H NMR

experiments show the species to be fluxional via inversion at the bridging sulfurs, with no evidence of the trans isomer and the cis conformer favoured at low temperature. It was proposed that either the trans isomer is in low equilibrium concentration or the mechanism of inversion is a symmetrical concerted process involving cis to cis conversion. Based on other MoS_2M species which had been structurally characterized and exhibit similar fluxional behaviour, the present compounds were proposed to have puckered MoS_2M cores. Treatment of the metalloligand with HCl gas replaces the thiolates bound to molybdenum with chloride. Subsequent reaction of the modified ligand with $((COD)RhCl)_2$ gives the bimetallic species $[Cl_2Mo(C_5H_4(CH_2)_2\text{-}\mu\text{-}SPh)_2Rh(COD)]Cl$ in which the rhodium is coordinated through the thiolates on the rings, as shown in Figure 1.7.

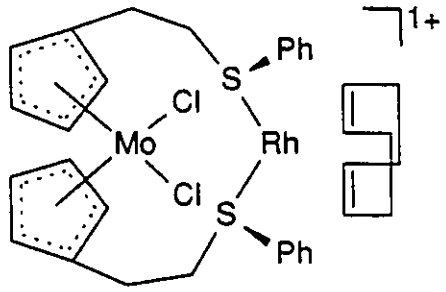

Figure 1.7: Schematic Drawing of $[Cl_2Mo(C_5H_4(CH_2)_2\text{-}\mu\text{-}SPh)_2Rh(COD)]^{1+}$

In addition to the mono- and bis-cyclopentadienyl molybdenum thiolates discussed above, another type of molybdenum metalloligand, $Mo(S\text{-}t\text{-}Bu)_4$, has been used by Otsuka et al. to prepare mixed-metal species.[93,94] The reaction of $Mo(S\text{-}t\text{-}Bu)_4$ or $(t\text{-}BuNC)_4\text{-}Mo(S\text{-}t\text{-}Bu)_2$ with $CuBr(t\text{-}BuNC)_3$ or $(t\text{-}BuNC)_4Mo(S\text{-}t\text{-}Bu)_2$ with $Pd(t\text{-}BuNC)_2$ gives bimetallic thiolate products (Figure 1.8). By NMR studies, the product was found to exist in two isomeric forms, due to different arrangement of the *t*-butyl groups (i.e., syn or anti). Reaction of the bimetallic with diphenylacetylene allows isolation of the anti isomer, although the acetylene is not coordinated. The structures of the syn and anti forms of

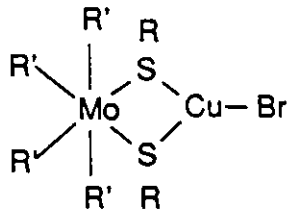

R = Me; R' = t-BuCN

Figure 1.8: Schematic Drawing of $R'_4Mo(\mu\text{-}SR)_2CuBr$

$(t\text{-}BuNC)_4Mo(\mu\text{-}S\text{-}t\text{-}Bu)_2CuBr$ were assigned on the basis of crystallographic studies. Molybdenum has a distorted octahedral geometry, while the copper is in a trigonal-planar environment. It was found that the angles at the bridging sulfurs are quite closed down, with values of about 68.6° for both the anti and syn forms. The angles at the metals are obtuse with S-Mo-S values of about 105° for the anti and syn forms, while at Cu the values are ca. 117.7° for the anti and syn forms. The angles, coupled with short M-M' distances and IR stretching frequencies for the isocyanide ligands, led to assignment of the oxidation states of the metals as Mo(II) (d^4) and Cu(I) (d^{10}). The Mo/Pd structure was assigned on the basis of spectroscopic data and was found to be similar to the anti-form of the Mo/Cu bimetallic.

The metalloligand $(RNC)_4Mo(S\text{-}t\text{-}Bu)_2$ has been used to prepare mixed-metal iron complexes. McDonald and coworkers have reacted $(RNC)_4Mo(S\text{-}t\text{-}Bu)_2$ (R = cyclohexyl or *t*-Bu) with FeX_2 (X = Cl or Br), which leads to the dinuclear species $(RNC)_4Mo(\mu\text{-}S\text{-}t\text{-}Bu)_2FeX_2$.[95] These species undergo reversible, one-electron oxidations, resulting from a Mo(II)/Mo(III) redox couple. Unlike the previously described bimetallics, these species are paramagnetic, and thus the existence of cis/trans forms could not be confirmed by NMR spectroscopy, although they are expected to exist.

When $Mo(S\text{-}t\text{-}Bu)_4$ is reacted with $Fe_2(CO)_9$ a trinuclear species, $[(CO)_4Fe(\mu\text{-}S\text{-}t\text{-}Bu)]_2Mo$ is obtained.[96] The structure was proposed on the basis of

elemental analysis, IR and NMR spectroscopy and mass spectrometry and subsequently, confirmed by X-ray crystallography. In this complex, there are Mo-Fe bonds based on the M-M' distances (2.754(1) and 2.759(1) Å) and the geometry about molybdenum. The molybdenum is described as a distorted, flattened trigonal prism if the iron atoms are not considered. The carbonyls are considered to be semi-bridging based on the low IR stretching frequencies.

Molybdenum and iron or cobalt compounds have also been prepared by reaction of $[MCl_4]^{2-}$ with $[Mo(CO)_4(SR)_2]^{2-}$ or $[M(SR)_4]^{2-}$ with $(C_7H_8)Mo(CO)_4$ (R = Ph or Bz).[97] The products of these reactions are trimers of the form $[M(\mu\text{-}SR)_4(Mo(CO)_4)_2]^{2-}$. For the phenyl species it is possible to obtain the trimer by refluxing $Mo(CO)_6$, $[NEt_4]_2[MCl_4]$, $[NEt_4]Cl$, and NaSPh, indicating that the thiolates of iron and cobalt are intermediates in the synthesis. The trimetallic species were studied by IR and cyclic voltammetry, and the cobalt complexes by EPR spectroscopy. A related trinuclear species is prepared by reaction of the iron-molybdenum species, where R = Ph, with cyclohexyl and *tert*-butyl isocyanides in MeCN, shown in Figure 1.9. The product has two MeCN molecules

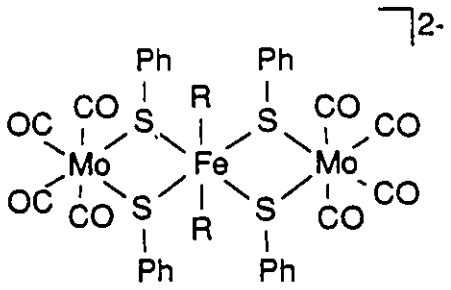

R = CyNC or t-BuNC

Figure 1.9: Schematic Drawing of $[((CO)_4Mo(\mu\text{-}SPh)_2)_2FeR_2]^{2-}$

coordinated to the iron centre resulting in an eighteen electron configuration. The electrochemistry showed reversible two-electron oxidations at essentially the same potential. It was proposed that when the species are oxidized there is formation of two metal-metal bonds, allowing each metal to keep an eighteen-electron configuration.

Chemical oxidation of the trimers with iodine yields the neutral species. The results from this experiment support the conclusions drawn from the electrochemical experiments.

Complexes have been prepared which involve metal coordination of a multidentate, thiolate or mercaptoamine ligand. Jicha and Busch have prepared trimetallic complexes by reaction of two equivalents of $[M(NH_2CH_2CH_2S)_2]$ with the appropriate metal halide (M = Ni(II), Pd(II), Co(II), or Cd(II)) to give $[M(M(NH_2CH_2CH_2S)_2)_2]X_2$, (Figure 1.10).[98] Molar susceptibilities and conductance measurements led to the

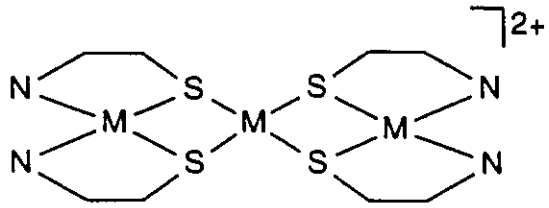

M = Ni, Pd, Co, or Cd
N = NH_2

Figure 1.10: Schematic Drawing of $[M(M(NH_2CH_2CH_2S)_2)_2]^{2+}$

conclusion that the species were trinuclear.

Mixed-metal and homonuclear trimers which contain noble metals have been prepared by Roundhill.[99] When $[Ni(H_2O)_6][ClO_4]_2$ is added to two equivalents of $(PPh_3)_2Pt(SR)_2$ or (dppe)$M(SR)_2$ (M = Pt or Ni, R = *i*-Pr or Ph) a linear trimer results. Reaction of the Pd monomer of 1,4,8,11-tetrathiaundecane (TTU) with Ni(II) gives a trinuclear product. The analogous TTU monomers of Ni and Zn cannot be prepared; however, the trinuclear species can be obtained by reaction of Ni(II) or Zn(II) with the TTU species.

Braterman and Wilson have used functionalized noble metal metalloligands to prepare dimeric compounds.[100] The species (L-L)$M(SR)_2$ (M = Pt or Pd, R = Me or P, L-L = dppe or *o*-phenylenebis(diethylarsine) can react with $C_7H_8M'(CO)_4$ (M' = Cr, Mo, or W), to give species of the type (L-L)$M(\mu\text{-}SR)_2M'(CO)_4$. By examination of the

spectroscopic data, it was determined that no metal-metal bonding exists in these complexes.

Molybdenum or palladium complexes have been prepared using functionalized platinum. Reaction of $(PPh_3)_2Pt(SPh)_2$ with $((NBD)Mo(CO)_4)$ or $((MeCN)_2PdCl_2)$ gives the complexes $(PPh_3)_2Pt(\mu\text{-}SPh)_2Mo(CO)_4$ or $(PPh_3)_2Pt(\mu\text{-}SPh)_2PdCl_2$, respectively.[101] The IR data for these complexes were not consistent with those of other species determined to have a metal-metal interaction, therefore a M-M bond was not suggested.

Dance et al. have prepared bimetallic species containing copper.[102] The metalloligand CuSPh is added to triphenylphosphine which upon work-up yielded $(Ph_3P)_2Cu(\mu\text{-}SPh)_2Cu(PPh_3)_2$. Assignment of the structure was based on similar compounds containing bridging chlorides and was confirmed by an X-ray study. This compound is the first one reported which possesses strictly planar geometry of the $Cu_2(SPh)_2$ core. Due to the steric requirements of the phenyl rings, the copper centres are quite far apart. The large metal-metal separation and the angles at the bridging sulfur and copper atoms preclude a metal-metal interaction.

1.3(ii) Early/Late Metal Thiolato-Bridged Complexes

The SMSI phenomenon is seen in systems containing an early and a late metal in close proximity. Various ligand systems have been used to this end and have been recently reviewed.[103] The first thiolato-bridged, early/late heterobimetallic complex, reported in 1969 by Köpf and Räthlein, was prepared by photolysis of $Cp_2Ti(SPh)_2$ and $Mo(CO)_6$ (Figure 1.11).[104] The structure was assigned on the basis of the observed CO stretching frequencies and proton NMR shifts. As well, related species of the type $Cp_2Ti(\mu\text{-}SR)_2M'(CO)_4$ (M' = Cr, Mo, or W, R = Me or Ph) were prepared and studied by spectroscopy and X-ray crystallography.[105-107] These species can be prepared by the reaction of $Cp_2Ti(SR)_2$ and $(C_7H_8)M(CO)_4$ to give the heterobimetallic complexes. The NMR and IR data indicate that electron transfer from the late metal to the empty d orbital

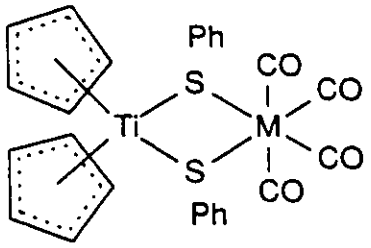

M = Cr, Mo, or W

Figure 1.11: Schematic Drawing of $Cp_2Ti(\mu\text{-}SPh)_2Mo(CO)_4$

of titanium is appreciable, and was described as shown in Figure 1.12. From the crystal

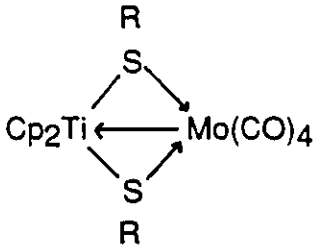

R = Me or Ph

Figure 1.12: Schematic Drawing of Bonding Mode for $Cp_2Ti(\mu\text{-}SR)_2Mo(CO)_4$

structure, it was found that the TiS_2M' core is planar with acute angles at the bridging sulfur atoms and obtuse angles at the metals. This evidence is consistent with the criteria established by Dahl et al. to indicate metal-metal bonding.

Metalloligands of the type $Cp_2Ti(SH)_2$ have been used to prepare tungsten and molybdenum bimetallic species by Rauchfuss and Ruffing.[108] The product obtained from $(RC_5H_4)_2Ti(SH)_2$ plus $(C_7H_8)M'(CO)_4$, $(RC_5H_4)_2Ti(\mu\text{-}SH)_2M'(CO)_4$ (R = H or Me, M' = Mo; R = H, M' = W), is similar to the products obtained from reaction of the late metal species with $Cp_2Ti(SMe)_2$. The proton NMR data indicates syn and anti isomers due to the orientation of the methyl groups. The activation energy necessary for interconversion

in $Cp_2Ti(SH)_2Mo(CO)_4$ was determined to be 76 ± 0.8 kJ/mol based on line shape analysis. Reactions of the bimetallics, in which R = H or Me and M' = Mo, with CH_2=$CHCO_2Me$ led to new bimetallic species of the form, $(RC_5H_4)_2Ti(\mu$-$SCH_2CH_2CO_2Me)_2Mo(CO)_4$.

Reaction of $[Cp_3Ni_2]BF_4$ with $Cp_2Ti(SR)_2$ (R = Me or Ph) yields the mixed-metal species $[Cp_2Ti(\mu$-$SR)_2NiCp]BF_4$ which is similar to the species in Figure 1.5.[90] This molecule exhibits fluxional behaviour which occurs rapidly on the NMR time scale above 35 °C. The mechanism of conversion from the cis to trans form is proposed to be inversion at sulfur.

Wardle and coworkers have also reported the synthesis of $(Cp_2Ti(\mu$-$SMe)_2CuCl)_2$ achieved by reacting the titanium methanethiolate metalloligand with $((COD)CuCl)_2$.[109] The structure was assigned on the basis of analytical data and IR spectroscopy. In related work, the preparation of $((Cp_2Ti(\mu$-$SR)_2CuX)_n$ (R = Me or Ph, X = Cl or Br) has been described.[131] Based on electronic data, there was proposed to be some type of Cu(I) to Ti(IV) electron transfer, best described as a Ti-Cu bond.

Mixed-metal species have also been prepared using chelating, tetradentate phosphinothiolate ligands. White and Stephan have reported the synthesis of a series of compounds of the type $[Cp_2Ti(\mu$-$S(CH_2)_xPPh_2)_2M]^{n+}$ (M = Cu, x = 2, n = 1; M = Rh, x = 3, n = 1; M = Pd or Ni, x = 3, n = 0).[111-113] All of these complexes have been spectroscopically examined and, with the exception of the Pd species, have been structurally characterized. Preparation of the Ti/Cu species is achieved by reaction of $Cp_2Ti(SCH_2CH_2PPh_2)_2$ with $[(MeCN)_4Cu]BF_4$ (Figure 1.13). This species undergoes reversible electrochemical reduction, indicative of a Ti(IV)/Ti(III) redox couple. The crystal structure revealed the titanium and copper atoms to be in pseudo-tetrahedral environments. As seen with previously described mixed-metal species, there are acute angles at the bridging sulfur atoms (78.1(1)° and 78.0(1)°) and obtuse angles at the metals (S-Ti-S 97.5(1)° and S-Cu-S 91.2(1)°). This evidence, together with the M-M' separation

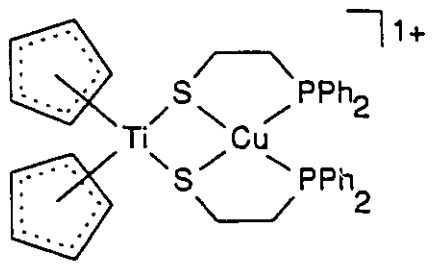

Figure 1.13: Schematic Drawing of $[Cp_2Ti(\mu\text{-}SCH_2CH_2PPh_2)_2Cu]^{1+}$

and a butterfly of the TiS_2Cu core, led to the proposal of a Cu → Ti dative bond.

The Ti/Rh species is prepared by reaction of $Cp_2Ti(SCH_2CH_2CH_2PPh_2)_2$ and $[(NBD)_2Rh]BF_4$. Fluxional behaviour is exhibited by this system as determined by ^1H NMR spectroscopy, with the cis conformer favoured at low temperature. The mechanism of conversion from the trans conformer to the cis conformer was proposed to be pyramidal inversion at sulfur. The crystal structure showed the chelating ligands to be cis, coordinating to rhodium in a square planar geometry, with the titanium in a pseudo-tetrahedral environment. In this complex the core is planar; however, the angles found in the TiS_2Rh core and the M-M' separation were used to identify a metal-metal interaction. The Ti/Rh species was also studied by cyclic voltammetry and was found to be reversibly reduced. As with the Ti/Cu species, the reduction was assigned to a Ti(IV)/Ti(III) redox couple. In order to investigate the reduced species further, the initial Ti/Rh complex was reacted with Cp_2Co and the reduced species investigated by EPR spectroscopy. The *g* value of 1.979 indicated a Ti(III) species with hyperfine coupling to two equivalent phosphorus atoms of 2.8 G and to one rhodium atom of 1.8 G. The magnitudes of the couplings were similar to those seen for other systems in which direct, through space interactions had been proposed. Therefore, the mechanism proposed for electronic communication was a transannular interaction between the Ti and Rh centres.

The Ti/Ni complex is prepared by addition of $(COD)_2Ni$ to $Cp_2Ti(SCH_2CH_2CH_2PPh_2)_2$. A schematic drawing of the Ti/Ni and Ti/Rh species appears

in Figure 1.14. Two, one-electron reversible oxidations are exhibited by this system,

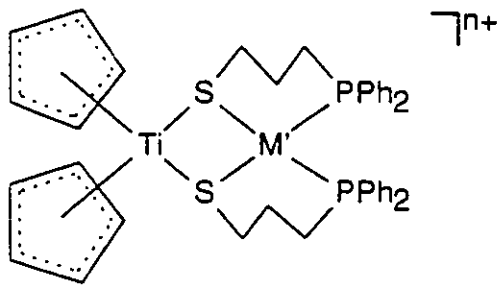

M' = Ni, n = 0; M' = Rh, n = 1

Figure 1.14: Schematic Drawing of $[Cp_2Ti(\mu\text{-}SCH_2CH_2CH_2PPh_2)_2M]^{n+}$

corresponding to Ni(0) being oxidized, sequentially, to Ni(I) and Ni(II). The electrochemistry exhibited by this system is in contrast to that seen for the copper and rhodium species, in which the titanium undergoes one-electron reduction. An X-ray study revealed the TiS_2Ni core to have a butterfly shape. Angles at the bridging sulfurs are again closed down, with the angles at the metals opened up and a Ni-Ti distance shorter than the M-M' distances seen for the related Ti/Cu heterobimetallics. Donation of electron density from the electron rich Ni(0) centre to the electron deficient Ti(IV) centre was proposed. By reaction with CO, the Ti/Ni complex is converted from an 'inside' species in which the Ni is coordinated to the two sulfur and the two phosphorus atoms, to an 'outside' complex where the nickel is bound to two phosphorus atoms and to two carbonyl ligands. The Ti/Pd species was not structurally characterized, but the spectroscopic data is consistent with a species analogous to the Ti/Ni species. Comparison of the crystal data shows the Ti-Ni species to have the shortest M-M' (2.825(3) Å) separation, followed by the Ti/Cu system (3.024(1) Å and then the Ti/Rh species (3.127(2) Å). This trend is related to the electron density and charge on the late metal. Since Ni(0) is neutral and d^{10}, it is capable of donating the most electron density, while Rh is d^8 and cationic and thus, is a poorer donor. All of the complexes prepared

using the phosphinothiolate ligands are proposed to have a late metal to early metal electron donation across the four-membered ring.

Niobium based thiolate ligands have been used to prepare mixed metal species. When the metalloligand $Cp_2Nb(SR)_2$ (R = Me or Ph) is reacted with $(C_7H_8)Mo(CO)_4$, the product is $Cp_2Nb(\mu\text{-}SR)_2Mo(CO)_4$, analogous to that seen for $Cp_2Ti(SR)_2$.[114-115] However, when the same metalloligand is reacted with $NiCl_2$, $(PhCN)_2PdCl_2$, or $(PhCN)_2PtCl_2$, the product is a trinuclear mixed metal species, as seen in Figure 1.15, assigned on the basis of spectroscopic data. The Nb/Ni species is diamagnetic which was

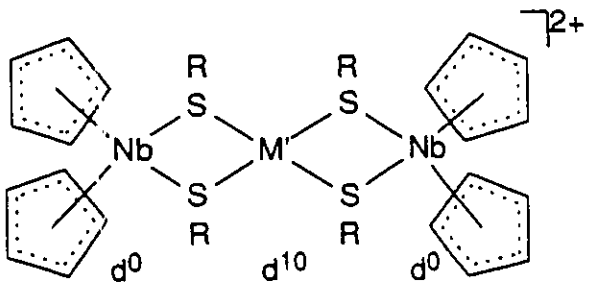

R = Me or Ph; M' = Ni, Pd, Pt

Figure 1.15: Schematic Drawing of $[(Cp_2Nb(\mu\text{-}SR)_2)_2M']^{2+}$

proposed to be due to electron donation from Ni→Nb. Therefore, the oxidation states of the metals were assigned as Ni(0) and Nb(V), locating the positive charge on niobium. A subsequent crystallographic study of $[(Cp_2Nb(\mu\text{-}SMe)_2)_2Ni][BF_4]_2$ supported the initial interpretation.[116] Based on the crystallographic data, it was confirmed that the nickel is d^{10}, in a tetrahedral environment and the niobium atoms are five coordinate, d^0, if metal-metal bonding is invoked.

Darensbourg et al. have recently reported the use of a phenylthiolate niobium metalloligand to prepare mixed metal species.[117] The reaction of $Cp_2Nb(SPh)_2$ and $(C_7H_8)Mo(CO)_4$ gave $Cp_2Nb(\mu\text{-}SPh)_2Mo(CO)_4$, a species analogous to that obtained when the thiolate metalloligand is $Cp_2Nb(SMe)_2$. As this compound is quite insoluble in all

normal solvents, it was oxidized with $[NO][PF_6]$ to improve the chances of obtaining crystals. The complexes were studied by IR, ^{13}C, and ^{1}H NMR spectroscopy, as well as, cyclic voltammetry. In the IR spectra, the carbonyl stretches are at a higher frequency for the oxidized species relative to the unoxidized species, suggesting that the positive charge is delocalized over the entire heterobimetallic species. Variable temperature proton NMR spectroscopy was performed on the oxidized species. The results are consistent with two conformers of the complex, resulting from both syn and anti disposition of the phenyl rings. Cyclic voltammetry studies were performed; however, the reduction of the bimetallic species was found to be only quasi-reversible. Of the two reduction potentials, one (-0.32 V) is similar to those found for the monomeric species $Cp_2Nb(SPh)_2$ and $[Cp_2Nb(SPh)_2][PF_6]$; however, one is at a much lower potential (-0.70 V). Upon reduction in acetone, the dimer exhibited another reduction wave at -1.1 V corresponding to $Cp_2Nb(SPh)_2^+$, indicating that the dimer had been disrupted.

X-ray crystallography was used to examine the oxidized Nb/Mo species. Molybdenum is in regular octahedral geometry, bonded to four carbonyl ligands and to the sulfur atoms of the metalloligand. The NbS_2Mo core is planar with the phenyl rings disposed in the anti conformation. The angles at sulfur are acute (77.7(1)° and 77.4(1)°), but the angle at Nb (101.8(1)°) is the same as that found for the uncoordinated metalloligand. The Nb-Mo distance (3.116(2) Å) was found to be less than the sum of the covalent radii (3.24 Å). Of the resonance forms possible for the heterobimetallic, the one which is thought to be the most correct is the one in which the Mo donates electron density to the niobium centre via a donor-acceptor interaction.

Tantalum metalloligands have been use to prepare bimetallic platinum complexes.[118] When $Cp_2Ta(SMe)_2$ is reacted with $(PhCN)_2PtCl_2$, the result is a trinuclear mixed-metal species, $[Cp_2Ta(\mu\text{-}SMe)_2Pt(\mu\text{-}SMe)_2TaCp_2]^{2+}$, which was crystallized as the PF_6^- salt. An X-ray crystallographic study revealed this species to be similar to that resulting from the reaction of $Cp_2Nb(SMe)_2$ or $Cp_2Mo(SMe)_2$ and $NiCl_2$ (Figure 1.15).

The system is best described as two tantalum d^0 centres and one platinum d^{10} atom with two M-M' bonds.

Iron and cobalt species have been reacted with early metal thiolates in order to prepare mixed-metal species. The reaction of $Cp_2M(SR)_2$ (M = Ti, R = Me or Ph; M = Nb, R = Ph) and $Hg[Fe(CO)_3NO]_2$ to give $Cp_2M(\mu\text{-}SR)_2Fe(NO)L$ (M = Ti, L = NO; M = Nb, L = CO).[119] Also, $Cp_2Nb(SPh)_2$ could be reacted with $Hg[Co(CO)_4]_2$ to give the heterobimetallic species, $Cp_2Nb(\mu\text{-}SPh)_2Co(CO)_2$. The complexes were examined by IR and NMR spectroscopy. From the spectroscopic data, it was determined that the bimetallic complexes are fluxional and exist in cis and trans forms. Also, the niobium species are diamagnetic, indicating bonding between the early and late metal centres. This result is consistent with other bimetallic species discussed previously.

The utility of thiolate metalloligands for the preparation of bimetallic and trimetallic complexes can be seen from the preceding discussion. This type of ligand system has been used most often to prepare species containing similar or adjacent metals; however, the metalloligand approach has been not been as extensively used to link two widely divergent transition metals.

1.4 Scope of Thesis

At the outset of this work, there were only a small number of complexes reported which contained both an early and a late transition metal held in close proximity by any type of bridging system. A number of these early/late heterobimetallic complexes have been prepared by extending the use of titanium and vanadium alkylthiolates as metalloligands. During the course of these investigations, other workers have reported the use of different metalloligands such as phenylthiolates[117] and phosphinopropanethiolates.[112,113]

The focus of the work reported herein is the syntheses and characterization of mixed metal species. These discrete, early/late metal complexes have been examined by

various spectroscopic methods and X-ray crystallography. By studying these compounds, it may be possible to elucidate the nature of SMSI observed in heterogeneous catalytic systems.

CHAPTER TWO

USE OF $Cp_2Ti(SEt)_2$ AS A METALLOLIGAND FOR THE PREPARATION OF HETEROBIMETALLIC, THREE-COORDINATE COPPER COMPLEXES

2.1 Introduction

Köpf and Räthlein reported the first early/late metal, thiolato-bridged transition metal complexes using a titanium metalloligand.[104] However, few complexes with bridging thiolates have been prepared which contain both of the constituent metals of a system exhibiting SMSI. Prior to the initiation of this work, our group reported the synthesis and X-ray structure of the Ti/Cu complex, $[Cp_2Ti(\mu\text{-}SCH_2CH_2PPh_2)Cu]BF_4$, shown in Figure 1.1.[111] In this complex the four-coordinate copper is bound by two, bidentate, phosphinoethanethiolate ligands. This ligand arrangement may be involved in the reversible electrochemistry exhibited by this system which corresponds to a Ti(IV)/Ti(III) redox couple. Also, the proximity of the metals may be affected by the chelate. In order to elucidate the effect of the chelate, attempts were made to prepare related Ti/Cu complexes containing two thiolate bridges and two ancillary ligands not joined to the sulfur atoms by carbon backbones. The unchelated ligand would give a less restrained geometry about the core which may be flexible enough to allow a closer approach of the metals.

Reaction of the metalloligand $Cp_2Ti(SEt)_2$ with $[(MeCN)_4Cu]PF_6$, in the presence of trisubstituted phosphines or pyridine, gave complexes containing only one ancillary ligand, as opposed to the disubstituted product. These complexes were studied using NMR spectroscopy, cyclic voltammetry and X-ray crystallography.

2.2 Experimental Section

All preparations were done under an atmosphere of dry, O_2-free N_2. Solvents were

reagent grade, distilled from the appropriate drying agents under N_2, and degassed by the freeze-thaw method at least three times prior to use. ^1H and ^{13}C NMR spectra were recorded on a General Electric QE-300 spectrometer located at Wayne State University, using the trace of protonated solvent as the reference. The chemical shifts are reported in ppm relative to $SiMe_4$ for both the ^1H and ^{13}C NMR data. Variable temperature ^1H NMR spectra were recorded on a Bruker WH-400 spectrometer at the Southwestern Ontario Regional NMR Facility at the University of Guelph. $^{31}P\{^1H\}$ NMR spectra were recorded on a General Electric GN-300 spectrometer located at Wayne State University. $^{31}P\{^1H\}$ NMR chemical shifts are reported in ppm relative to external 85% H_3PO_4. UV-Vis data were recorded on a Shimadzu 240 spectrometer or a Hewlett-Packard 8451A diode array spectrophotometer. Cyclic voltammetry experiments were performed using a BAS CV-27 electrochemistry unit with a platinum working electrode and a saturated calomel reference electrode. The supporting electrolyte used in the electrochemistry was $[NBu_4]PF_6$. The melting points were determined using a Fisher stage melting point apparatus and were not corrected. Combustion analyses were performed by Guelph Chemical Laboratories, Guelph, Ontario. Cp_2TiCl_2, HSEt, PPh_3, PEt_3, and $Ph_2P(CH_2)_2PPh_2$ were purchased from the Aldrich Chemical Co.; pyridine was purchased from the J. T. Baker Chemical Co. and PBz_3 and PCy_3 were purchased from the Strem Chemical Company. $[(MeCN)]_4CuPF_6$ was prepared by the literature method.[120] Physical data and spectroscopic data appear in Tables 2.1 and 2.2, respectively, for compounds **3-8**.

(i) Preparation of NaSEt (1) To a 100 mL THF solution of HSEt (6.44 mL, 87 mmoles) was added sodium metal (2.0 g, 87 mmoles) and the mixture stirred overnight. An additional 2 mL of the thiol was added to the reaction flask and the mixture stirred for another 4 h to ensure complete reaction. The air-sensitive sodium salt was filtered under nitrogen and dried *in vacuo*. (Yield based on sodium metal used: 7.3 g, 100%).

(ii) Preparation of $Cp_2Ti(SEt)_2$ (2) To Cp_2TiCl_2 (1.0 g, 4.0 mmoles) in 50 mL THF was added NaSEt (675 mg, 8.0 mmoles) and the mixture stirred overnight. Activated neutral alumina was added, the mixture stirred for 10 min and filtered. The alumina was washed with 5 x 20 mL portions of THF which were combined with the mother liquor. The resulting THF solution was stripped to dryness and the residue washed with 2 x 10 mL of pentane. The red-purple microcrystalline solid was dried *in vacuo*. (Yield 1.08 g, 95%). ^1H NMR (d_6-benzene): δ, 6.10 (s, 5 H), 3.07 (q, 2 H), 1.18 (t, 3 H). $^{13}C\{^1H\}$ NMR (d_6-benzene): δ, 111.12 (Cp) 39.08 (CH_2), 18.55 (CH_3).

(iii) Preparation of $[Cp_2Ti(\mu\text{-}SEt)_2CuPPh_3]PF_6$ (3) To a 30 mL THF suspension of $[(MeCN)_4Cu]PF_6$ (633 mg, 1.7 mmoles) was added PPh_3 (892 mg, 3.4 mmoles) and the solution stirred for 10 min. Upon addition of a 20 mL THF solution of purple $Cp_2Ti(SEt)_2$ (500 mg, 1.7 mmoles), the solution became dark red immediately. After 30 min of stirring, the volume was reduced to 15 mL and the solution cooled to -10 °C. Red-orange microcrystalline solid was evident after 1 h. The solid was collected by filtration and washed with two, 5 mL portions of n-hexane. The addition of n-hexane to the mother liquor caused precipitation of a second crop of product which was also isolated by filtration. (Combined yield: 1.17 g, 89%). $^{13}C\{^1H\}$ NMR (THF, -80 °C): δ, 134.4 (d, J|P-C| = 14.3 Hz), 132.0 (s), 130.2 (s), 112.3, 110.7 (Cp), 34.1 (CH_2), 18.7 (CH_3).

(iv) Preparation of $[Cp_2Ti(\mu\text{-}SEt)_2CuL]PF_6$ (L = PCy_3 (4); PEt_3 (5); PBz_3 (6); $Ph_2P(CH_2)_2PPh_2$ (7); NC_5H_5 (8)) These compounds were prepared in a manner analogous to that used for **3** utilizing the appropriate phosphine or pyridine.

(v) X-ray Data Collection and Reduction Orange crystals of **3**·1.62 THF were obtained by crystallization from a THF solution of **3** cooled to -10 °C. Alternatively, orange crystals of **3** could be obtained by vapour diffusion of n-hexane into a THF solution of **3**.

Table 2.1: Physical Data for $[Cp_2Ti(\mu\text{-}SEt)_2CuL]PF_6$ (3-8)

Compound		Melting Point (°C)	C(%)		H(%)		S(%)	
			Calcd	Found	Calcd	Found	Calcd	Found
3	$C_{32}H_{35}CuF_6PS_2Ti$	141-143	49.84	49.49	4.57	4.35	8.32	8.39
4	$C_{32}H_{52}CuF_6P_2S_2Ti$	155-157	48.70	48.81	6.77	7.08	8.12	8.49
5	$C_{20}H_{35}CuF_6P_2S_2Ti$	147-148	38.31	43.68	5.63	6.65	10.23	10.70
6	$C_{35}H_{41}CuF_6P_2S_2Ti$	95 (d)[a]	51.69	52.69	5.08	5.54	7.88	7.74
7	$C_{40}H_{44}CuF_6P_2S_2Ti$	110 (d)[a]	54.95	47.09	4.88	4.84	7.07	7.26
8	$C_{19}H_{25}CuF_6NPS_2Ti$	128 (d)[a]	38.81	33.01	4.28	4.21	10.91	10.73

[a] decomposes

Table 2.2: Spectroscopic Data for $[Cp_2Ti(\mu\text{-}SEt)_2CuL]PF_6$ (3-8)

Compound L =	^1H NMR[a] δ (ppm)	$^{31}P\{^1H\}$[b] NMR δ (ppm)	|J| (Hz)	UV-Vis[c] λ (ε, $M^{-1}cm^{-1}$
3 PPh_3	7.59 (m, 15H) 6.28 (br s, 10H) 2.90 (q, 4H) 1.02 (t, 6H)	6.0 (s) -144.5 (septet)	$\|CH_2\text{-}CH_3\| = 7.2$ $\|P\text{-}F\| = 712.9$	4500 (3185) 370 (3923)
4 PCy_3	6.20 (br s, 10H) 2.90 (q, 4H) 2.2-1.3 (br m, 33H) 1.34 (t, 6H)	27.1 (s) -144.7 (septet)	$\|CH_2\text{-}CH_3\| = 7.5$ $\|P\text{-}F\| = 720.4$	462 (5580) 354 (5709)
5 PEt_3	6.13 (br s, 10H) 2.91 (q, 4H) 1.85 (d of q, 6H) 1.33 (t, 6H) 1.16 (d of t, 9H)	2.1 (s) -142.9 (septet)	$\|CH_2\text{-}CH_3\| = 7.5$ $\|CH'_2\text{-}P\| = 7.7$ $\|CH'_2\text{-}CH'_3\| = 7.6$ $\|CH_3'\text{-}P\| = 17.1$ $\|P\text{-}F\| = 711.4$	456 (5349) 352 (5858)

6 PBz_3	7.4 (m, 15H) 6.11 (br s, 10H) 3.49 (d, 6H) 2.6 (m, 4H) 1.09 (t, 6H)	6.3 (s) -143.2 (septet)	$\|CH_2\text{-}P\| = 8.8$ $\|CH_2\text{-}CH_3\| = 7.5$ $\|P\text{-}F\| = 712.4$	454 (2823) 348 (3547)
7 $PPh_2(CH_2)_2PPh_2$	7.4-7.2 (m, 20H) 6.44 (s, 10H) 2.6 (m, 8H) 1.18 (t, 6H)	9.2 (br s) -142.9 (septet)	$\|CH_2\text{-}CH_3\| = 7.5$ $\|P\text{-}F\| = 709.9$	466 (1190)
8 NC_5H_5	8.79 (d of d, 2H) 8.18 (d of t, 1H) 7.74 (d of d, 2H) 6.23 (br s, 10H) 3.05 (q, 4H) 1.37 (t, 6H)		$\|CH_o\text{-}CH_p\| = 1.3$[d,e] $\|CH_m\text{-}CH_p\| = 7.7$[d,f] $\|CH_o\text{-}CH_m\| = 6.1$[e,f] $\|CH_2\text{-}CH_3\| = 7.4$	470 (3673) 362 (5170)

NMR Solvent: d_6-acetone
[b]NMR Solvent: THF
[c]UV-Vis Solvent: THF
[d]H_p refers to para protons
[e]H_o refers to ortho protons
[f]H_m refers to meta protons

Orange crystals of **4** were obtained by vapour diffusion of n-hexane into a THF solution of **4**. Diffraction experiments were performed on a four-circle Syntex $P2_1$ diffractometer with graphite-monochromatized Mo Kα radiation. The initial orientation matrix for each compound was obtained from 15 machine-centred reflections selected from rotation photographs. These data were used to determine the crystal systems. Partial rotation photographs around each axis were consistent with a monoclinic crystal system in each case. Ultimately, 30 high-angle reflections ($15°<2\theta<30°$) were used to obtain the final lattice parameters and the orientation matrices. Machine parameters, crystal data, and data collection parameters are summarized in Table 2.3. The observed extinctions were consistent with the space group $P2_1/c$ for **3·1.62 THF** and $P2_1/n$ for **4**. $\pm h,+k,+l$ data for **3·1.62 THF** were collected in two shells ($4.5°<2\theta<35°$ and $35°<2\theta<40°$), while $\pm h,k,l$ data for **4** were collected in one shell ($4.5°<2\theta<45°$). Three standard reflections, for each species, were recorded regularly throughout data collection. In the case of **3·1.62 THF**, decay of the crystal was indicated by the change in the intensities of the standard reflections. After approximately a 12% decay in the average intensities of the standards, a second crystal was employed to collect the higher angle data ($35°<2\theta<40°$). Decay of the second crystal of approximately 12% was also seen. This decay is undoubtedly due to partial loss of the THF molecules in the crystal lattice, even though the crystals were sealed in capillaries. A decay correction was applied to the data for **3·1.62 THF** and the standard reflection intensities were used to scale the two portions of the data obtained from the two crystals. For compound **4**, the standards showed no statistically significant change over the duration of data collection. The data were processed using the SHELX-76 program package. The total number of reflections with $F^2o>3\sigma(Fo^2)$ for each compound, are listed in Table 2.3. No absorption corrections were applied to the data.

(vi) Structure Solutions and Refinements Non-hydrogen atomic scattering factors were taken from the literature tabulations.[121-123] The Cu atom position was determined using

the heavy atom (Patterson) method for **3·1.62 THF**, while the Cu atom position in **4** was determined using the direct methods program, MULTAN. The remaining non-hydrogen atoms were located from successive difference Fourier map calculations. Refinement was carried out by using full-matrix least squares techniques on F, minimizing the function $\Sigma w(|Fo|-|Fc|)^2$, where the weight, w, is defined as $4Fo^2/\sigma^2(Fo^2)$ and Fo and Fc are the observed and calculated structure factor amplitudes. In the final cycles, in which a block-diagonal refinement was employed, the Cu, Ti, S, P, F, O and cyclopentadienyl carbons of **3·1.62 THF** were assigned anisotropic temperature factors. The phenyl ring carbons were described by isotropic thermal parameters and the ring geometries were constrained to that of regular hexagons with C-C bond distances of 1.39 Å. For **4**, all non-hydrogen atoms were assigned anisotropic temperature factors. For both refinements, hydrogen atom positions were allowed to ride on the carbon to which they are bonded assuming a C-H bond length of 0.95 Å. In each case, hydrogen atom temperature factors were fixed at 1.10 times the isotropic temperature factor of the carbon atom to which they are bonded. In all cases, the hydrogen atom contributions were calculated, but not refined. For compound **3·1.62 THF**, the THF molecules of crystallization were not of full site occupancy. After location and refinement of the positional parameters of the THF molecules, the site occupancy factors were refined. Site occupancies of 0.85 and 0.77 were found for the two THF sites. In addition to the fractional occupancy, rotational disordering of the THF molecules was evident. Thus, it was necessary to constrain the geometries of the THF molecules to that of pentagonal structures in which the C-O bond distances were 1.44 Å and the C-C bond distances were 1.52 Å. For compound **4**, a disordering of one of the cyclohexyl rings was evident. The disorder was sufficiently blurred such that no acceptable model involving two conformations of the disordered ring could be obtained. Thus, in order to maintain a chemically reasonable geometry, the C-C bond distances for this ring were fixed at 1.52 Å and markedly anisotropic thermal parameters were accepted as a result. The final values of $R = \Sigma||Fo|-|Fc||/\Sigma|Fo||$ and $Rw =$

$[\Sigma w(|Fo|-|Fc|)^2/\Sigma w(Fo^2)]^{1/2}$, for each species and the maximum Δ/σ on any of the parameters in the final cycles of refinement are given in Table 2.3. Final difference Fourier map calculations showed no peaks of chemical significance. The magnitudes and locations of the largest residual peaks are described in Table 2.3. The Crystallographic Parameters (Table 2.3), Positional Parameters (Table 2.4) and Selected Bond Distances and Angles (Table 2.5) are included in this chapter. Tables of Thermal Parameters, Hydrogen Atom Parameters and Distances and Angles Associated with the Cyclopentadienyl and Phenyl Rings and the PF_6 Anions appear in Appendix One.

2.3 Results and Discussion

The complex $Cp_2Ti(SEt)_2$ (2) was prepared by reaction of Cp_2TiCl_2 with two equivalents of the thiolate sodium salt in THF. Unreacted Cp_2TiCl_2, as well as, any monosubstituted species $Cp_2TiCl(SEt)$, were separated from the product by stirring the reaction mixture with activated neutral alumina. Filtration and removal of solvent gave the dark red-purple, microcrystalline product 2 in 95% yield. The proton NMR spectrum of 2 shows a singlet in the cyclopentadienyl region and a triplet and a quartet corresponding to the ethyl groups, consistent with literature values.[124] A schematic drawing of the metalloligand appears in Figure 2.1. The disposition of the ethyl groups can be either cis or trans with respect to the S-Ti-S plane. Variable temperature ^1H NMR spectra show only one singlet in the cyclopentadienyl region over the entire temperature range and no change in the methylene resonance. These data suggest that the ethyl groups are on opposites sides of the S-Ti-S plane. However, it may be that the conversion is rapid even at low temperature and an averaging of the signals due to the cis and trans isomers results.

The mixed metal species 3-8 were prepared by addition of $Cp_2Ti(SEt)_2$ to THF solutions containing $[(MeCN)_4Cu]PF_6$ and either one or two equivalents of trisubstituted phosphine or pyridine. Upon addition of the metalloligand, the colour of the reaction mixture rapidly changed from purple to orange-red. Reduction of the solvent volume,

Table 2.3: Crystallographic Parameters for $[Cp_2Ti(\mu\text{-}SEt)_2CuPPh_3]PF_6 \cdot 1.62$ THF and $[Cp_2Ti(\mu\text{-}SEt)_2CuPCy_3]PF$

	3·1.62 THF	4
Formula	$C_{32}H_{35}CuF_6P_2S_2Ti$ $C_{6.48}H_{12.96}O_{1.62}$	$C_{32}H_{53}CuF_6P_2S_2Ti$
Crystal colour, form	orange blocks	orange blocks
Crystal system	monoclinic	monoclinic
a (Å)	15.157(4)	9.389(2)
b (Å)	15.809(6)	36.333(6)
c (Å)	18.527(7)	11.584(3)
β (deg)	100.86(3)	107.81(2)
Space group	$P2_1/c$	$P2_1/n$
Volume ($Å^3$)	4359(3)	3762(1)
Density (gcm^{-3})	1.35	1.39
Z	4	4
Crystal dimens (mm)	0.46 x 0.46 x 0.42 0.42 x 0.46 x 0.39	0.50 x 0.27 x 0.62
Abs coeff, μ (cm^{-1})	8.32	9.60
Radiation, λ (Å)	Mo Kα (0.71069)	Mo Kα (0.71069)
Temperature (°C)	24	24
Scan speed (deg/min)	2.0-5.0 (θ/2θ scan)	2.0-5.0 (θ/2θ scan)
Scan range (deg)	1.0 below Kα1 1.0 above Kα2	1.0 below Kα1 1.0 above Kα2
Bkgd/scan time ratio	0.5	0.5
Data collected	4458	5391

No. of unique data		
$F\sigma^2>3\sigma(F\sigma^2)$	2317	3330
No. of variables	285	397
R (%)	9.86	6.22
Rw (%)	10.55	6.80
Largest Δ/σ in the final least squares cycle	0.001	0.026
Maximum residual electron density ($e/Å^3$)	1.20	0.080
Atom associated	Ti	C31, C36

Table 2.4: Positional Parameters for $[Cp_2Ti(\mu\text{-}SEt)_2CuPPh_3]PF_6 \cdot 1.62$ THF and $[Cp_2Ti(\mu\text{-}SEt)_2CuPCy_3]PF_6$[1]

$[Cp_2Ti(\mu\text{-}SEt)_2CuPPh_3]PF_6 \cdot 1.62$ THF (3·1.62 THF)

Atom	x	y	z	Atom	x	y	z
Cu	2172(1)	3965(1)	463(1)	Ti	3092(2)	5453(2)	3244(2)
S1	2829(3)	4157(3)	2491(2)	S2	2490(3)	4972(3)	4323(2)
P1	1358(3)	2835(3)	3629(2)	P2	4075(4)	7407(5)	737(4)
F1	3300(12)	6919(17)	929(11)	F2	3855(19)	8188(17)	1111(19)
F3	4874(9)	7930(12)	567(9)	F4	4623(17)	7110(19)	1389(15)
F5	3505(16)	7682(20)	43(14)	F6	4298(16)	6701(18)	291(18)
C1	4517(11)	4961(13)	3786(14)	C2	4575(11)	5155(14)	3107(14)
C3	4441(12)	6009(18)	2986(12)	C4	4299(12)	6352(14)	3666(13)
C5	4362(13)	5706(15)	4166(11)	C6	2629(23)	6684(15)	2591(28)
C7	2260(21)	6077(24)	2169(13)	C8	1610(21)	5672(15)	2567(30)
C9	1644(17)	6092(24)	3183(21)	C10	2203(32)	6673(27)	3194(19)
C11	288(6)	3100(7)	3878(6)	C12	285(6)	3715(7)	4418(6)
C13	-520(6)	3942(7)	4628(6)	C14	-1322(6)	3555(7)	4298(6)
C15	-1318(6)	2940(7)	3758(6)	C16	-514(6)	2713(7)	3548(6)
C21	1951(6)	2189(7)	4375(6)	C22	1523(6)	1815(7)	4898(6)
C23	2017(6)	1332(7)	5463(6)	C24	2938(6)	1223(7)	5506(6)
C25	3366(6)	1597(7)	4983(6)	C26	2872(6)	2080(7)	4417(6)
C31	1084(8)	2099(8)	2847(5)	C32	1067(8)	1226(8)	2955(5)
C33	906(8)	682(8)	2351(5)	C34	762(8)	1011(8)	1640(5)
C35	780(8)	1884(8)	1532(5)	C36	941(8)	2427(8)	2136(5)

C41	3739(12)	3348(13)	2652(11)	C42	3359(13)	2522(13)	2296(11)
C51	3294(14)	4441(12)	5079(11)	C52	2806(19)	4138(17)	5649(15)
O1	4699(18)	9103(22)	3417(18)	C61	3914(26)	8715(15)	2986(19)
C62	3281(18)	9447(22)	2727(16)	C63	3577(21)	10147(15)	3285(19)
C64	4359(23)	9766(22)	3823(14)	O2	360(16)	9275(19)	3812(18)
C71	238(20)	9041(32)	4537(21)	C72	1183(28)	9006(32)	4995(14)
C73	1788(16)	8859(29)	4438(22)	C74	1147(23)	8820(25)	3700(16)

$[Cp_2Ti(\mu\text{-}SEt)_2CuPCy_3]PF_6$ (4)

Atom	x	y	z	Atom	x	y	z
Cu	3205(1)	3635(1)	6952(1)	Ti	838(1)	3117(1)	6187(1)
S1	3520(2)	3016(1)	7086(2)	S2	869(2)	3782(1)	5783(2)
P1	4926(2)	4056(1)	7878(2)	P2	5511(4)	6624(1)	7530(3)
F1	6449(15)	6956(3)	7390(12)	F2	4341(12)	6896(3)	7730(12)
F3	6506(15)	6386(4)	7118(19)	F4	4549(13)	6296(3)	7697(9)
F5	6181(15)	6655(4)	8856(8)	F6	4603(18)	6623(4)	6190(9)
C11	4120(10)	4422(3)	8613(8)	C12	2953(11)	4643(3)	7694(10)
C13	2264(14)	4930(3)	8339(14)	C14	1628(16)	4746(5)	9284(18)
C15	2808(16)	4524(4)	10175(13)	C16	3422(12)	4244(3)	9535(10)
C21	5692(11)	4306(3)	6806(9)	C22	6758(11)	4615(3)	7304(10)
C23	7203(19)	4824(4)	6322(16)	C24	7569(17)	4600(4)	5426(15)
C25	6523(14)	4286(4)	4930(11)	C26	6053(15)	4076(3)	5900(11)
C31	6553(13)	3892(2)	9011(10)	C32	7480(10)	4138(2)	10024(9)
C33	8994(13)	3987(3)	10761(14)	C34	9034(15)	3585(3)	11127(10)
C35	8089(9)	3333(2)	10142(8)	C36	6651(12)	3481(3)	9263(13)
C1	943(11)	3006(3)	4212(8)	C2	1193(11)	2671(3)	4803(8)

C3	70(12)	2569(3)	5109(8)	C4	1132(10)	2850(3)	4637(9)
C5	544(10)	3111(3)	4106(8)	C6	909(13)	2851(3)	8091(9)
C7	570(11)	2842(3)	7333(10)	C8	1056(10)	3210(3)	7104(10)
C9	81(12)	3432(3)	7732(9)	C10	1301(11)	3217(4)	8346(9)
C41	4618(9)	2926(2)	6051(8)	C42	5392(10)	2555(3)	6337(10)
C51	1159(14)	3918(3)	4315(9)	C52	1284(19)	4289(4)	4161(11)

[1]Parameters multiplied by 10^4

Table 2.5: **Selected Bond Distances and Angles for $[Cp_2Ti(\mu\text{-}SEt)_2CuPPh_3]PF_6 \cdot 1.62$ THF and $[Cp_2Ti(\mu\text{-}SEt)_2CuPCy_3]PF_6$[1]**

$[Cp_2Ti(\mu\text{-}SEt)_2CuPPh_3]PF_6.1.62$ THF (3·1.62 THF)

Distances (Å)

Cu...Ti	2.803(3)	Cu-S1	2.238(5)	Cu-S2	2.240(5)
Cu-P1	2.226(5)	Ti-S1	2.470(5)	Ti-S2	2.468(5)
Ti-C1	2.34(2)	Ti-C2	2.36(2)	Ti-C3	2.36(2)
Ti-C4	2.33(2)	Ti-C5	2.35(2)	Ti-C6	2.33(3)
Ti-C7	2.36(3)	Ti-C8	2.38(3)	Ti-C9	2.40(3)
Ti-C10	2.35(5)	S1-C41	1.86(2)	S2-C51	1.87(2)
C41-C42	1.53(3)	C51-C52	1.48(4)		

Angles (Degrees)

Cu-S1-Ti	72.9(1)	Cu-S2-Ti	72.9(2)	S1-Cu-S2	114.1(2)
S1-Ti-S2	99.1(2)	S1-Cu-P1	124.2(2)	S2-Cu-P1	121.6(2)
Cu-P1-C11	113.2(4)	Cu-P1-C21	110.4(4)	Cu-P1-C31	116.6(4)
P1-C11-C12	117.8(7)	P1-C11-C16	122.2(8)	P1-C21-C22	122.6(7)
P1-C21-C26	117.4(9)	P1-C31-C32	121.3(8)	P1-C31-C36	118.6(9)
Ti-S1-C41	116.3(6)	Cu-S1-C41	101.9(7)	S1-C41-C42	108(1)
Ti-S2-C51	117.1(7)	Cu-S2-C51	103.6(6)	S2-C51-C52	110(2)
C1-C2-C3	111(2)	C2-C3-C4	106(2)	C3-C4-C5	108(2)
C4-C5-C1	106(2)	C5-C1-C2	109(2)	C6-C7-C8	106(3)
C7-C8-C9	107(3)	C8-C9-C10	108(4)	C9-C10-C6	114(4)
C10-C6-C7	105(3)				

$[Cp_2Ti(\mu\text{-}SEt)_2CuPCy_3]PF_6$ (4)

Distances (Å)

Cu...Ti	2.840(2)	Cu-S1	2.269(2)	Cu-S2	2.261(2)
Cu-P1	2.243(2)	Ti-S1	2.440(2)	Ti-S2	2.461(3)
Ti-C1	2.36(1)	Ti-C2	2.37(1)	Ti-C3	2.366(9)
Ti-C4	2.356(9)	Ti-C5	2.362(8)	Ti-C6	2.39(1)
Ti-C7	2.36(1)	Ti-C8	2.36(1)	Ti-C9	2.41(1)
Ti-C10	2.43(1)	S1-C41	1.84(1)	S2-C51	1.87(1)
C41-C42	1.52(1)	C51-C52	1.37(2)		

Angles (Degrees)

Cu-S1-Ti	74.1(1)	Cu-S2-Ti	73.8(1)	S1-Cu-S2	110.9(1)
S1-Ti-S2	99.1(1)	S1-Cu-P1	125.6(1)	S2-Cu-P1	123.5(1)
Cu-P1-C11	111.8(3)	Cu-P1-C21	112.6(3)	Cu-P1-C31	117.0(3)
P1-C11-C12	111.6(7)	P1-C11-C16	109.4(7)	P1-C21-C22	117.4(8)
P1-C21-C26	115.0(8)	P1-C31-C32	122.0(6)	P1-C31-C36	117.2(7)
Ti-S1-C41	117.4(2)	Cu-S1-C41	102.7(3)	S1-C41-C42	110.0(7)
Ti-S2-C51	116.5(3)	Cu-S2-C51	102.9(4)	S2-C51-C52	114.9(9)
C1-C2-C3	109.4(9)	C2-C3-C4	105.4(9)	C3-C4-C5	110.3(9)
C4-C5-C1	107.8(8)	C5-C1-C2	107.0(9)	C6-C7-C8	107.2(9)
C7-C8-C9	107.9(8)	C8-C9-C10	109(1)	C9-C10-C6	107.8(9)
C10-C6-C7	108(1)				

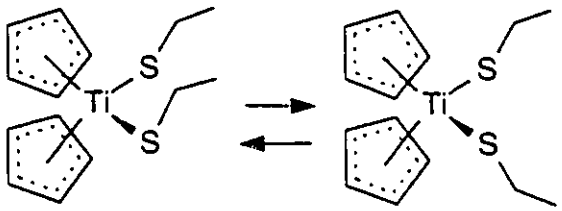

Figure 2.1: Schematic Drawing of the Metalloligand $Cp_2Ti(SEt)_2$

followed by cooling or slow addition of hexane caused precipitation of orange-red crystalline solids. The best yields were obtained when two equivalents of the ancillary ligand were employed. These compounds are air-stable in the solid state; however, in solution they are much more air sensitive. Acetone or THF solutions of these compounds are suitable for the acquisition of spectral data; however, the bimetallic complexes decompose in acetonitrile. For compounds **3-7**, degradation in THF or acetone solution is seen after several days as the colour changes from red-orange to pale yellow. Compound **8** is even more unstable, as decomposition in concentrated solution is evident after several hours, while in dilute solution, decomposition is apparent almost immediately. The products of decomposition are unknown, but loss of the intense colour implies cleavage of at least one Ti-S bond, yielding perhaps a Cu(I) phosphine-thiolate species.

The proton and phosphorus NMR data are consistent with the assignment of the products as titanium/copper species with only one coordinated ancillary ligand. The $^{31}P\{^1H\}$ NMR spectra of the phosphine complexes **3-7** show resonances with chemical shifts indicative of phosphine coordination to a metal atom, as well as, the characteristic septet of resonances arising from the PF_6 anions. In the case of the diphos complex, the $^{31}P\{^1H\}$ NMR resonance arising from the phosphorus coordinated to Cu was broad at 25 °C (1200 Hz at half-height). At -90 °C, this linewidth narrows to 300 Hz at half-height. Further, the UV-Vis spectrum of complex **7** is similar to the monophosphine complexes **3-6**, and markedly dissimilar from the spectral data for the chelated, Ti/Cu bis-phosphine

complex. These data suggest that the diphosphine is not chelating in **7** and that exchange of coordinated and dangling phosphine groups occurs rapidly in solution.

The ^1H NMR spectra of compounds **3** and **4** were examined over the temperature range 50 to -80 °C (Figure 2.2). In both cases, the cyclopentadienyl proton resonances show variation with temperature. At higher temperatures (50 °C), a single resonance is observed at approximately 6.25 ppm. On cooling, this signal broadens and splits into two sharp resonances at about 6.5 and 6.0 ppm. Similarly, the $^{13}C\{^1H\}$ NMR singlet arising from the cyclopentadienyl carbons becomes two separate resonances at low temperature. At the same time, the quartet in the ^1H NMR spectra that is assigned to the methylene protons, of the ethanethiolate groups, broadens and splits into two sets of overlapping doublets of quartets. The coalescence temperatures for all of these signals are approximately 10 °C and 0 °C for **3** and **4**, respectively. The E_a values for the signal averaging processes were determined from line shape analyses[2] and were found to be 71 KJ/mol for **3** and 74 KJ/mol for **4**. The low temperature spectra are assigned to the conformer in which the ethyl substituents of the thiolate moieties are cis. This is consistent with the observation of two inequivalent cyclopentadienyl groups. In addition, the methylene protons of the μ-thiolato groups are inequivalent (i.e., exo and endo) and thus, geminal coupling is seen at low temperature. At higher temperatures, the dynamic process which results in signal averaging, probably involves the interconversion of the cis (syn) -trans (anti) -cis (syn) conformers, although no direct evidence for the trans form is observed. The mechanism for this process may involve metal-sulfur bond cleavage, rotation and bond reformation. Cleavage of the Cu-S bond would yield a two-coordinate Cu(I) intermediate, a geometry which is common for Cu(I). Alternatively, the mechanism may involve pyramidal inversion at the bridging sulfur atoms. This mechanism has been proposed for other thiolato-bridged heterobimetallic complexes[92] and the activation energies for related systems were found to be about 70-77 KJ/mol.[108,113] These data imply that the cis form of these complexes is favoured thermodynamically. The greater

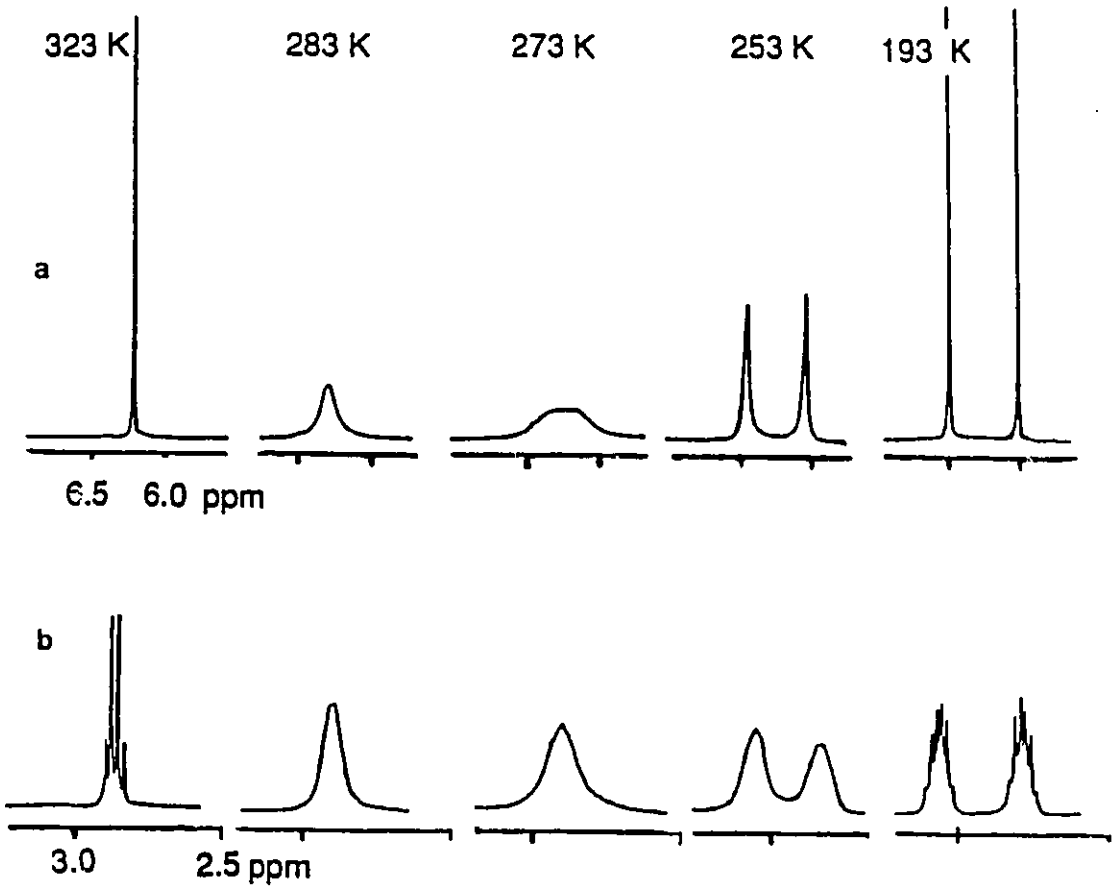

Figure 2.2: Variable Temperature ^1H NMR Spectra for $[Cp_2Ti(\mu\text{-}SEt)_2CuPCy_3]PF_6$:
(a) cyclopentadienyl region
(b) methylene region

stability of the cis form may result from the minimization of steric interactions between the ethyl groups of the μ-thiolato groups and the substituents on the phosphine bound to Cu. Based on the NMR data, the bimetallic complexes were proposed to have the structure shown in Figure 2.3.

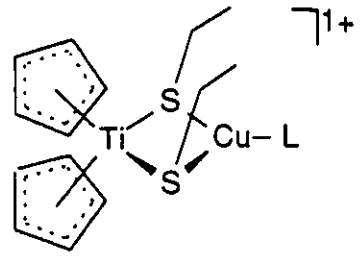

L = PPh_3, PCy_3, PEt_3, PBz_3, NC_5H_5, or $Ph_2P(CH_2)_2PPh_2$

Figure 2.3: Schematic Drawing of the Cation of $[Cp_2Ti(\mu\text{-}SEt)_2CuL]PF_6$

Compounds 3-8 were studied by cyclic voltammetry. All species show irreversible reductions between -0.8 and -1.0 V vs. SCE as represented in Figure 2.4. This is in contrast to the chelated, phosphinoethanethiolate Ti/Cu complex where a reversible reduction wave attributable to a formal Ti(IV)/Ti(III) couple is seen. The presence of the chelate in $[Cp_2Ti(\mu\text{-}SCH_2CH_2PPh_2)_2Cu]^+$ may serve to hold the bimetallic complex together such that it does not decompose upon reduction. Reversible oxidation processes are also not observed. Presumably oxidation at copper or thiolate leads to compound degradation.

The present complexes are dark orange-red, while the chelated Ti/Cu phosphinoethanethiolate complex is green-black. The difference between the pseudo-trigonal copper geometry in complexes 3-8 and the pseudo-tetrahedral copper geometry found in the phosphinoethanethiolate Ti/Cu complex is clearly reflected by perturbation of the Ti-S chromaphore. The UV-Vis spectra of compounds 3-8 show absorptions that are blue-shifted relative to the heterobimetallic complex $[Cp_2Ti(\mu\text{-}SCH_2CH_2PPh_2)_2Cu]^+$.

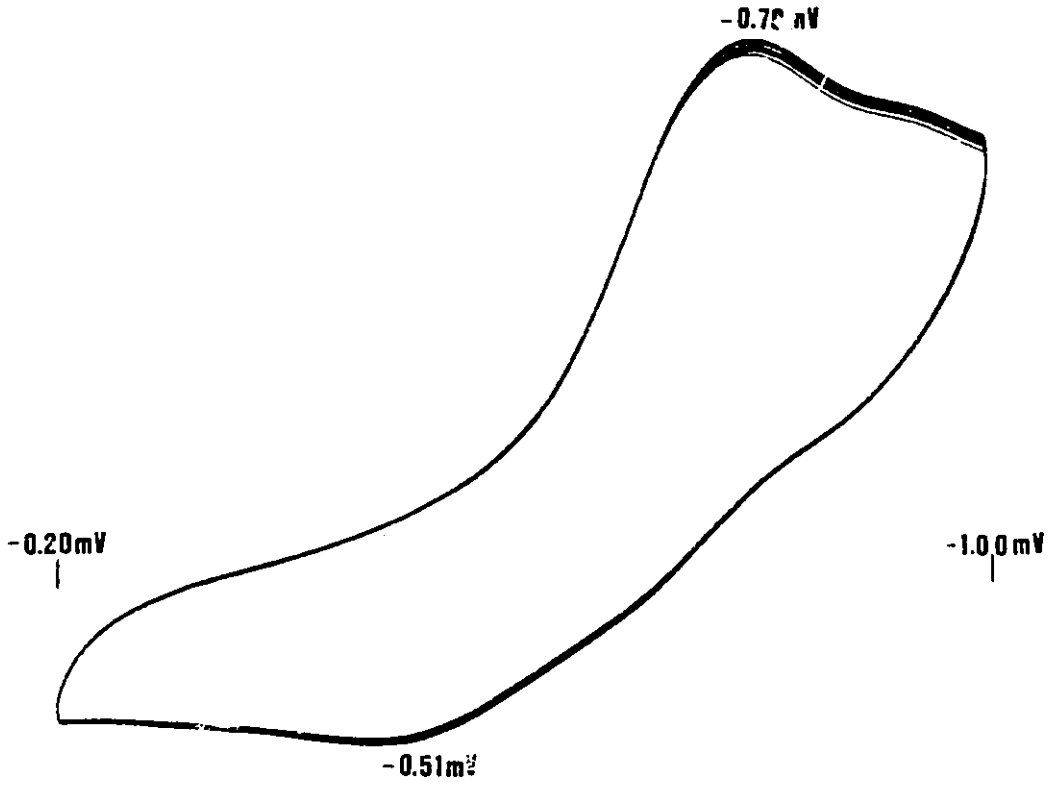

Figure 2.4: Cyclic Voltammogram of $[Cp_2Ti(\mu\text{-}SEt)_2CuPPh_3]PF_6$

Single crystals of **3·1.62 THF** were obtained by cooling a saturated THF solution of **3**. An X-ray crystallographic study revealed that the crystals are made up of monoclinic unit cells each containing discrete cations and anions, as well as, THF molecules of crystallization. The closest approach of any cation to any anion is 2.542 Å (F4-H3). There are two sites where THF molecules exist in the lattice; however, these sites are not fully occupied. The closest approach of a THF molecule to either the cation or anion is 2.331 Å (H74B- H33). The geometry of the anion is typical. Selected bond distances and angles within the cation are given in Table 2.5. An ORTEP drawing of the cation is shown in Figure 2.5 and details of the core appear in Figure 2.6. The coordination geometry of Ti is pseudo-tetrahedral, while the Cu atom is in a pseudo-trigonal environment. The two π-bonded cyclopentadienyl rings and the two thiolato-sulfur atoms comprise the Ti coordination sphere. The Ti-C distances are typical and average 2.36(7) Å. The average Ti-S distance observed was 2.469(1) Å, which is similar to that seen in the chelated Ti/Cu complex, but significantly longer than the 2.378(6) Å found for the Ti-S bond distance in $Cp_2Ti(SCH_2CH_2CH_2PPh_2)_2$. The Cu atom coordination sphere consists of the thiolato-sulfur atoms and the phosphorus atom of the bound PPh_3. The Cu-S bond lengths average 2.239(1) Å, while the Cu-P distance is 2.226(5) Å. These values are similar to those seen for $[Cp_2Ti(\mu\text{-}SCH_2CH_2PPh_2)_2Cu]^+$.

Crystals of **4** were obtained by diffusion of hexane into a THF solution of **4** under anaerobic conditions. The X-ray study of this compound showed the lattice is made up of monoclinic unit cells comprised of discrete anions and cations. The closest approach of a cation to an anion is 2.570 Å (F1- H7). Again, the geometry of the anion is as expected and some selected bond distances and angles for the cation are given in Table 2.5. Figure 2.7 shows an ORTEP drawing of the cation of **4** and details of the core are given in Figure 2.8. The general structural features of this complex are similar to those found for **3·1.62 THF**. The coordination sphere is pseudo-tetrahedral for Ti and pseudo-trigonal for Cu. Ti-C bond distances average 2.39(2) Å, while Ti-S and Cu-S distances average 2.451(8)

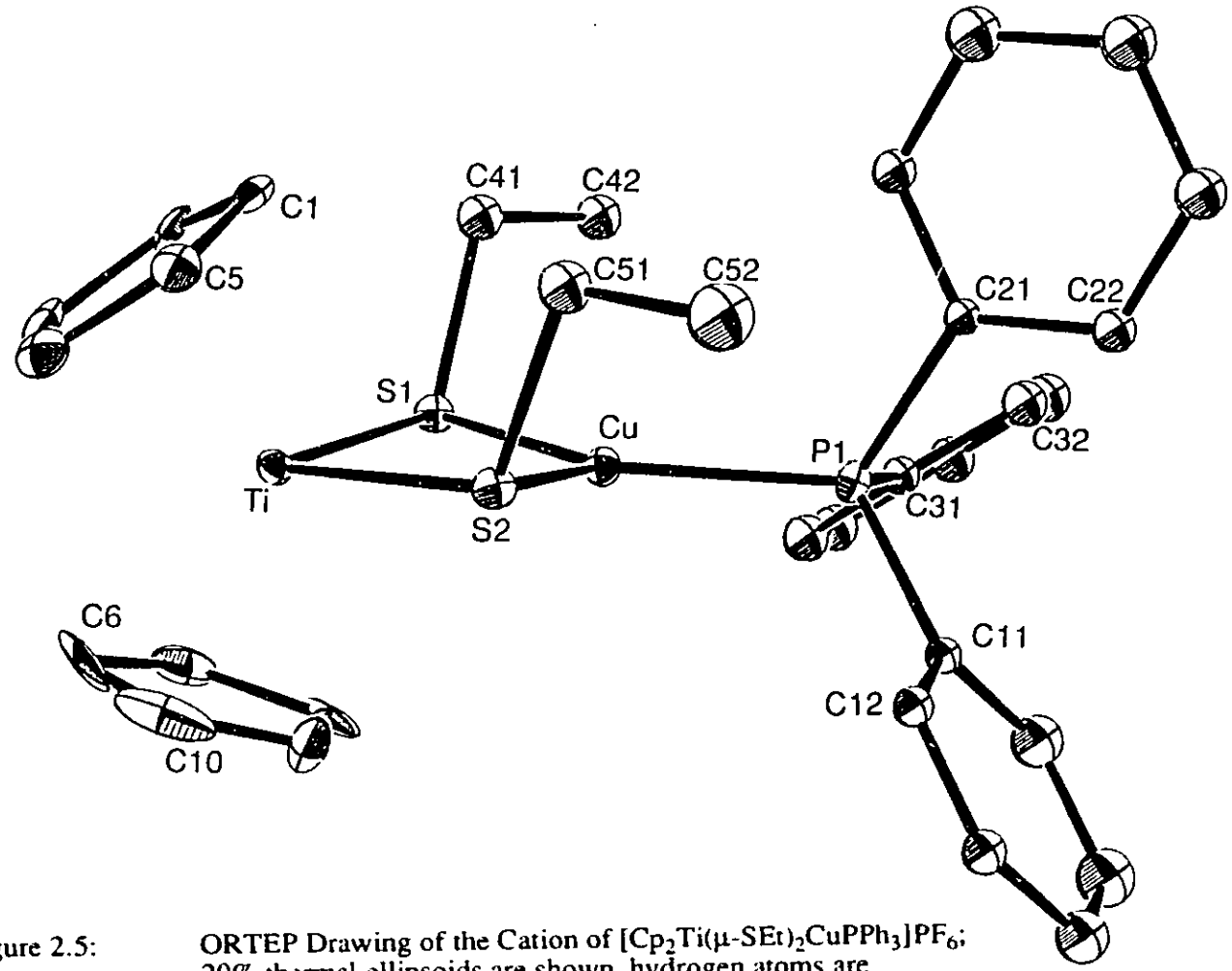

Figure 2.5: ORTEP Drawing of the Cation of $[Cp_2Ti(\mu\text{-}SEt)_2CuPPh_3]PF_6$; 20% thermal ellipsoids are shown, hydrogen atoms are omitted for clarity

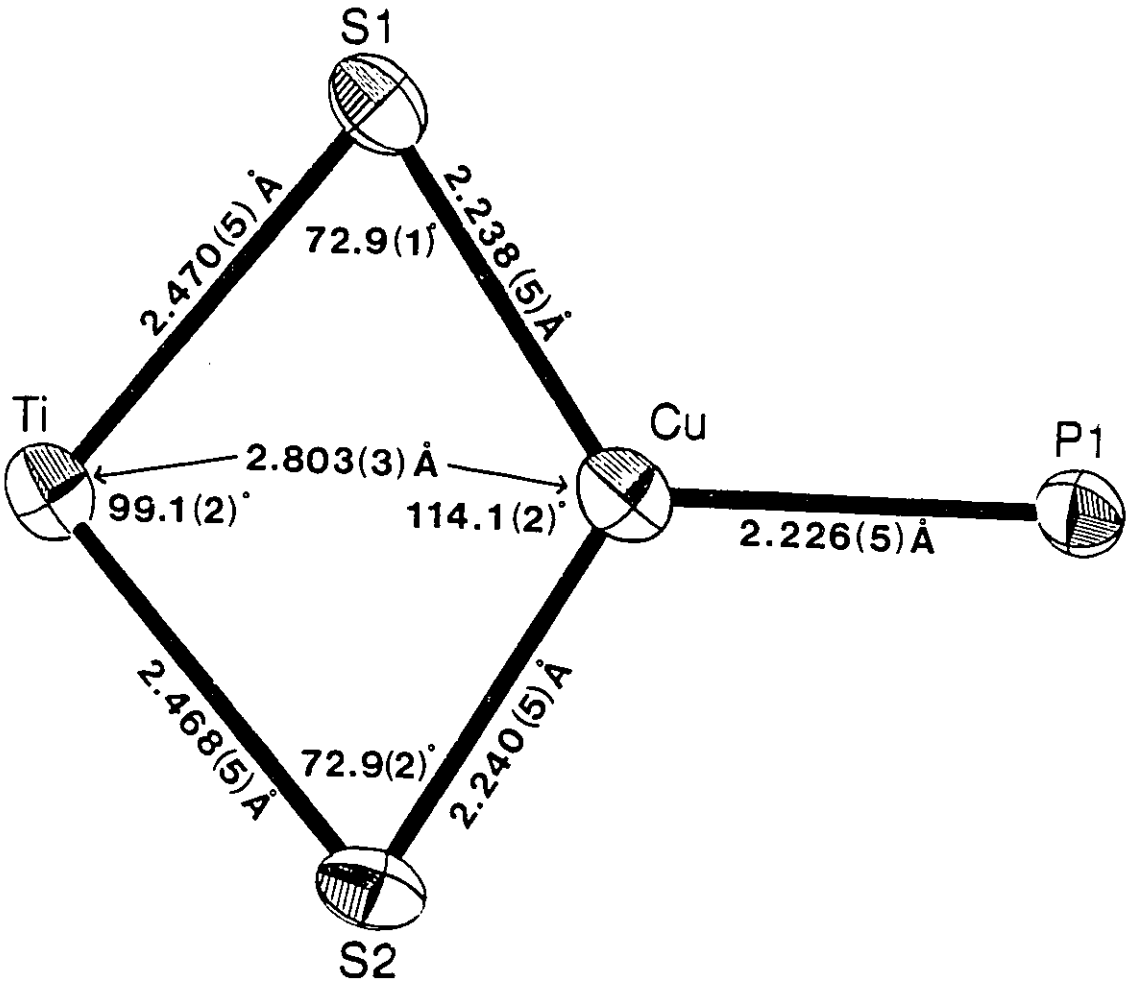

Figure 2.6: ORTEP Drawing of the TiS_2CuP Core of the Cation of $[Cp_2Ti(\mu\text{-}SEt)_2CuPPh_3]PF_6$

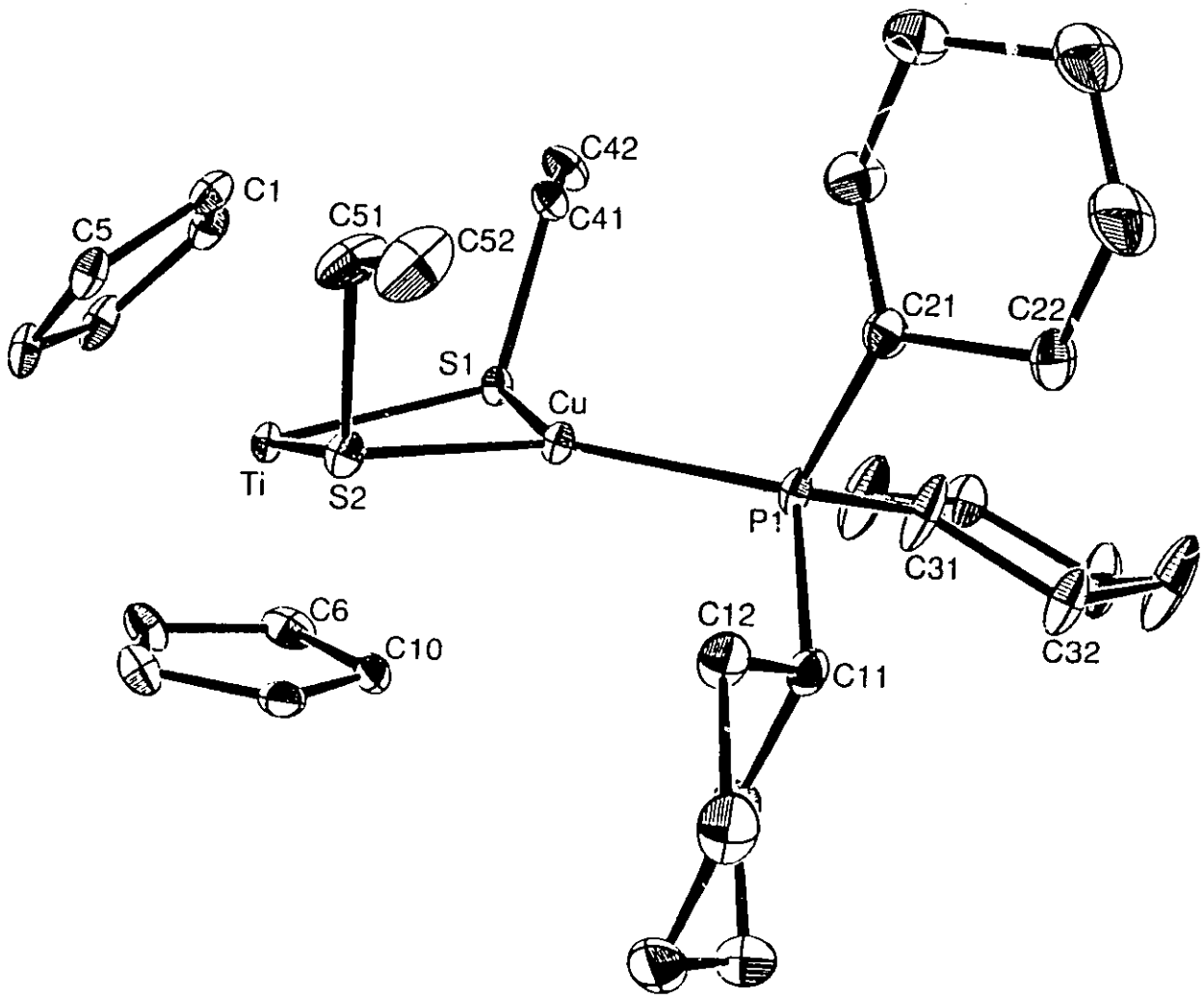

Figure 2.7: ORTEP Drawing of the Cation of $[Cp_2Ti(\mu\text{-}SEt)_2CuPCy_3]PF_6$: 20% thermal ellipsoids are shown, hydrogen atoms are omitted for clarity

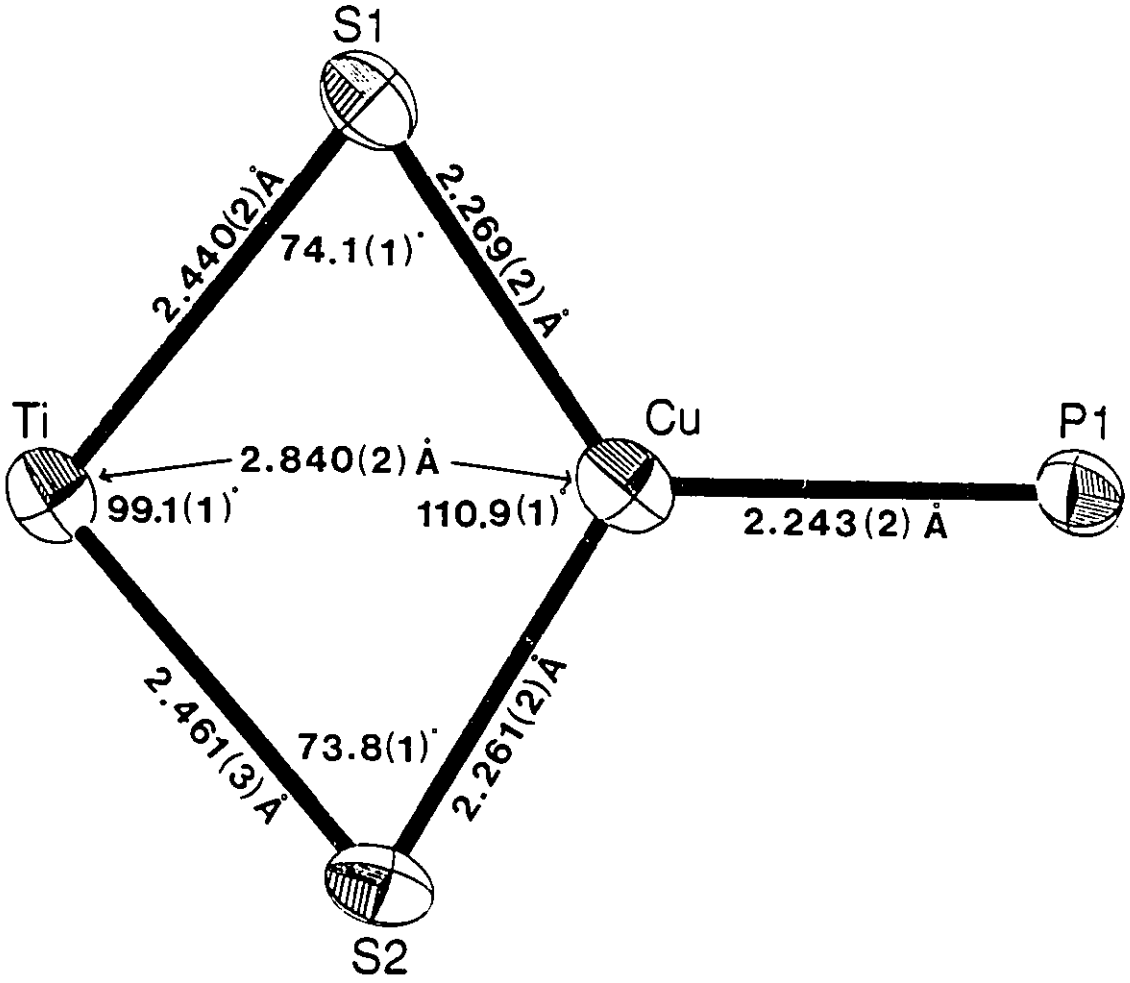

Figure 2.8: ORTEP Drawing of the TiS_2CuP Core of the Cation of $[Cp_2Ti(\mu\text{-}SEt)_2CuPCy_3]PF_6$

and 2.265(4) Å, respectively. The Cu-P distance observed was 2.243(2) Å. The slight lengthening of the Cu-S and Cu-P bonds in **4** compared to the analogous bonds in **3**·1.62 THF can be attributed to the increase in the steric demands of PCy_3 versus PPh_3. The orientation of the substituents of the bridging thiolato groups is cis for both **3**·1.62 THF and **4**. In this orientation, the substituents on the phosphine are staggered with respect to the bridging ethanethiolate groups, thereby minimizing any destabilizing steric interactions.

The TiS_2Cu cores of **3**·1.62 THF and **4** are not planar, rather they are puckered. The angles between the CuS_2 and the TiS_2 planes are 13.02° and 17.92° for **3**·1.62 THF and **4**, respectively. This result is in contrast to that seen for $[Cp_2Ti(\mu\text{-}SCH_2CH_2PPh_2)_2Cu]^+$, where the presence of the chelating phosphinoethanethiolate ligands restricts the four atoms of the TiS_2Cu core to a coplanar geometry. In the present complexes, the absence of the chelating ligands permits a distortion from planarity. The distortion may relieve some of the steric congestion between the μ-thiolato groups and the substituents on the phosphorus. In addition, the puckering of the core may be caused by the Ti centre exhibiting Lewis acidity towards the electron-rich Cu centre. The Cu-S-Ti angles average 72.9(1)° and 73.9(2)° for **3**·1.62 THF and **4**, respectively. These angles are 4-6° less than the Cu-S-Ti angles seen in $[Cp_2Ti(\mu\text{-}SCH_2CH_2PPh_2)_2Cu]^+$. In both compounds the S-Ti-S angles are 99.1(1)°, while the S-Cu-S angle is 114.1(2)° for **3**·1.62 THF and 110.9(1)° for **4**. Both of the angles at Ti and Cu are larger than the corresponding values seen in the chelated complex. The Ti-Cu distances in **3**·1.62 THF and **4** are 2.803(3) and 2.840(2) Å, respectively, which are 0.16-0.20 Å shorter than the metal-metal separation found for $[Cp_2Ti(\mu\text{-}SCH_2CH_2PPh_2)_2Cu]^+$.

The "butterfly" shape of the core, the angles about the CuS_2Ti core and the Cu-Ti distances are consistent with $d^{10} \rightarrow d^0$ dative interactions in the present compounds. Such interactions, in which Ti(IV) acts as a Lewis acid towards an electron-rich metal centre,

have been proposed for $Cp_2Ti(\mu\text{-}SMe)_2Mo(CO)_4$[107] and $[Cp_2Ti(\mu\text{-}SCH_2CH_2PPh_2)_2Cu]^+$.[111] In complexes 3 and 4, the Cu-Ti distances are markedly shorter than either the Ti/Mo complex or the Ti/Cu chelated complex where the Ti-M distances are 3.321(2) and 3.024(1) Å, respectively.

2.4 Summary

Employing complex 2 as a metalloligand offers a useful method for the synthesis of early/late heterobimetallic complexes. The absence of the chelate backbone allows a closer approach of the metals in compounds 3-8 compared to the phosphinoethanethiolate chelated bimetallic. Also, 3-8 do not undergo reversible electrochemistry, therefore it may be concluded that the bidentate ligands keep the complex intact during the reduction. The crystallographic and spectroscopic data are consistent with dative interactions between electron-poor and electron-rich metal centres. This communication may be similar to that occurring in systems exhibiting SMSI. The nature of the metal-metal interactions in these compounds is best described as a $d^{10} \rightarrow d^0$ dative bond and further investigation of this assignment is discussed in the following chapter.

CHAPTER THREE

USE OF $Cp_2Ti(SMe)_2$ AND $Cp_2Ti(SEt)_2$ AS METALLOLIGANDS FOR THE PREPARATION OF HETEROBIMETALLIC, THREE- AND FOUR-COORDINATE COPPER COMPLEXES

3.1 Introduction

The titanium species $Cp_2Ti(SEt)_2$ is useful for preparing three-coordinate, heterobimetallic Ti/Cu compounds containing one ancillary ligand. However, attempted synthesis of four-coordinate copper complexes analogous to $[Cp_2Ti(\mu\text{-}SCH_2CH_2PPh_2)_2Cu]BF_4$, using the ethanethiolate metalloligand and various ancillary ligands, were unsuccessful. The steric requirements of the ethyl substituent on sulfur or the large cone angles of trisubstituted phosphines may preclude isolation of the tetrahedral copper species. Reported in this chapter is the investigation of the steric requirements of the thiolate substituents and of the ancillary ligands with respect to their effect on the preparation of four-coordinate copper compounds. The steric effects of the alkyl substituent on sulfur were probed by utilizing methanethiolate in place of ethanethiolate in the metalloligand. In the case of ancillary ligand modification, the use of less sterically demanding ligands such as trimethylphosphine and acetonitrile was explored instead of the larger tricyclohexylphosphine and triphenylphosphine.

The methanethiolate metalloligand, as well as, a four-coordinate Cu(I) complex prepared using the methanethiolate species have been crystallized and studied by X-ray crystallography. Direct comparison between the starting ligand and the bimetallic provides insight into the geometric perturbations caused by the close proximity of the constituent metals. A trimetallic species containing a tetrahedral copper centre was prepared by the reaction of two equivalents of the methanethiolate metalloligand with $[(MeCN)_4Cu]PF_6$. However, attempts to prepare four-coordinate copper complexes with

two copper-bound phosphines using $Cp_2Ti(SMe)_2$ were unsuccessful. In the reaction of the methanethiolate ligand with copper and PCy_3, the product was a species similar to 3 and 4, while the analogous reaction employing trimethylphosphine gave the titanium/copper trimetallic complex.

3.2 Experimental Section

All preparations were done under an atmosphere of dry, O_2-free N_2. Solvents were reagent grade, distilled from the appropriate drying agents under N_2, and degassed by the freeze-thaw method at least three times prior to use. ^1H NMR spectra were recorded on a Bruker AC-300 spectrometer operating at 300 MHz. Trace amounts of protonated solvents were used as references and chemical shifts are reported in ppm relative to $SiMe_4$. $^{31}P\{^1H\}$ NMR spectra were recorded on a Bruker AC-200 spectrometer operating at 81 MHz and are reported relative to external 85% H_3PO_4. Cyclic voltammetry experiments were performed using a BAS CV-27 electrochemistry unit with a platinum working electrode and a Ag/AgCl reference electrode. $[NBu_4]BF_4$ was used as the supporting electrolyte. Combustion analyses were performed by Galbraith Laboratories Inc. Knoxville, TN. Cp_2TiCl_2, Me_2S_2, and PPh_3 were purchased from the Aldrich Chemical Co. and PCy_3 was purchased from the Pressure Chemical Co. $[(MeCN)_4Cu]PF_6$ was prepared by the literature method[120] and $Cp_2Ti(SEt)_2$ was prepared as described in Chapter Two.

(i) Preparation of NaSMe (9) To a 100 mL THF solution of Me_2S_2 (3.9 mL, 43.5 mmoles) was added sodium metal (2.0 g, 87 mmoles) and the mixture stirred overnight. An additional 2 mL of the disulfide was added to the reaction flask and the mixture stirred for an additional 4 h to ensure complete reaction. The air-sensitive, sodium salt was filtered under nitrogen and dried *in vacuo*. (Yield based on sodium metal used: 6.3g, 100%).

(ii) Preparation of $Cp_2Ti(SMe)_2$ (10) To Cp_2TiCl_2 (1.0 g, 4.0 mmoles) in 50 mL THF was added NaSMe (563 mg, 8.0 mmoles) and the mixture stirred overnight. Activated neutral alumina was added, the mixture stirred for 10 min and then filtered. The alumina was washed with 5 x 20 mL portions of THF which were combined with the mother liquor. The resulting THF solution was stripped to dryness and the residue washed with 2 x 10 mL of pentane. The red-purple, microcrystalline solid was dried *in vacuo*. (Yield: 1.0 g, 92%). ^1H NMR (d_6-benzene): δ, 6.23 (s, 5 H), 2.45 (s, 3 H). Anal. Calcd for $C_{12}H_{16}S_2Ti$: C, 52.94; H, 5.92. Found: C, 53.06; H, 5.95.

(iii) Preparation of $[Cp_2Ti(SMe)_2CuPCy_3]PF_6$ (11) To a 30 mL THF suspension of $[(MeCN)_4Cu]PF_6$ (136 mg, 0.36 mmoles) was added PCy_3 (205 mg, 0.72 mmoles). To the clear, colourless solution was added a purple THF solution of $Cp_2Ti(SMe)_2$ (100 mg, 0.36 mmoles), resulting in a colour change to red-orange and precipitation of a bright orange solid. After the mixture was stirred for 10 min, the solution was filtered, washed with 2 x 10 mL pentane and dried in vacuo. The bright orange microcrystalline solid was isolated by filtration, washed with 2 x 10 mL pentane and dried *in vacuo*. (Yield: 227 mg, 80%). Anal. Calcd for $C_{30}H_{49}CuF_6P_2S_2Ti$: C, 47.34; H, 6.49. Found: C, 47.22; H, 6.47. ^1H NMR (d_3-MeCN): δ, 6.03 (s, 10 H), 2.50 (s, 6 H), 1.96-1.27 (br m, 33 H). $^{31}P\{^1H\}$ NMR (d_3-MeCN): δ, 29.90 (s), -142.99 (septet).

(iv) Preparation of $[Cp_2Ti(\mu\text{-}SMe)_2Cu(NCMe)_2]PF_6$ (12) To $[(MeCN)_4Cu]PF_6$ (136 mg, 0.36 mmoles) in 30 mL MeCN was added dropwise $Cp_2Ti(SMe)_2$ (100 mg, 0.36 mmoles) in 10 mL MeCN, which resulted in a colour change from purple to dark, red-orange. After the mixture was stirred for 30 min, the solvent was removed under vacuum and the residue washed with 2 x 10 mL pentane. The product was collected by filtration, washed with 2 x 10 mL pentane and dried *in vacuo*. (Yield: 142 mg, 70 %).

Anal. Calcd for $C_{16}H_{22}CuF_6N_2PS_2Ti$: C, 35.92; H, 4.15. Found: C, 35.12; H, 4.08. ^1H NMR (d_3-MeCN): δ, 6.00 (s, 5 H), 2.46 (s, 3 H), 1.95 (s, 3 H).

(v) **Preparation of $[Cp_2Ti(\mu\text{-}SEt)_2Cu(NCMe)_2]PF_6$ (13)** This species is prepared in a manner analogous to that used for the methanethiolate species using $[(MeCN)_4Cu]PF_6$ (136 mg, 0.36 mmoles) and $Cp_2Ti(SEt)_2$ (108 mg, 0.36 mmoles). (Yield: 138 mg, 65%). ^1H NMR (d_3-MeCN): δ, 5.98 (s, 5 H), 2.84 (q, 2 H), 2.05 (s, 3 H), 1.14 (t, 3 H).

(vi) **Preparation of $[(Cp_2Ti(\mu\text{-}SMe)_2)_2Cu]PF_6$ (14)** To a 30 mL THF suspension of $[(MeCN)_4Cu]PF_6$ (68 mg, 0.18 mmoles) was added $Cp_2Ti(SMe)_2$ (100 mg, 0.36 mmoles) and the mixture stirred. Upon stirring the colour of the solution changed from purple to red-purple and after 20 min precipitation of a dark solid was evident. The solution was filtered and the solid washed with 2 x 10 mL pentane and the solid dried *in vacuo*. (Yield 90 mg, 65%). Anal. Calcd for $C_{24}H_{32}CuF_6PS_4Ti_2$: C, 38.28; H, 4.28. Found: C, 37.22; H, 4.21. ^1H NMR (d_6-acetone): δ, 6.23 (s, 5 H), 2.77 (s, 3 H).

(vii) **Reaction of $[Cp_2Ti(\mu\text{-}SMe)_2Cu(NCMe)_2]PF_6$ with PCy_3** To a 20 mL THF solution of $[Cp_2Ti(\mu\text{-}SMe)_2Cu(NCMe)_2]PF_6$ (30 mg, 0.053 mmoles) was added PCy_3 (0.15 mg, 0.05 mmoles). The solution changed from dark red-orange to bright orange immediately and orange solid precipitated. $^{31}P\{^1H\}$ NMR (d_6-acetone): δ, 30.39 (s), -143.80 (septet).

(viii) **Reaction of $[Cp_2Ti(\mu\text{-}SMe)_2Cu(NCMe)_2]PF_6$ with PMe_3** To a 20 mL THF solution of $[Cp_2Ti(\mu\text{-}SMe)_2Cu(NCMe)_2]PF_6$ (30 mg, 0.053 mmoles) was added PMe_3 (0.08 mg, 0.10 mmoles). The colour of the solution immediately changed from dark red-orange to purple. $^{31}P\{^1H\}$ NMR (THF): δ, -45.88 (br s), -143.80 (septet).

(ix) X-ray Data Collection and Reduction Diffraction experiments were performed on a four-circle Syntex $P2_1$ diffractometer with graphite-monochromatized Mo Ka radiation (λ = 0.71069 Å). The initial orientation matrices for **10** and **12** were obtained from 15 machine-centred reflections selected from rotation photographs. These data were used to determine the crystal systems and in the case of **10** the final lattice parameters and orientation matrix. Partial rotation photographs around each axis were consistent with a tetragonal crystal system for **10** and a triclinic crystal system for **12**. The final lattice parameters and the final orientation matrix for **12** were determined from 64 high-angle reflections (20°<2θ<25°). Machine parameters, crystal data, and data collection parameters are summarized in Table 3.1. The observed extinctions were consistent with the space group $P4_12_12$ for **10** and $P\bar{1}$ for **12**. $+h,+k,+l$ data were collected (4.5°<2θ<45.0°) for **10** and $\pm h,\pm k,+l$ data were collected (4.5°<2θ<45.0°) for **12**. Three standard reflections were recorded every 197 reflections with no statistically significant change in their intensities over the duration of the data collection. The data were processed using the SHELX-76 program package. An empirical absorption correction was applied to the data of **12** employing a locally modified version of ABSORB.

(x) Structure Solution and Refinement Non-hydrogen atomic scattering factors were taken from the literature tabulations.[121-123] The heavy atoms positions were determined using direct methods. The remaining non-hydrogen atoms were located from successive difference Fourier map calculations. The refinement was carried out by using full-matrix least squares techniques on F, minimizing the function $w(|Fo|-|Fc|)^2$ where the weight, w, is defined as $4Fo^2/\sigma(Fo^2)$ and Fo and Fc are the observed and calculated structure factor amplitudes. In the final cycles of refinement all the non-hydrogen atoms were assigned anisotropic temperature factors. Hydrogen atom positions were calculated and allowed to ride on the carbon to which they are bonded assuming a C-H bond length of 0.95 Å. Hydrogen atom temperature factors were fixed at 1.10 times the isotropic temperature

factor of the carbon atom to which they are bonded. In all cases the hydrogen atom contributions were calculated, but not refined. Tables of Positional Parameters (Table 3.2) and Selected Bond Distances and Angles (Table 3.3) appear in this chapter, Thermal Parameters (Table A1.1), and Hydrogen Atom Parameters (Table A1.2) are reported in Appendix One.

3.3 Results and Discussion

The metalloligand $Cp_2Ti(SMe)_2$ (**10**) was prepared by reaction of titanocene dichloride and the methanethiol sodium salt. The solution changes from red-orange to purple over a period of hours. Purification of the compound was achieved by addition of activated neutral alumina to remove any starting material or monosubstituted species, $Cp_2TiCl(SMe)$. After work-up, a dark purple-red microcrystalline solid was obtained. The proton NMR spectrum shows a singlet in the cyclopentadienyl region and another singlet in the methyl region with the appropriate integration, consistent with the proposed formulation.[124]

The bimetallic complex $[Cp_2Ti(\mu\text{-}SMe)_2CuPCy_3]PF_6$ (**11**) was prepared by addition of the metalloligand to a THF solution of $[(MeCN)_4Cu]PF_6$ and the trisubstituted phosphine. Upon addition of the purple metalloligand to the clear, colourless solution containing Cu(I) and the phosphine, the solution colour changed to red-orange. The bright orange product precipitated and was isolated by filtration.

Complexes **11** was studied by NMR spectroscopy. The $^{31}P\{^1H\}$ NMR spectrum for **11** shows a singlet with a chemical shift corresponding to coordinated phosphine and the characteristic septet due to the PF_6 anion. In the ^1H NMR spectrum of **11** there are the expected singlets due to the cyclopentadienyl and methyl groups and a multiplet corresponding to the cyclohexyl groups. Integration of the proton spectrum reveals only one phosphine bound to copper as was found for complexes 3 and 4. The NMR data suggest the structure of **11** is as shown in Figure 3.1.

Table 3.1: Crystallographic Parameters for $Cp_2Ti(SMe)_2$ and $[Cp_2Ti(\mu\text{-}SMe)_2Cu(NCMe)_2]PF_6$

	10	**12**
Formula	$C_{12}H_{16}S_2Ti$	$C_{16}CuF_6H_{22}N_2PS_2Ti$
Crystal colour, form	dark red prisms	orange blocks
Crystal system	tetragonal	triclinic
a (Å)	9.288(5)	8.038(2)
b (Å)		13.169(3)
c (Å)	14.487(5)	11.732(3)
α (deg)		109.31(2)
β (deg)		106.12(2)
γ (deg)		89.29(2)
Space group	$P4_12_12$	$P\bar{1}$
Volume ($Å^3$)	1249(1)	1122(1)
Density (gcm^{-3}) calcd	1.45	1.67
Z	4	2
Crystal dimens (mm)	0.48 x 0.29 x 0.38	0.35 x 0.40 x 0.45
Abs coeff, μ (cm^{-1})	9.10	15.30
Radiation, λ (Å)	Mo Kα (0.71069)	Mo Kα (0.71069)
Temperature (°C)	24	24
Scan speed (deg/min)	2.0-5.0(θ/2θ)scan	2.0-5.0(θ/2θ scan)
Scan range (deg)	1.0 below Kα1	1.0 below Kα1
	1.0 above Kα2	1.0 above Kα2
Bkgd/scan time ratio	0.5	0.5
Data collected	988	3368
No. of unique data		

$Fo^2>3\sigma(Fo^2)$	771	1901
No. of variables	68	262
R (%)	2.76	5.85
Rw (%)	3.19	6.20
Largest Δ/σ in the final least squares cycle	0.001	0.003
Maximum residual electron density (e/A^3)	0.28	0.78
Atom associated	Ti	Cu, S1

Table 3.2: Positional Parameters for $Cp_2Ti(SMe)_2$ and $[Cp_2Ti(\mu\text{-}SMe)_2Cu(NCMe)_2]PF_6$[1]

$Cp_2Ti(SMe)_2$ (10)

Atom	x	y	z	Atom	x	y	z
Ti	-361(1)	-361(1)	10000	S	1696(1)	81(1)	9038(1)
C1	-1350(6)	-538(5)	8486(3)	C2	-1366(5)	935(5)	8721(3)
C3	-2308(5)	1090(6)	9465(3)	C4	-2849(5)	-249(7)	9706(3)
C5	-2299(5)	-1251(6)	9096(3)	C6	3318(5)	138(6)	9739(4)

$[Cp_2Ti(\mu\text{-}SMe)_2Cu(NCMe)_2]PF_6$ (12)

Atom	x	y	z	Atom	x	y	z
Ti	3436(2)	7338(1)	7479(1)	Cu	2350(1)	5631(1)	8166(1)
S1	482(3)	6674(2)	7329(2)	S2	5159(3)	6242(2)	8625(2)
N1	1980(12)	5617(6)	9779(9)	N2	2124(11)	4020(7)	7059(8)
P	1617(4)	9208(2)	12842(2)	F1	1262(13)	9579(8)	11723(7)
F2	3009(13)	10129(7)	13487(9)	F3	173(12)	8323(8)	2141(13)
F4	355(10)	9917(7)	13387(8)	F5	2094(17)	8833(12)	13958(10)
F6	2839(11)	8504(7)	12240(10)	C1	3550(13)	8680(7)	9417(9)
C2	2428(14)	8993(7)	8479(10)	C3	3391(17)	9197(8)	7744(11)
C4	5106(16)	9003(8)	8244(11)	C5	5204(13)	8700(7)	9267(9)
C6	2275(21)	6131(14)	5380(11)	C7	2472(19)	7077(13)	5300(11)
C8	4135(21)	7407(10)	5663(10)	C9	5096(16)	6610(15)	6067(9)
C10	3869(29)	5775(10)	5866(12)	C11	1992(14)	5742(8)	10779(11)

C12	1965(15)	5894(8)	12069(10)	C21	4263(14)	3152(9)	6598(100
C22	2512(17)	1997(10)	6036(13)	C31	-383(13)	7409(9)	8633(11)
C41	5871(14)	6805(9)	10338(9)				

[1]Parameters multiplied by 10^4

Table 3.3: Selected Bond Distances and Angles for $Cp_2Ti(SMe)_2$ and $Cp_2Ti(\mu\text{-}SMe)_2Cu(NCMe)_2]PF_6$

$Cp_2Ti(SMe)_2$ (10)

Distances (Å)

Ti-S	2.400(1)	Ti-C1	2.383(4)	Ti-C2	2.399(4)
Ti-C3	2.385(40	Ti-C4	2.352(5)	Ti-C5	2.375(4)
S-C6	1.817(5)	C1-C2	1.409(6)	C2-C3	1.396(6,
C3-C4	1.386(8)	C4-C5	1.381(7)	C1-C5	1.412(7)

Angles (Degrees)

S-Ti-S'	93.7(1)	C6-S-Ti	109.9(2)	Cp-Ti-Cp'	127.0(1)

$[Cp_2Ti(\mu\text{-}SMe)_2Cu(NCMe)_2]PF_6$ (12)

Distances (Å)

Ti-S1	2.480(3)	Ti-S2	2.451(3)	Cu-S1	2.265(3)
Cu-S2	2.263(3)	Cu-N1	2.002(9)	Cu-N2	2.067(9)
S1-C31	1.832(11)	S2-C41	1.818(10)	N1-C11	1.127(12)
C11-C12	1.465(15)	N2-C21	1.111(12)	C21-C22	1.481(16)
		Ti...Cu	2.847(2)		

Angles (Degrees)

S2-Ti-S1	99.3(1)	S2-Cu-S1	112.2(1)	Cu-S1-Ti	73.6(1)
Cu-S2-Ti	74.2(1)	C31-S1-Ti	115.9(3)	C31-S1-C:	102.7(4)
C41-S2-Ti	117.7(4)	C41-S2-Cu	103.9(4)	N1-Cu-S1	110.6(3)

N1-Cu-S2	106.9(3)	N2-Cu-S1	115.5(3)	N2-Cu-S2	106.3(3)
N2-Cu-N1	104.7(3)	C11-N1-Cu	168.5(9)	C12-C11-N1	179(1)
C21-N2-Cu	168(1)	C22-C21-N2	177(1)		

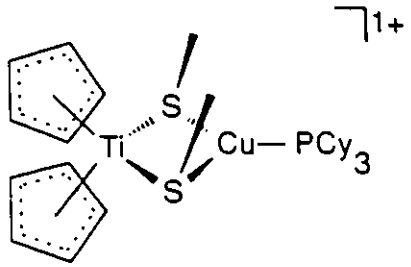

Figure 3.1: Schematic Drawing of the Cation of $[Cp_2Ti(\mu\text{-}SMe)_2CuPCy_3]PF_6$

Variable temperature proton NMR was carried out on complex **11** and the cyclopentadienyl region of the spectra is shown in Figure 3.2. As can be seen from the spectra, the cyclopentadienyl signal is a singlet at high temperature (327 K) and broadens as the temperature is lowered. At 243 K, the spectrum shows two sharp singlets, indicating two different cyclopentadienyl environments. As seen with species **3** and **4**, these results indicate a cis arrangement of the alkyl groups on sulfur. There is no evidence for the trans isomer, suggesting that the trans isomer is in low equilibrium concentration or does not exist. A concerted interconversion with the sulfurs inverting simultaneously is one mechanism which would explain the latter case. The mechanism for the former situation may involve inversion of only one sulfur at a time or breaking of a S-Cu bond, rotation and bond reformation. Using line shape analysis, the activation energy for the interconversion was found to be 77 kJ/mol, which is similar to that found for **3** and **4**, as well as, related complexes reported in the literature.[108,113] From the variable temperature NMR data the methyl groups were determined to be in a cis disposition as suggested in the structure shown in Figure 3.1.

Reactions of $Cp_2Ti(SMe)_2$ and $Cp_2Ti(SEt)_2$ with $[(MeCN)_4Cu]PF_6$ in acetonitrile lead to red-orange, microcrystalline solids **12** and **13**, respectively. The products were purified by removal of the solvent and washing of the residue with pentane. Proton NMR experiments were performed on complexes **12** and **13**. In the cyclopentadienyl region there are the expected singlets for both species, and for **12** a singlet in the methyl region and for **13** a quartet and a triplet due to the ethyl groups. In both cases, a multiplet at

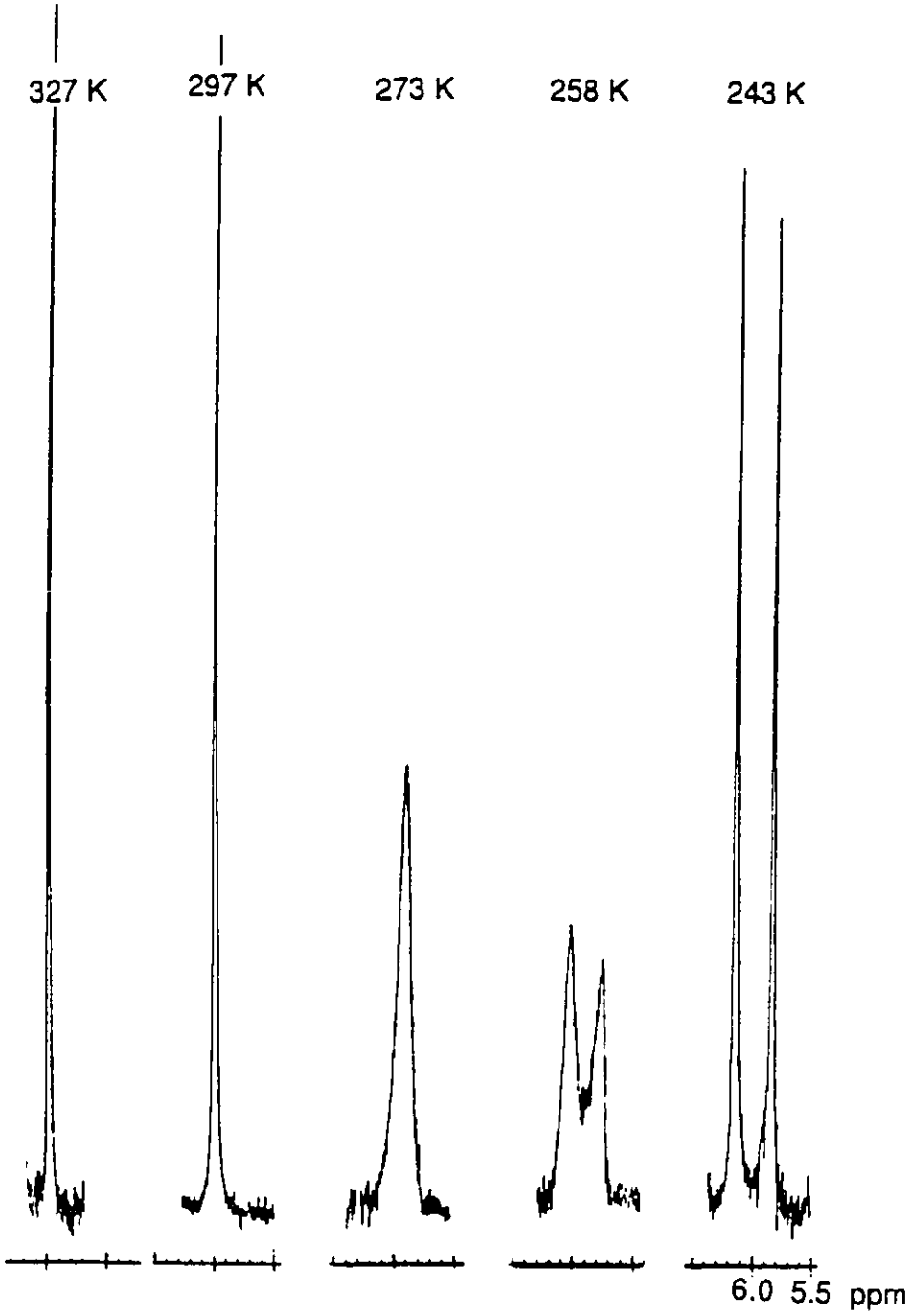

Figure 3.2: Variable Temperature ^1H NMR Spectra for $[Cp_2Ti(\mu\text{-}SMe)_2CuPCy_3]PF_6$; cyclopentadienyl region is shown

about 1.93 appears which corresponds to two coordinated acetonitriles. Based on the NMR data, the structures of **12** and **13** were assigned as shown in Figure 3.3.

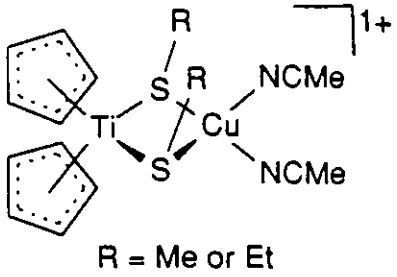

Figure 3.3: Schematic Drawing of the Cation of $[Cp_2Ti(\mu\text{-}SMe)_2Cu(NCMe)_2]PF_6$

A variable temperature NMR study was performed on complex **12**. The cyclopentadienyl region is the area of interest in the proton spectra and is shown in Figure 3.4. At 327 K, there is one peak corresponding to an averaged cyclopentadienyl environment. As the temperature is lowered, the signal broadens and eventually splits into two singlets. The spectrum at 243 K shows two sharp singlets, indicating two different cyclopentadienyl environments. These results correspond to the methyl substituents on the sulfur atoms being in a cis disposition. The activation energy, as determined from line shape analysis was found to be 80 kJ/mol which is similar to that found for complexes **3** and **4**. The mechanism may be similar to that discussed for the variable temperature results of **11**.

Reaction of two equivalents of the titanium methanethiolate ligand with $[(MeCN)_4Cu]PF_6$ leads to a trimetallic complex $[(Cp_2Ti(\mu\text{-}SMe)_2)_2Cu]PF_6$ (**14**). The dark, red-brown solid precipitates out of THF and is isolated by filtration. The ^1H NMR data and elemental analyses are consistent with the formulation depicted in Figure 3.5.

Changing the steric bulk of the phosphine by using PMe_3 instead of tricyclohexylphosphine did not lead to a four-coordinate copper species analogous to $[Cp_2Ti(\mu\text{-}SCH_2CH_2PPh_2)_2Cu]BF_4$. Rather complex **14** is obtained when one equivalent of $Cp_2Ti(SMe)_2$ is reacted with $[(MeCN)_4Cu]PF_6$ and two equivalents of PMe_3. Trimethylphosphine reacts with the Cu(I) centre to give a copper-phosphine species

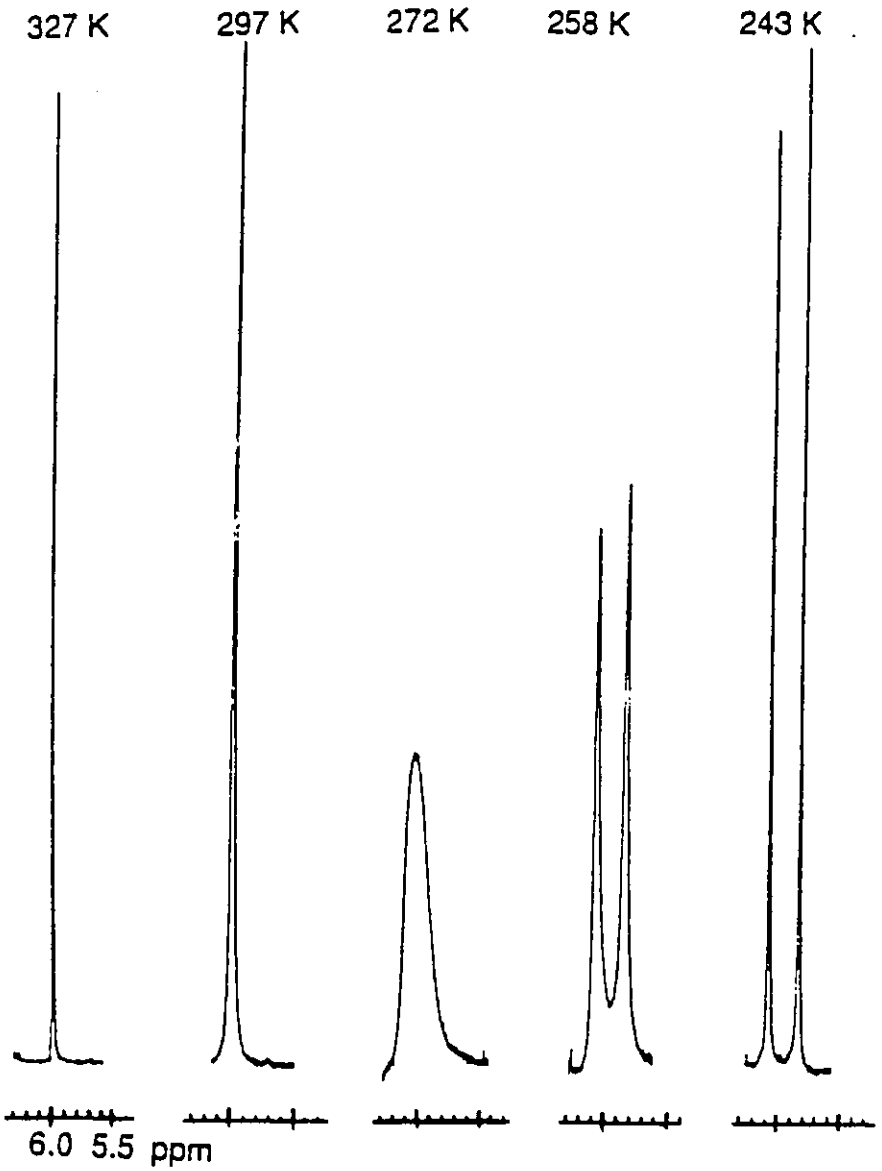

Figure 3.4: Variable Temperature ^1H NMR Spectra for $[Cp_2Ti(\mu\text{-}SMe)_2Cu(NCMe)_2]PF_6$; cyclopentadienyl region is shown

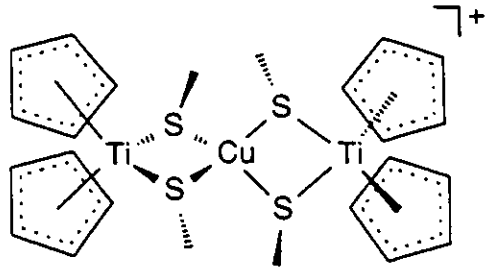

Figure 3.5: Schematic Drawing of the Cation of $[(Cp_2Ti(\mu\text{-}SMe)_2)_2Cu]PF_6$

leaving half of the Cu(I) species to react with the titanium metalloligand in a 2:1 ratio.

Complex **11** will not undergo substitution of the phosphine in the presence of large excesses of acetonitrile to give **12**. The phosphine complex is sufficiently stable in MeCN to allow acquisition of spectral data; however, after approximately four days, the compound decomposes to give a copper-phosphine species, uncoordinated phosphine and the titanium metalloligand. Complexes **12** and **13** will not undergo displacement of the coordinated acetonitriles when two equivalents of tricyclohexylphosphine are added to MeCN solutions of **12** or **13**. However, if **12** or **13** are dissolved in THF, the phosphine will displace the acetonitriles. When excess PMe_3 is used, the colour of the solution changes immediately from orange to dark purple. The small phosphine is so basic that it displaces the acetonitriles and the thiolates of the metalloligands. The syntheses and the results from the substitution experiments are summarized in Scheme 3.1.

Cyclic voltammetry experiments were performed on species **10** and **12**. The voltammograms appear in Figures 3.6 and 3.7, respectively. Neither of these complexes exhibits reversible reduction or oxidation, similar to the behaviour seen for **3** and **4**. A reduction potential of -0.93 mV was found for **10** and for **13** a reduction potential of -0.98 mV was found.

Crystals of **10** were obtained by vapour diffusion of pentane into a THF solution of **10**. An X-ray structural study for **10** showed the compound to be made up of tetragonal unit cells each containing four discrete formula units. The closest approach between these

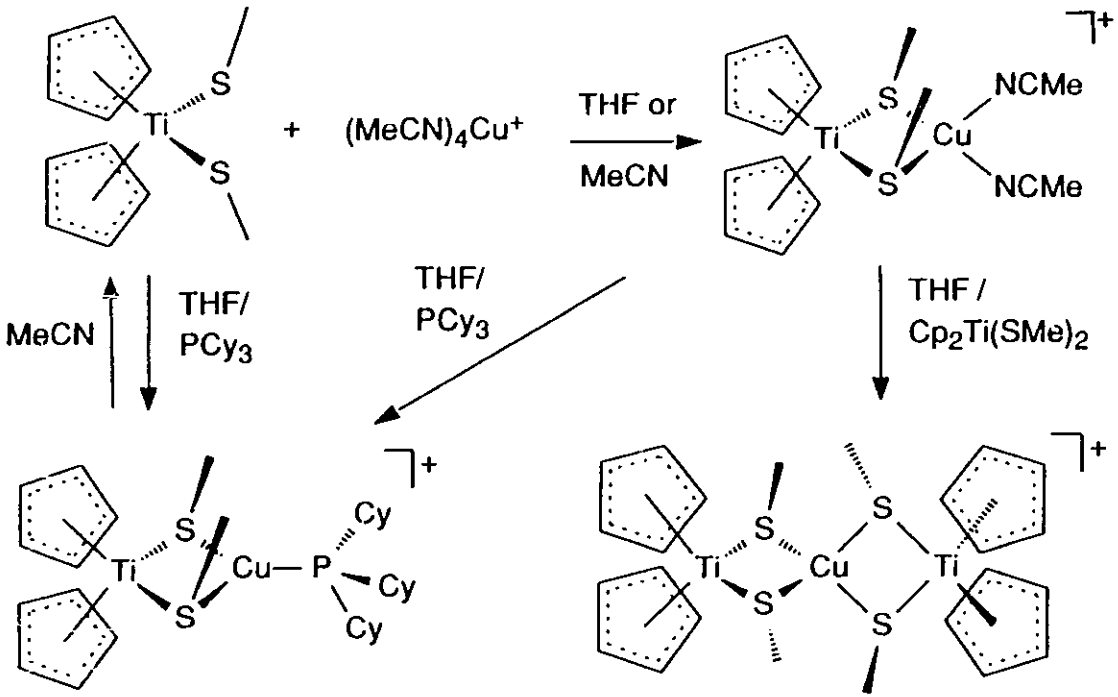

Scheme 3.1: Reaction Scheme for Preparation of 11-14 and Substitution Reactions

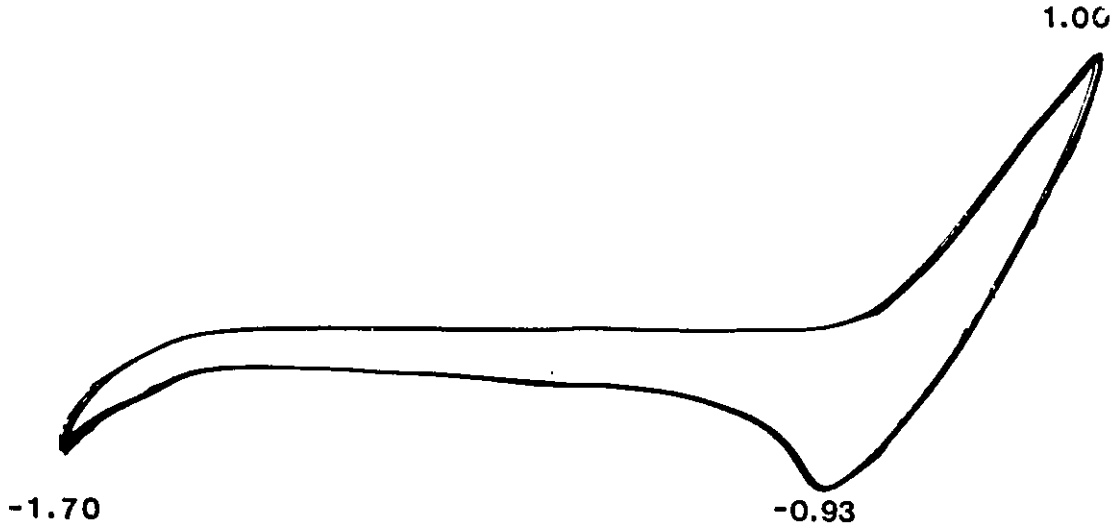

Figure 3.6: Cyclic Voltammogram of $Cp_2Ti(SMe)_2$; potentials in mV vs. Ag/AgCl

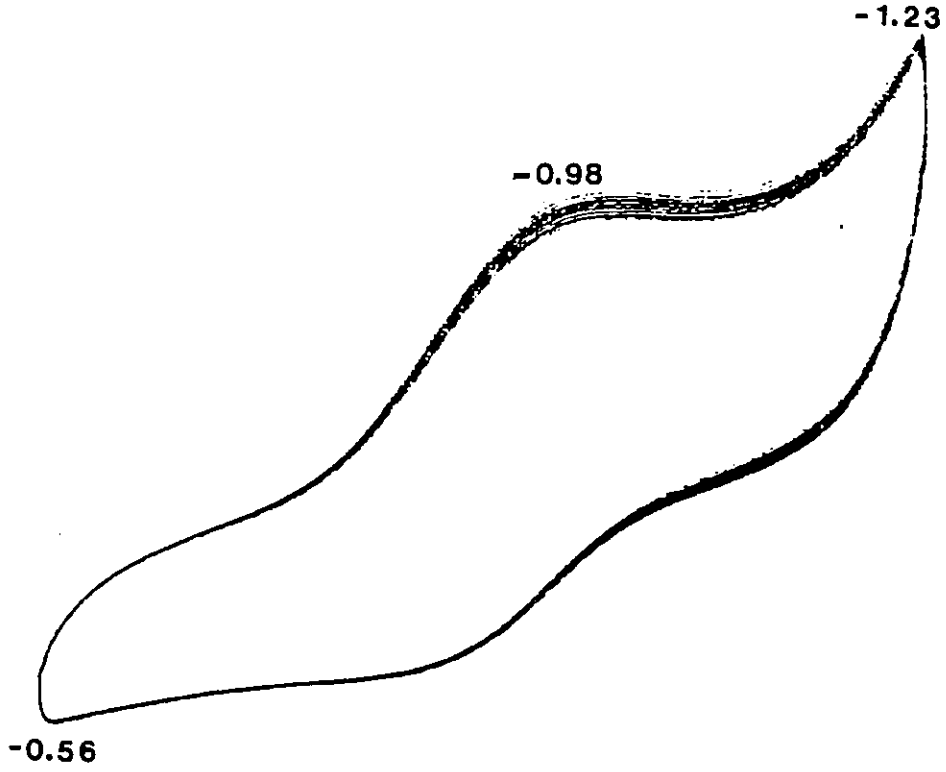

Figure 3.7: Cyclic Voltammogram of $[Cp_2Ti(\mu\text{-}SMe)_2Cu(NCMe)_2]PF_6$; potentials in mV vs. Ag/AgCl

molecules is 2.876 Å (S...H5). The symmetry of the unit cell demands that the metal atom of **10** sits on a crystallographically imposed two fold axis of symmetry. The coordination sphere of Ti is comprised of two π-bonded cyclopentadienyl rings and two methanethiolate moieties. Thus, the molecular geometry about the metal centre is best described as pseudo-tetrahedral with strict C_2 symmetry. A similar result was reported by other workers.[125] The imposed symmetry requires that the two cyclopentadienyl rings are exactly eclipsed. This is in contrast to that seen for $Cp_2M(SPh)_2$ (M = Ti, V) where the rings are rotated by 15.5° with respect to one another.[126] An ORTEP drawing of the molecule is shown in Figure 3.8 with the important structural details indicated. The accessibility of the eclipsed conformation in **10** may reflect the lesser steric demands of the methanethiolate substituents versus those of the phenylthiolate ligands.

The Ti-S distances in **10** are shorter than those seen in the related complexes $Cp_2Ti(SPh)_2$ (2.4395(8) Å),[126] $Cp_2^*Ti(SH)_2$ (2.409(2) Å and 2.418(3) Å),[127] and $Cp_2Ti(S_2PCy_2)$ (2.420(3) Å and 2.427(3) Å).[128] The angle at titanium is 93.7° which is smaller than the corresponding angle seen in $Cp_2Ti(SPh)_2$.[126] This difference reflects the smaller steric demands of the methanethiolate as compared to the phenylthiolate.

X-ray quality crystals of **12** were obtained by anaerobic diffusion of diethyl ether into an acetonitrile solution of **12**. A crystallographic study showed the complex to be made up of monoclinic unit cells containing discrete anions and cations. The closest approach between these ions is 2.511 Å (H4-F2). The cation of **12** is depicted in the ORTEP drawing in Figure 3.9. The pseudo-tetrahedral coordination sphere of Ti is comprised of two π-bonded cyclopentadienyl rings and two methanethiolate moieties, similar to complexes **3** and **4**. Copper is pseudo-tetrahedral with a coordination sphere consisting of the two sulfurs of the metalloligand and two acetonitriles. As was proposed on the basis of variable temperature NMR data, the alkyl substituents are in a cis disposition. Details of the TiS_2CuN_2 core are given in Figure 3.10. Typical bond lengths are found for the Ti-S and Cu-S bonds, as well as, the Ti-C bonds. Angles at the bridging

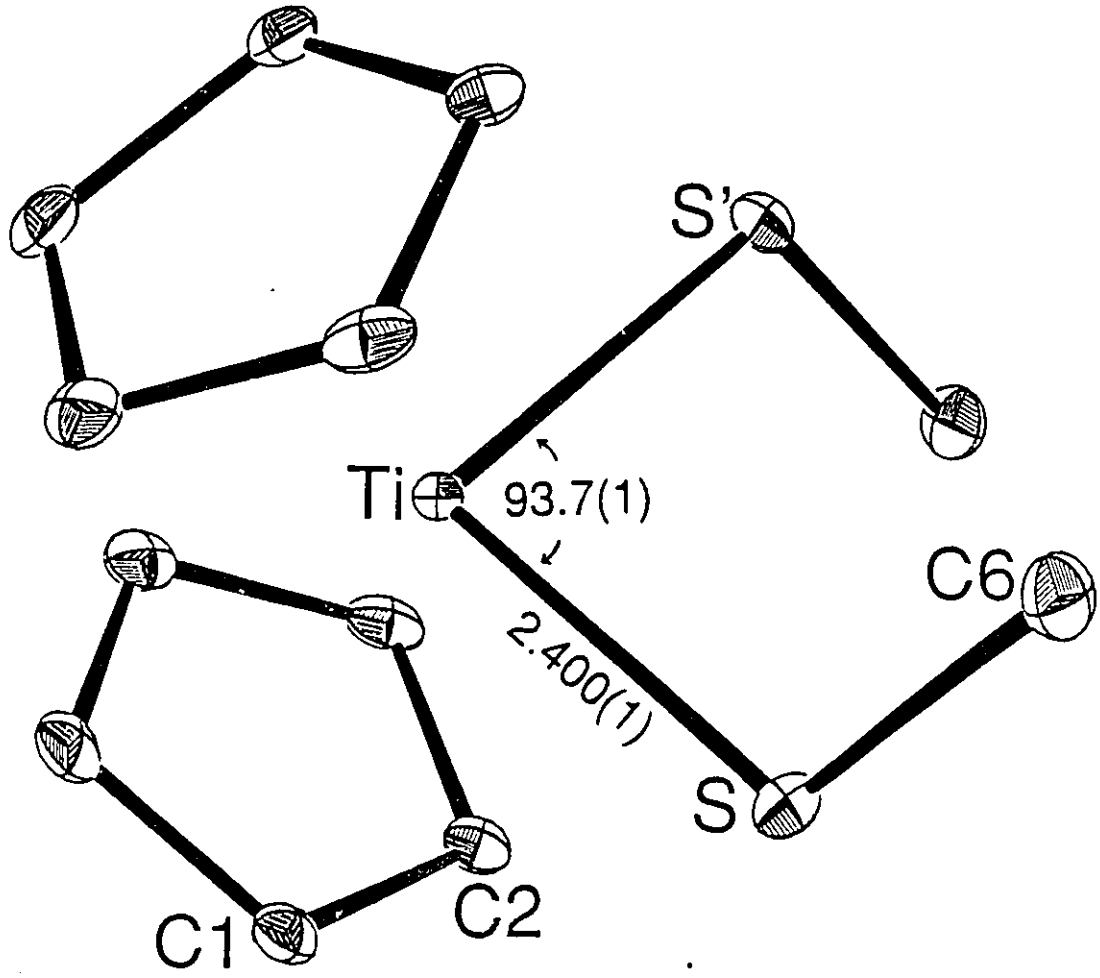

Figure 3.8: ORTEP Drawing of $Cp_2Ti(SMe)_2$; 20% thermal ellipsoids are shown, hydrogen atoms are omitted for clarity; distances in Å, angles in degrees

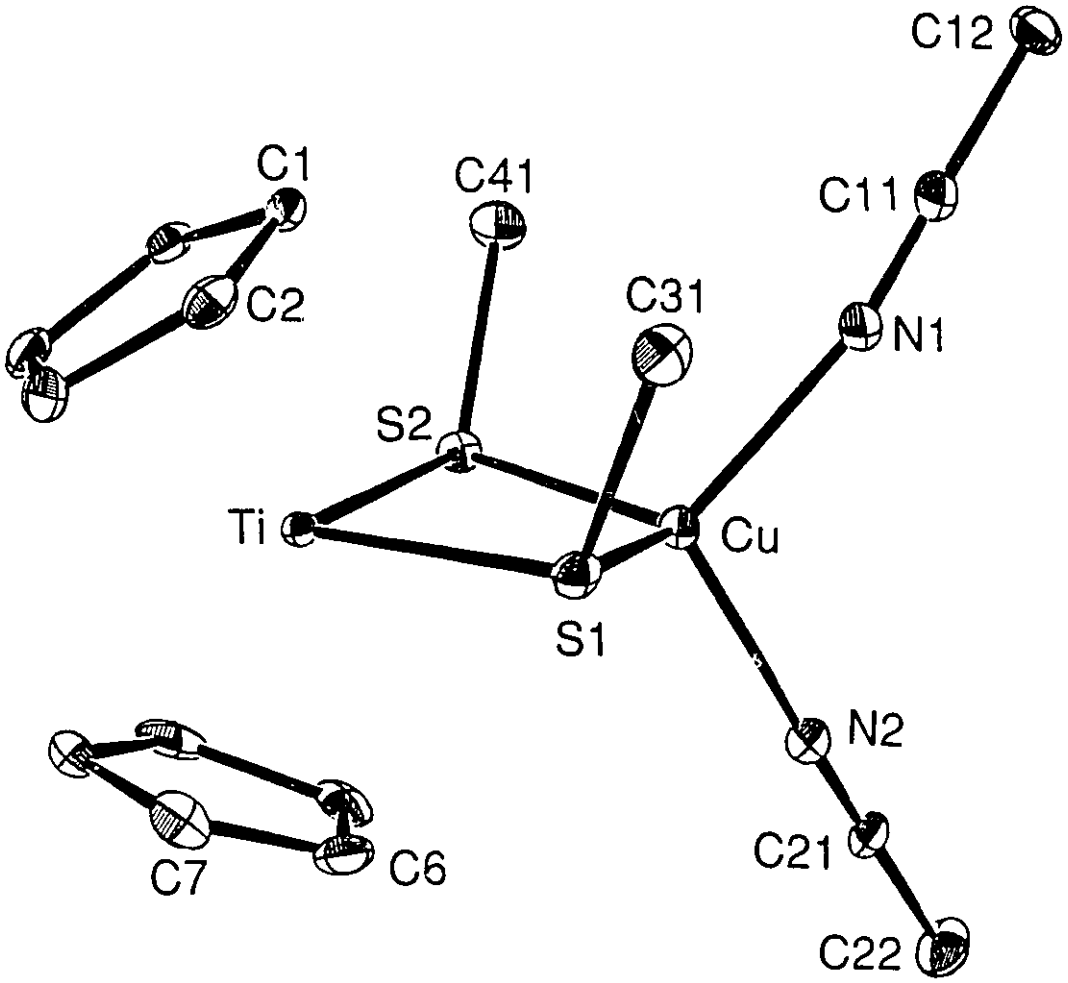

Figure 3.9: ORTEP Drawing of the Cation of $Cp_2Ti(\mu\text{-}SMe)_2Cu(NCMe)_2]PF_6$; 20% thermal ellipsoids are shown

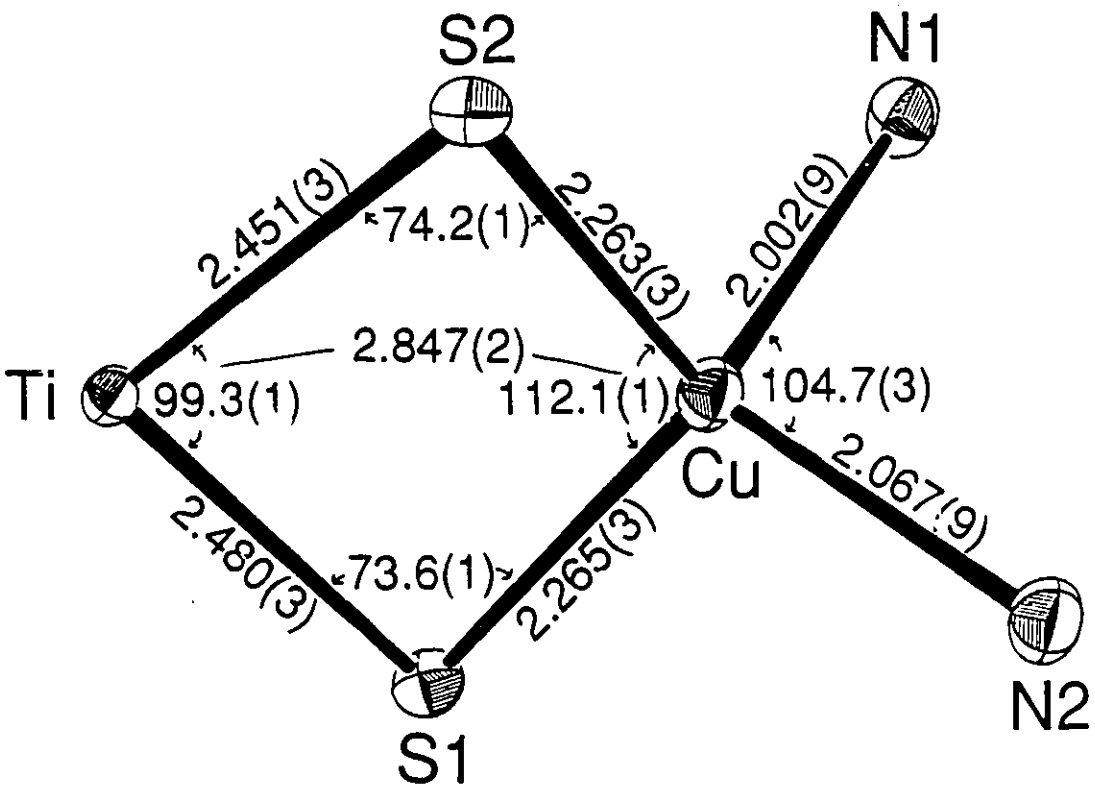

Figure 3.10: ORTEP Drawing of the TiS_2CuN_2 Core of the Cation of $Cp_2Ti(\mu\text{-}SMe)_2Cu(NCMe)_2]PF_6$; distances in Å, angles in degrees

sulfur atoms are 74.2° and 73.6° with an S1-Ti-S2 angle of 99.3° and an S1-Cu-S2 angle of 112.1°. These angles are similar to those found in complexes **3** and **4**, again suggesting a metal-metal interaction. The sulfur angles in **12** are 4° smaller than the corresponding angles in $[Cp_2Ti(\mu\text{-}SCH_2CH_2PPh_2)_2Cu]^+$, while the angles at the metals in **12** are greater than the analogous angles in the chelated complex. The S1-Ti-S2 angle in **12** is 5° greater in the bimetallic complex than in the metalloligand **10**. This suggests that opening of the angle at titanium facilitates interaction between the metals. As seen in related, four-atom core species, the TiS_2Cu core is puckered, with an angle of 11° between the S1-Cu-S2 and the S1-Ti-S2 planes. The distance between the metals is 2.847 Å which is similar to the M-M' separation seen in **3** and **4**, but less than the 3.024 Å separation found in the chelated phosphinoethanethiolate Ti/Cu complex.

3.4 Summary

Three- and four-coordinate Ti/Cu complexes using the metalloligands $Cp_2Ti(SMe)_2$ and $Cp_2Ti(SEt)_2$ have been prepared successfully. The methanethiolate species can be employed to synthesize bimetallic species analogous to **3** and **4**. Both of the titanium metalloligands give Ti/Cu complexes in which the copper is in a tetrahedral environment bound to two acetonitriles. Also, $Cp_2Ti(SMe)_2$ can be used to prepare a trimetallic complex containing two metalloligands bound to one central copper atom. The steric requirements of the methane- and ethanethiolate ligands appear to be similar based on the preparation of analogous complexes.

In addition to the steric bulk of the trisubstituted phosphines, the basicity is a consideration when choosing an ancillary ligand. Trimethylphosphine is very basic and does not give a heterobimetallic species with a four-coordinate copper centre. The equilibrium for the reaction lies to the side of the copper-phosphine complex. This equilibrium is also seen for **11** in the presence of acetonitrile, since this species decomposes to a Cu-P complex, free phosphine and the starting metalloligand.

Acetonitrile is less basic than PMe_3 and has small steric requirements, therefore it is a good ancillary ligand to employ in order to prepare compounds containing tetrahedral copper.

The trigonal copper complexes **3** and **4** have similar structural features compared to the tetrahedral species **12**. In particular, the approach of the Ti and Cu centres is independent of the geometry at copper. The S-Ti-S angles in **12** are opened up compared to the metalloligand **10** and related Cp_2TiS_2 species. Also, the angles at sulfur in **12** are less than 80°. These structural features are consistent with a metal-metal interaction assigned as $d^{10} \cdot d^0$ dative donation of electron density. This type of communication may be similar to that seen for systems exhibiting SMSI.

CHAPTER FOUR

USE OF $Cp_2V(SMe)_2$ AND $Cp_2V(SEt)_2$ AS METALLOLIGANDS FOR THE PREPARATION OF PARAMAGNETIC, HETEROBIMETALLIC, THREE- AND FOUR-COORDINATE COPPER COMPLEXES

4.1 Introduction

In systems exhibiting SMSI there is evidence for Ti(III) centres. The Ti(IV)/Cu(I) complexes reported in the previous chapter; however, do not undergo reversible, electrochemical reduction to give stable Ti(III) species. In order to model the reduced oxidation state, the synthetic method developed for the preparation of the Ti(IV)/Cu(I) complexes has been applied to synthesize V(IV)/Cu(I) species. These complexes, prepared using the metalloligands $Cp_2V(SMe)_2$ and $Cp_2V(SEt)_2$, are analogous to complexes **3**, **4**, and **11-13** and contain a d^1 centre which is isoelectronic with Ti(III).

The vanadium species $Cp_2V(SMe)_2$ has been prepared and studied by X-ray crystallography. Using the methane- and ethanethiolate metalloligands vanadium(IV)/copper(I) compounds have been prepared. These complexes are paramagnetic, and thus EPR spectroscopy becomes useful for characterization of the bimetallic complexes. The hyperfine coupling seen in the EPR spectra provides insight into the electronic communication which may occur between the constituent metals.

4.2 Experimental Section

All preparations were done under an atmosphere of dry, O_2-free N_2. Solvents were reagent grade, distilled from the appropriate drying agents under N_2, and degassed by the freeze-thaw method at least three times prior to use. EPR experiments were performed on a Varian E-12 Spectrometer using DPPH as the reference. Cyclic voltammetry experiments were performed using a BAS CV-27 electrochemistry unit with a platinum

working electrode and a Ag/AgCl reference electrode. PPh_3 was purchased from the Aldrich Chemical Co. and Cp_2VCl_2 and PCy_3 were purchased from the Strem Chemical Co. $[(MeCN)_4Cu]PF_6$ was prepared by the literature method,[120] and the preparations of NaSEt and NaSMe were described in Chapters Two and Three, respectively.

(i) Preparation of $Cp_2V(SMe)_2$ (15) To Cp_2VCl_2 (300 mg, 1.2 mmoles) in 30 mL THF was added NaSMe (167 mg, 2.4 mmoles) and the mixture stirred for 4 h. Activated neutral alumina was added, the mixture stirred for 10 min and then filtered. The alumina was washed with 5 x 20 mL portions of THF which were combined with the mother liquor. The volume of the resulting THF solution was reduced to 10 mL and pentane added to precipitate a dark, blue-black microcrystalline solid. (Yield: 200 mg, 61%). EPR (THF): g = 1.997, $a<^{51}V>$ = 58.75 G.

(ii) Preparation of $Cp_2V(SEt)_2$ (16) This compound was prepared in a manner analogous to that described for the corresponding methyl species, using Cp_2VCl_2 (300 mg, 1.2 mmoles) and NaSEt (202 mg, 2.4 mmoles). The product is a microcrystalline, dark green-black solid. (Yield: 235 mg, 70%). EPR (THF): g = 1.994, $a<^{51}V>$ = 57.5 G.

(iii) Preparation of $[Cp_2V(\mu\text{-}SEt)_2CuPPh_3]PF_6$ (17) To a 30 mL THF suspension of $[(MeCN)_4Cu]PF_6$ (123 mg, 0.33 mmoles) was added PPh_3 (173 mg, 0.66 mmoles) and the mixture stirred for 5 min. To the clear, colourless solution was added dropwise a green-black THF solution of $Cp_2V(SEt)_2$ (100 mg, 0.33 mmoles), which resulted in an immediate colour change to dark brown. The solution was stirred for 20 min and the volume then reduced to 5 mL. The product was precipitated by addition of n-hexane and isolated by filtration. The brown microcrystalline product was washed with 2 x 10 mL portions of pentane and dried in vacuo. (Yield: 153 mg, 60%). EPR (THF): g = 1.998, $a<^{51}V>$ = 58.9.

(iv) Preparation of $[Cp_2V(\mu\text{-}SEt)_2CuPCy_3]PF_6$ (18) These complexes were prepared in a manner similar to that described for **18**, using PCy_3 (185 mg, 0.66 mmoles) instead of PPh_3. (Yield: 170 g, 65%). EPR (THF): g = 2.001, $a<^{51}V>$ = 60.0 G.

(v) Preparation of $[Cp_2V(\mu\text{-}SR)_2Cu(NCMe)_2]PF_6$ (R = Me (19); R = Et (20)) To $[(MeCN)_4Cu]PF_6$ (136 mg, 0.36 mmoles) in 20 mL MeCN was added dropwise $Cp_2V(SMe)_2$ (100 mg, 0.36 mmoles) or $Cp_2V(SEt)_2$ (100 mg, 0.33 mmoles) in 10 mL of MeCN which resulted in a colour change from blue-black to brown. After the mixture was stirred for 10 min, a brown solid was precipitated with pentane and collected by filtration. The solid was washed with 2 x 20 mL portions of pentane and dried in vacuo. **19:** (Yield: 106 mg, 57 %). EPR (THF): g = 1.996, $a<^{51}V>$ = 67.5 G. **20:** (Yield: 97 mg, 50%). EPR (THF): g = 1.999, $a<^{51}V>$ = 60.0 G

(vi) X-ray Data Collection and Reduction Diffraction experiments were performed on a four-circle Syntex $P2_1$ diffractometer with graphite-monochromatized Mo Kα radiation (λ = 0.71069 Å). The initial orientation matrix was obtained from 15 machine-centred reflections selected from a rotation photograph. These data were used to determine the crystal system. Partial rotation photographs around each axis were consistent with a tetragonal crystal system for **15**. The final lattice parameters and the orientation matrix were determined from 64 high angle data ($20°<2\theta<25°$). The observed extinctions were consistent with the space group $P4_12_12$. $+h,+k,+l$ data were collected ($4.5°<2\theta<45.0°$) with three standard reflections recorded every 197 reflections. Their intensities showed no statistically significant change over the duration of the data collection. The data were processed using the SHELX-76 program package.

(vii) Structure Solution and Refinement Non-hydrogen atomic scattering factors were

taken from the literature tabulations.[121-123] The heavy atom position was determined using direct methods. The remaining non-hydrogen atoms were located from successive difference Fourier map calculations. The refinement was carried out by using full-matrix, least squares techniques on F, minimizing the function $w(|Fo|-|Fc|)^2$ where the weight, w, is defined as $4Fo^2/2\sigma(Fo^2)$ and Fo and Fc are the observed and calculated structure factor amplitudes. In the final cycles of refinement, all the non-hydrogen atoms were assigned anisotropic temperature factors. Hydrogen atom positions were calculated and allowed to ride on the carbon to which they are bonded assuming a C-H bond length of 0.95 Å. Hydrogen atom temperature factors were fixed at 1.10 times the isotropic temperature factor of the carbon atom to which they are bonded. The hydrogen atom contributions were calculated, but not refined. The residual electron densities were of no chemical significance. Crystal data and data collection parameters are summarized in Table 4.1. Tables of Positional Parameters (Table 4.2) and Selected Bond Distances and Angles (Table 4.3) are reported in this chapter, and Thermal Parameters (Table A1.1) and Hydrogen Atom Parameters (Table A1.2) appear in Appendix One.

4.3 Results and Discussion

The vanadium complexes $Cp_2V(SMe)_2$ (**15**) and $Cp_2V(SEt)_2$ (**16**) were prepared by reaction of vanadocene dichloride with two equivalents of the appropriate thiolate sodium salt. Treatment of the reaction mixtures with alumina and subsequent isolation lead to microcrystalline, blue-black **15** and green-black **16** in ca. 65% yield. In similar reactions of Cp_2VCl_2 with HSPh and NEt_3, reduction of V(IV) to V(III) resulted in the formation of $Cp_2V_2(\mu\text{-}SPh)_4$.[126] Some degree of reduction in the present reactions may account for the comparatively low yields relative to those obtained for $Cp_2Ti(SMe)_2$ and $Cp_2Ti(SEt)_2$. Furthermore, it may also explain the observed sensitivity of yields to variations in scale, concentration and duration of reaction.

The formulation of **15** and **16** as V(IV) species is substantiated by the EPR spectra

Table 4.1: Crystallographic Parameters for $Cp_2V(SMe)_2$

	15
Formula	$C_{12}H_{16}S_2V$
Crystal colour, form	brown blocks
Crystal system	tetragonal
a (Å)	9.276(4)
c (Å)	14.164(4)
Space group	$P4_12_12$
Volume (Å^3)	1218(1)
Density (gcm^{-3}) calcd	1.50
Z	4
Crystal dimens (mm)	0.46 x 0.27 x 0.31
Abs coeff, μ (cm^{-1})	10.46
Radiation, λ (Å)	Mo Kα (0.71069)
Temperature (°C)	24
Scan speed (deg/min)	2.0-5.0(θ/2θ scan)
Scan range (deg)	1.0 below Kα1
	1.0 above Kα2
Bkgd/scan time ratio	0.5
Data collected	957
No. of unique data	
$Fo^2>3\sigma(Fo^2)$	742
No. of variables	68
R (%)	3.66
Rw (%)	4.39
Largest Δ/σ in the final	

least squares cycle	0.003
Maximum residual electron density ($e/Å^3$)	0.37
Atom associated	V, S

Table 4.2: Positional Parameters for $Cp_2V(SMe)_2$[1]

$Cp_2V(SMe)_2$ (15)

Atom	x	y	z	Atom	x	y	z
V	-431(1)	-431(1)	10000	S	1709(1)	91(1)	9056(1)
C1	-1339(6)	-596(6)	8499(3)	C2	-1323(5)	8812(5)	8752(3)
C3	-2280(5)	1083(6)	9507(3)	C4	-2859(5)	-200(7)	9752(3)
C5	-2324(5)	-1283(6)	9130(3)	C6	3275(5)	284(6)	9810(4)

[1]Positions multiplied by 10^4

Table 4.3: Selected Bond Distances and Angles for $Cp_2V(SMe)_2$

$Cp_2V(SMe)_2$ (15)

Distances (Å)

V-S	2.442(1)	V-C1	2.292(4)	V-C2	2.300(4)
V-C3	2.324(4)	V-C4	2.289(5)	V-C5	2.286(5)
S-C6	1.811(5)	C1-C2	1.416(7)	C2-C3	1.403(6)
C3-C4	1.351(8)	C4-C5	1.426(7)	C1-C5	1.428(7)

Angles (Degrees)

S-V-S'	88.7(1)	C6-S-V	110.4(2)	Cp-V-Cp'	130.2(1)

which show eight line patterns, resulting from coupling of an unpaired electron to a ^{51}V nucleus (I = 7/2, natural abundance 100 %). The observed line widths for THF and benzene solutions of **15** are 5 G and 20 G at half height, respectively. The EPR spectrum of vanadocene dichloride appears in Figure 4.1 for comparison to the EPR spectrum for $Cp_2V(SEt)_2$ which is in Figure 4.2. Line-width variations have been attributed to anisotropy in hyperfine interactions arising from inhibited molecular tumbling caused by solute-solvent interactions.[126] The present observations imply that solute-solvent interactions occur to a much lesser extent for THF solutions of compound **15**, than for benzene solutions. Similar interactions with solvent have been described for $Cp_2V(SPh)_2$ in benzene. Treatment of the data by standard methods gives an isotropic <a> value of 58.85 G and a *g* value of 1.997 determined directly from the spectrum for **15**, while for **16**, the <a> value is 57.5 G and the *g* value is 1.994 G. These data are similar to those reported for other species of the form Cp_2VL_2.[126,129]

An X-ray structural study for **15** showed the compound to be isostructural with **10**. The crystals consist of tetragonal unit cells, each with four discrete formula units. The closest approach between these molecules is 2.629 Å (H6A...H2). As with the analogous titanium species, the coordination sphere of the V is comprised of two π-bonded cyclopentadienyl rings and two methanethiolate moieties. Again, the imposed symmetry requires that the two cyclopentadienyl rings are exactly eclipsed. An ORTEP drawing of molecule **15** appears in Figure 4.3 with the relevant structural details included.

The average M-C distances in **15** (2.298 Å) are similar to those seen in the related $Cp_2V(IV)$ complexes,[126,129,130] while the V-S distances of 2.442(1) Å in **15** are shorter than those seen in $Cp_2V(SPh)_2$ (2.448(3), 2.470(2) Å).[126] These differences may be attributed to the basicity and small steric demands of the methanethiolato ligand.

The S-M-S angles in **10** (93.7(1)°) and **15** (88.7(1)°) are significantly smaller than those seen in the related complexes $Cp_2M(SPh)_2$ (M = Ti, 99.3(1)°; V, 94.1(1)°), reflecting the lesser steric demands of the methanethiolato ligand. The differences in

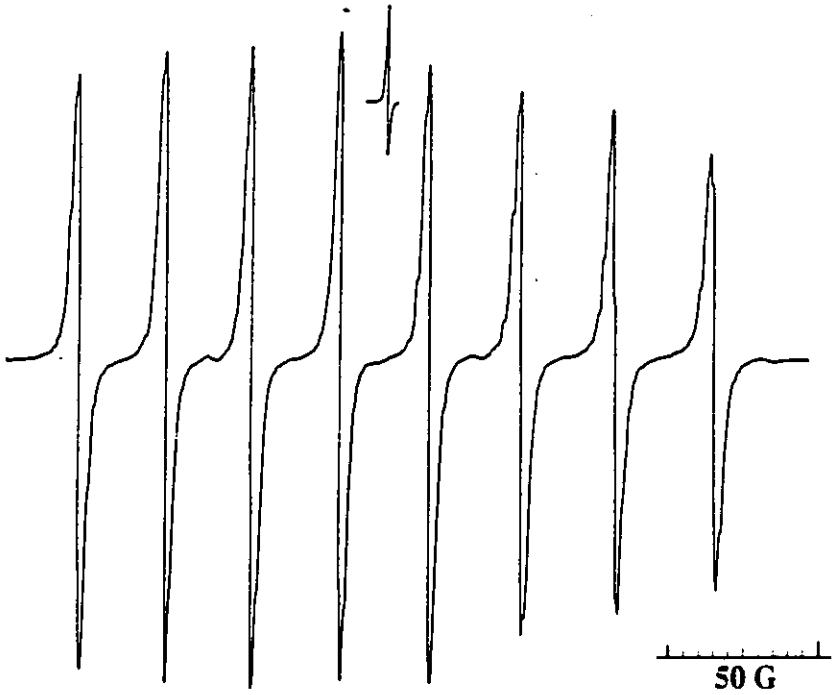

Figure 4.1: EPR Spectrum of Cp_2VCl_2

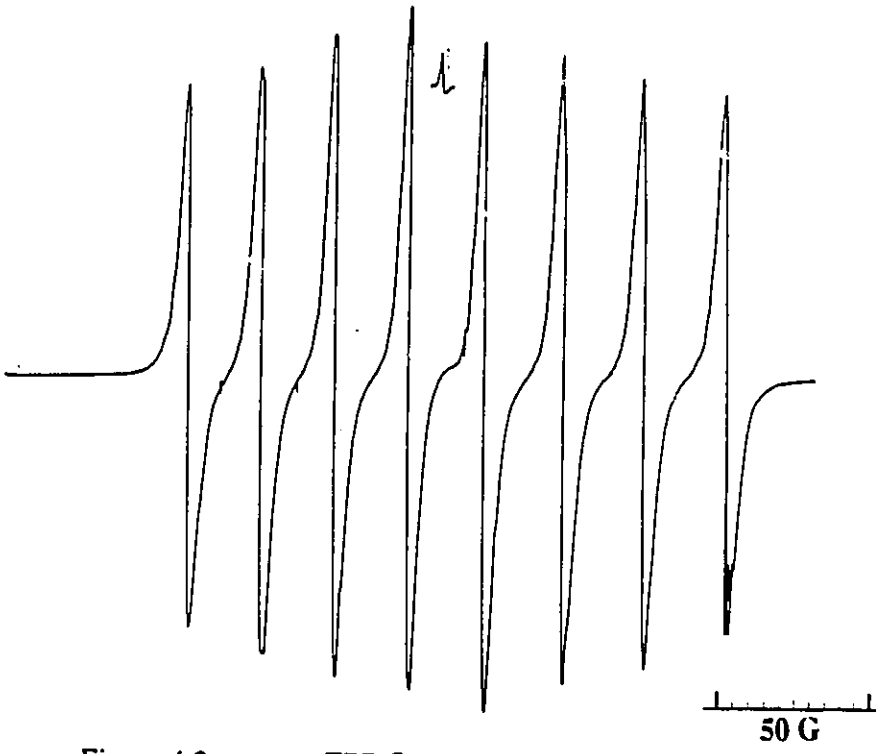

Figure 4.2: EPR Spectrum of $Cp_2V(SEt)_2$

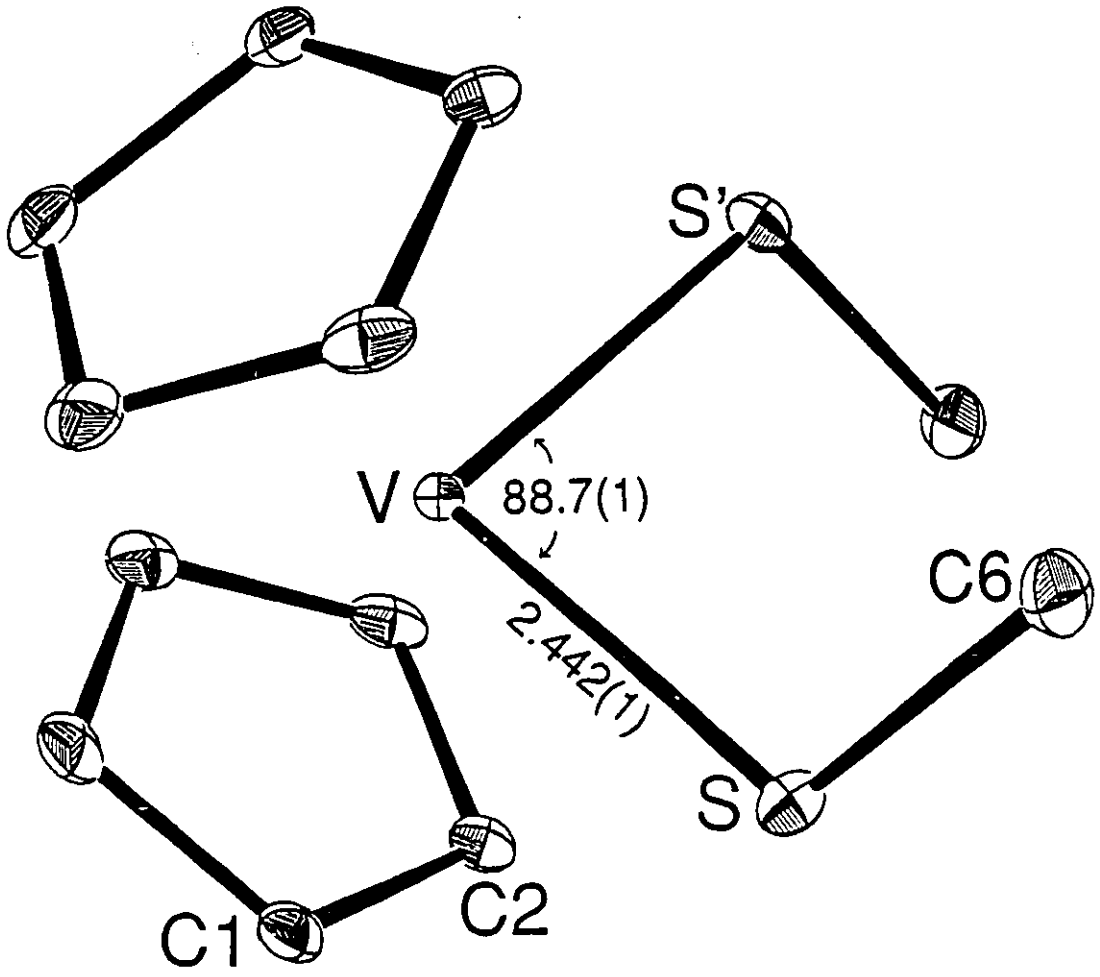

Figure 4.3: ORTEP Drawing of $Cp_2V(SMe)_2$; 20% thermal ellipsoids are shown, hydrogen atoms are omitted for clarity; distances in Å, angles in degrees

geometry of the d^0 Ti species and the d^1 V complex are consistent with predictions from Extended Hückel calculations,[131] as well as, the results of single crystal EPR studies.[129] Such work has shown that the single unpaired electron of d^1 complexes occupies the molecular orbital derived from the $1a_1$ frontier orbital of Cp_2M fragment. For the present complexes such an orbital lies in the MS_2 plane, perpendicular to the vector that bisects the S-M-S angle. Population of this non-bonding orbital by a single unpaired electron in d^1 complexes, results in electrostatic repulsions which decrease the S-M-S angle. Employing Extended Hückel methods, calculations were performed in which S-M-S angles of the model systems $Cp_2M(SH)_2$ (M = Ti, V) were optimized based on the minimization of the total energy. Analogous calculations described by Lauher and Hoffman[131] for Cp_2MH_2 show similar, but less distinct potential wells. The S-M-S angle values at minimum energy were found to be 93.5° and 87° for the Ti and V models, respectively. Interestingly, the S-M-S found in **10** and **15** approach these predicted values for the $Cp_2M(SH)_2$ models. This further suggests that the larger S-M-S angles seen for the complexes $Cp_2M(SPh)_2$ (M = Ti, V) are a result of steric demands of the substituents. Extended Hückel calculations also suggest that for Cp_2ML_2 systems, the better the π acceptor ability of the ligand, the greater the bending of the Cp_2M fragment and, thus, the smaller the Cp-M-Cp'angle. This is consistent with the present observations as the Cp-M-Cp' angles (i.e., the angle between the vectors joining the M and the centroids of the Cp rings) were found to be 127.0(1)° and 130.2(1)° for **10** and **15**, respectively; significantly smaller than the corresponding angles found in $Cp_2M(SPh)_2$ (M = Ti 132.4°, V 134.6°).[126]

Complex **15** showed only irreversible waves at -0.95 V and +0.75 V vs Ag/AgCl (Figure 4.4). Although it is uncertain, these features may arise from V(IV)-V(III) and V(IV)-V(V) redox chemistry. This is in contrast to the reversible behaviour seen for the related species $Cp_2Nb(SPh)_2$ which shows two, one-electron reductions, corresponding to sequential reduction of Nb(V) to Nb(IV) and Nb(III).[117]

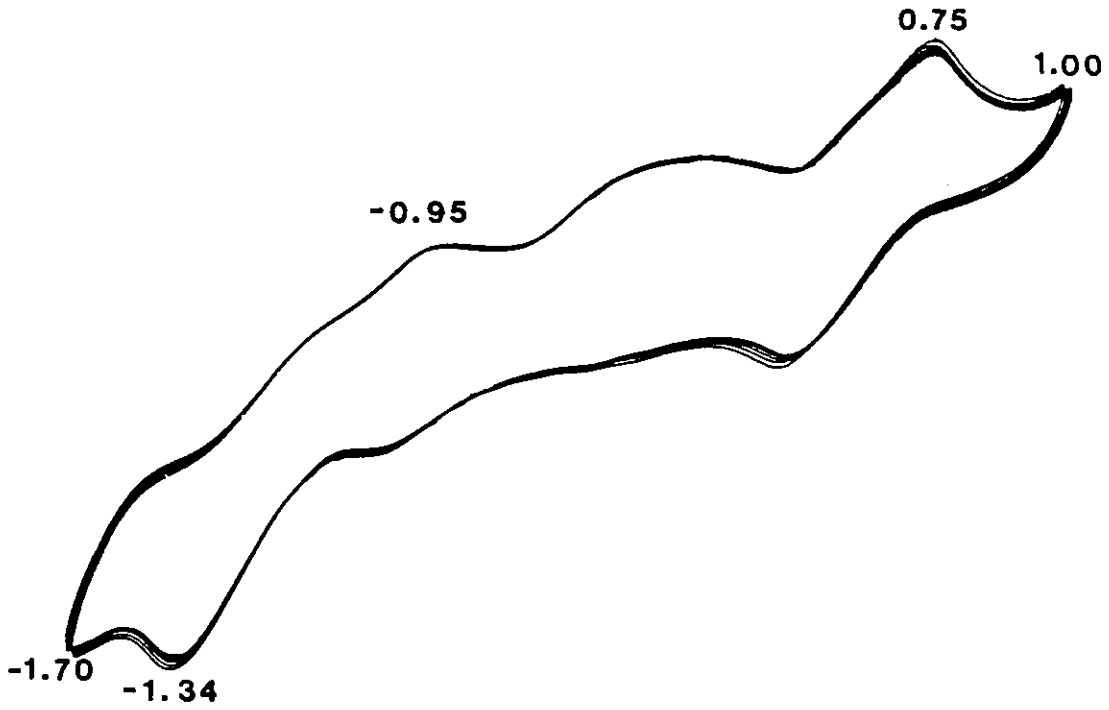

Figure 4.4: Cyclic Voltammogram of $Cp_2V(SMe)_2$; potentials in mV vs. Ag/AgCl

Bimetallic complexes containing three-coordinate copper were prepared by

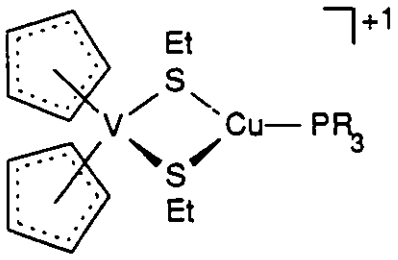

Figure 4.5: Schematic Drawing of the Cation of $[Cp_2V(\mu\text{-}SR)_2CuPR_3]PF_6$

addition of the metalloligand to a solution containing $[(MeCN)_4Cu]PF_6$ and a trisubstituted phosphine. Upon addition of a green THF solution of $Cp_2V(SEt)_2$ to a solution of Cu(I) and PPh_3 or PCy_3, the reaction mixtures changed from clear and colourless to brown. The heterobimetallic complexes were isolated by filtration after adding pentane to precipitate the products. The structures were expected to be similar to those found for the titanium/copper species **3**, **4**, and **11**, as depicted in Figure 4.5.

The V/Cu complexes containing coordinated phosphine, **17** and **18**, were studied by EPR spectroscopy. The spectra each show the expected eight line pattern due to coupling of the unpaired electron to the vanadium nucleus with additional hyperfine coupling. The EPR spectrum for $[Cp_2V(\mu\text{-}SEt)_2CuPCy_3]PF_6$ is shown in Figure 4.6. From computer simulation (Figure 4.7), the hyperfine coupling was determined to be due to coupling of the electron on vanadium to a copper atom with a value of 9.5 G and to one phosphorus centre with a value of 8 G. The magnitudes of these couplings are consistent with those determined for other four-atom core, bimetallic complexes in which cross-ring interaction has been proposed. For example, the EPR spectrum of the Ti(III) species $[Cp_2Ti(\mu\text{-}SCH_2CH_2CH_2PPh_2)_2Rh]^\circ$ shows coupling to rhodium of 1.8 G and to two equivalent phosphorus atoms of 2.8 G.[113] Transannular interaction has been supported by theoretical calculations performed by Lorenz and Wasson.[132] They found that in four-atom core species of the type $Cp_2VS_2PR_2$ (R = alkyl), the coupling observed in the

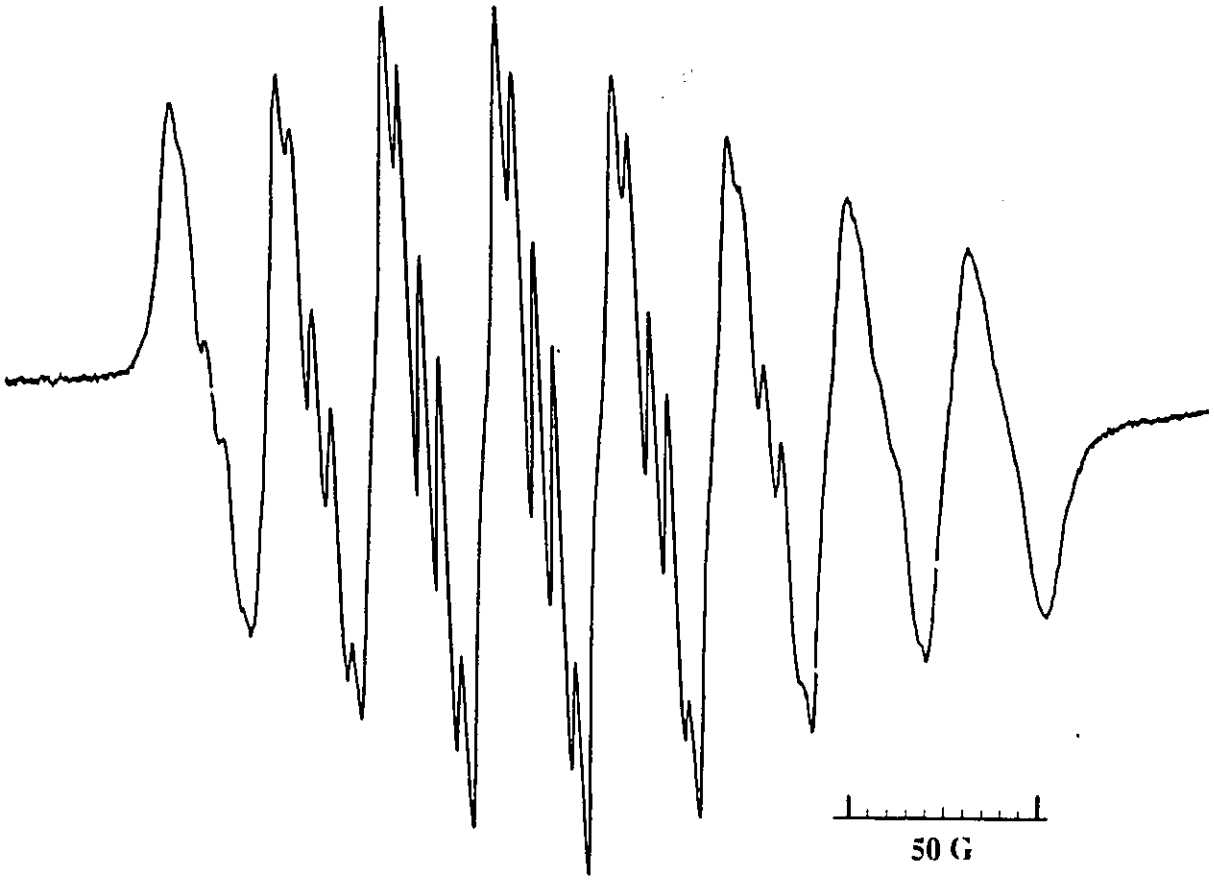

Figure 4.6: EPR Spectrum of $[Cp_2V(\mu\text{-}SEt)_2CuPCy_3]PF_6$

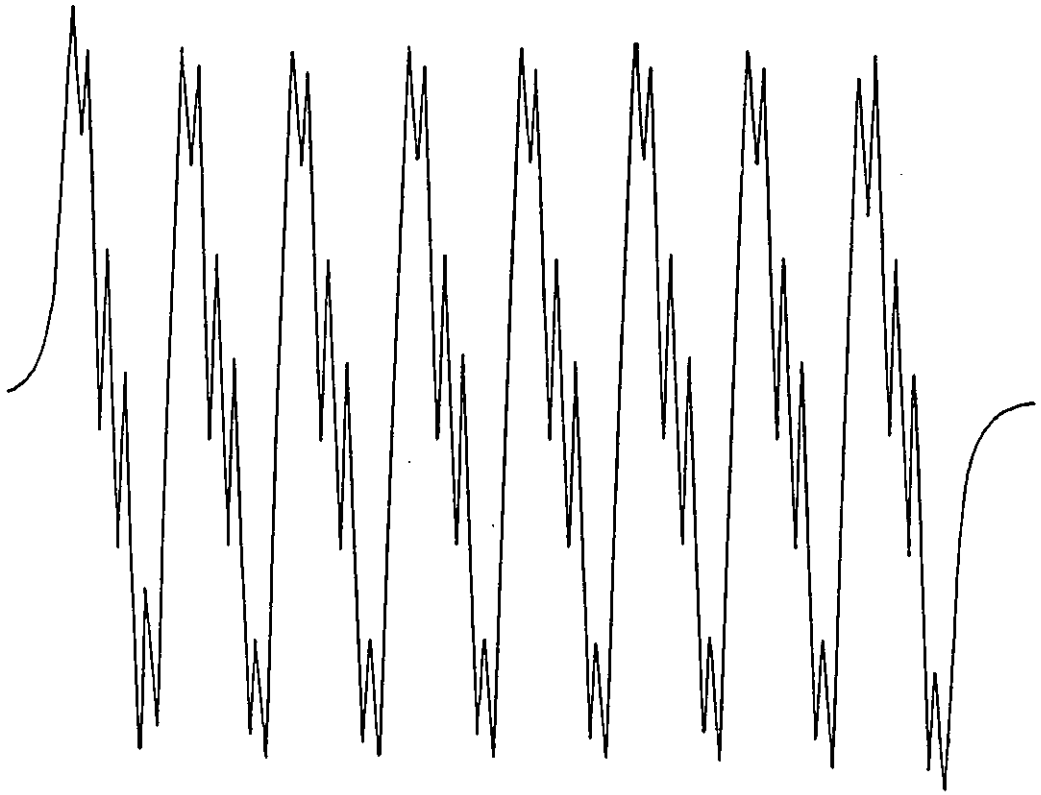

Figure 4.7: Computer Simulation of the EPR Spectrum of $[Cp_2V(\mu\text{-}SEt)_2CuPCy_3]PF_6$

EPR spectra is a result of direct interaction between the metal 3d orbital and the phosphorus 3s orbital. These results were found to be general for any d^1 species possessing C_{2v} symmetry. This type of interaction may explain the coupling seen in the EPR spectra of the Cp_2VS_2CuP complexes **17** and **18**.

Four-coordinate copper complexes (**19-20**) were prepared by the addition of the vanadium metalloligands to $[(MeCN)_4Cu]PF_6$ in MeCN. Isolation of these complexes was achieved by addition of hexane to cause precipitation, followed by filtration. The compounds were formulated as $[Cp_2V(\mu\text{-}SR)_2Cu(NCMe)_2]PF_6$, as seen in Figure 4.8, by

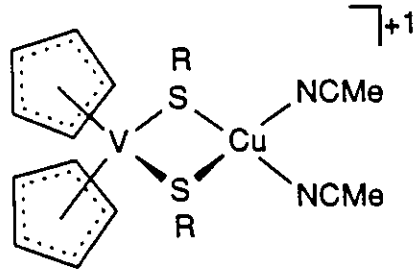

Figure 4.8: Schematic Drawing of the Cation of $[Cp_2V(\mu\text{-}SR)_2Cu(NCMe)_2]PF_6$

analogy to the Ti/Cu species. The EPR spectra of **19** and **20** each show eight line patterns, attributable to the electron on vanadium coupling to the vanadium nucleus. Unlike the phosphine complexes, the hyperfine coupling of the electron on vanadium to the other magnetic nuclei is not resolved. The line-width of the peaks is larger for complexes **19-20** compared to the metalloligands, possibly due to quadrupole broadening caused by the nitrogen centres.

4.4 Summary

Using vanadium methane- and ethanethiolate metalloligands, V(IV) complexes have been prepared which are isoelectronic to the reduced titanium centres existing in systems exhibiting SMSI. These three- and four-coordinate copper complex are analogous to the species prepared using $Cp_2Ti(SMe)_2$ and $Cp_2Ti(SEt)_2$. Also, comparison of the metalloligands $Cp_2Ti(SMe)_2$ and $Cp_2V(SMe)_2$ shows them to be isostructural. This

makes the V(IV) centre an appropriate model for the reduced titanium centre found in some heterogeneous catalytic systems.

The EPR spectra for **17** and **18** both show coupling between the unpaired electron on vanadium to the vanadium, copper and phosphorus centres. Based on the magnitude of the coupling found for these complexes compared to related systems and theoretical calculations, the interaction is assigned as transannular in nature. A similar cross-ring interaction is thought to occur for the tetrahedral copper species containing coordinated acetonitriles, although the coupling to copper and nitrogen could not be elucidated by computer simulation. The communication observed across the four-membered cores demonstrates that interaction between proximate metal centres occurs through space. In systems exhibiting SMSI, the metal of the support and the dispersed metal may interact in a similar fashion.

CHAPTER FIVE

USE OF THE METALLOLIGANDS $Cp_2Ti(SMe)_2$ AND $Cp_2V(SMe)_2$ FOR THE PREPARATION OF NICKEL COMPLEXES

5.1 Introduction

Heterobimetallic complexes containing copper and either titanium or vanadium have been prepared by utilizing thiolate metalloligands. In order to probe the generality of this synthetic approach to preparing mixed-metal species, the syntheses of complexes containing nickel and an early metal were attempted. Nickel was chosen as it is one of the metals used in heterogeneous catalysis for which SMSI have been seen. Use of a Ni(0) starting material, which is isoelectronic to Cu(I), allows investigation into the effect of charge on the late metal with respect to metal-metal separation.

The titanium metalloligand forms mixed-metal species when reacted with $(COD)_2Ni$, both in the presence and absence of tricyclohexylphosphine. These species were studied by NMR spectroscopy and one of the complexes by X-ray crystallography. Reaction of the vanadium metalloligand led, not to the expected bimetallic product, but to a nickel(II) hexamer which was characterized by X-ray crystallography.

5.2 Experimental Section

All preparations were done under an atmosphere of dry, O_2-free N_2 using either Schlenk line or dry-box techniques. Solvents were reagent grade, distilled from the appropriate drying agents under N_2 and degassed by the freeze-thaw method at least three times prior to use. ^1H NMR spectra were recorded on a Bruker AC-300 spectrometer operating at 300 MHz. Trace amounts of protonated solvents were used as a reference and chemical shifts are reported relative to $SiMe_4$. $^{31}P\{^1H\}$ NMR spectra were recorded using a Bruker AC-200 NMR spectrometer operating at 81 MHz and are reported using 85%

H_3PO_4 as an external reference. Cyclic voltammetric experiments were performed using a BAS CV-27 potentiostat, a platinum working electrode and a Ag/AgCl reference electrode. $[NEt_4]BPh_4$ was used as the supporting electrolyte. $(COD)_2Ni$ was purchased from the Strem Chemical Co. and PCy_3 was purchased from Pressure Chemical Co. The preparations of $Cp_2Ti(SMe)_2$ and $Cp_2V(SMe)_2$ were described in Chapters Three and Four, respectively.

(i) Preparation of $Cp_2Ti(\mu\text{-}SMe)_2NiPCy_3$ (21) To a 30 mL benzene solution of $(COD)_2Ni$ (100 mg, 0.36 mmoles) was added PCy_3 (205 mg, 0.72 mmoles). $Cp_2Ti(SMe)_2$ (100 mg, 0.36 mmoles) in benzene was added dropwise to the reaction flask with stirring. The purple mixture was stirred for 2 h, after which the solution was stripped to dryness. The resulting residue was dissolved in pentane and the solution filtered giving a purple-black solution and a gray solid. The pentane solution was stripped to dryness, giving a purple-black oil which solidified after being washed with diethyl ether. (Yield: 104 mg, 50%). ^1H NMR (d_6-benzene): δ, 5.28 (s, 10 H), 2.17-1.07 (br m, 39 H). $^{31}P\{^1H\}$ NMR (benzene): δ, 58.3 (s).

(ii) Preparation of $(Cp_2Ti(\mu\text{-}SMe)_2)_2Ni$ (22) To a 30 mL benzene solution of $Cp_2Ti(SMe)_2$ (100 mg, 0.36 mmoles) was added $(COD)_2Ni$ (50 mg, 0.18 mmoles) in benzene. After stirring for 3 h, there was a gradual colour change from red-purple to purple-black. The solvent was removed *in vacuo* and the residue washed with 2 x 10 mL pentane. The solid was isolated by filtration and washed with 2 x 10 mL portions of pentane. The black, microcrystalline product dried *in vacuo*. (Yield: 65 mg, 60%). ^1H NMR (d_6-benzene): δ, 5.37 (s, 5 H), 2.19 (s, 3 H).

(iii) Preparation of $(Ni(\mu\text{-}SMe)_2)_6$ (23) To a THF solution of $Cp_2V(SMe)_2$ (50 mg, 0.18 mmoles) was added dropwise a THF solution of $(COD)_2Ni$ (25 mg, 0.091 mmoles). Upon

addition of $(COD)_2Ni$, there was an instant colour change from green-black to brown. After stirring for 3 h, the solution volume was reduced to 5 mL and pentane added to precipitate a brown solid which was isolated by filtration and dried *in vacuo*.

(iv) **X-ray Data Collection and Reduction** Diffraction experiments were performed on a four-circle Syntex $P2_1$ diffractometer with graphite-monochromatized Mo Kα radiation ($\lambda = 0.71069$ Å). The initial orientation matrices for **22** and **23** were obtained from 15 machine-centred reflections selected from rotation photographs. These data were used to determine the crystal systems. Partial rotation photographs around each axis were consistent with a tetragonal crystal system for **22** and a monoclinic crystal system for **23**. Final lattice parameters and orientation matrices for **22** and **23** were determined from 64 and 45 high angle data ($20°<2\theta<25°$), respectively. The observed extinctions were consistent with the space group $I\bar{4}$ for **22** and $P2_1/n$ for **23**. $+h,+k,+l$ data were collected for **22** ($4.5°<2\theta<45.0°$), while for **23** ±h,+k,+l data were collected ($4.5°<2\theta<45.0°$). In each case, three standard reflections were recorded every 197 reflections. Their intensities showed no statistically significant change over the duration of the data collection. The data were processed using the SHELX-76 program package and an empirical absorption was applied to the data employing a locally modified version of ABSORB.

(v) **Structure Solutions and Refinements** Non-hydrogen atomic scattering factors were taken from the literature tabulations.[121-123] The heavy-atom positions for both structures were determined using direct methods. The remaining non-hydrogen atoms were located from successive difference Fourier map calculations. The refinements were carried out by using full-matrix least squares techniques on F, minimizing the function $w(|Fo|-|Fc|)^2$ where the weight, w, is defined as $4Fo^2/\sigma(Fo^2)$ and Fo and Fc are the observed and calculated structure factor amplitudes. In the final cycles of refinement all the non-hydrogen atoms were assigned anisotropic temperature factors. Hydrogen atom

positions were calculated and allowed to ride on the carbon to which they are bonded assuming a C-H bond length of 0.95 Å. Hydrogen atom temperature factors were fixed at 1.10 times the isotropic temperature factor of the carbon atom to which they are bonded. In all cases the hydrogen atom contributions were calculated, but not refined. The final values of *R* and *Rw* are given in Table 5.1. The maximum Δ/σ on any of the parameters in the final cycles of the refinement and the location of the largest peaks in the final difference Fourier map calculation are also given in Table 5.1. The residual electron densities were of no chemical significance. Machine parameters, crystal data, and data collection parameters are summarized in Table 5.1. Positional Parameters (Table 5.2) and Distances and Angles (Table 5.3) are tabulated in this chapter. Tables of Thermal Parameters (Table A1.1) and Hydrogen Atom Parameters (Table A1.2) appear in Appendix One.

5.3 Results and Discussion

The metalloligand $Cp_2Ti(SMe)_2$ was reacted with $(COD)_2Ni$ and PCy_3. Isolation of the purple-black product (**21**) leads initially to an oily species which, after being washed with diethyl ether, solidifies upon standing. The proton NMR spectrum shows a singlet in the cyclopentadienyl region and a broad multiplet between 2.17-1.07 which corresponds to the cyclohexyl and methyl protons. Phosphorus data indicate coordinated phosphine since a singlet is seen at 58.3 ppm. Based on the NMR data and the similarity to the isoelectronic copper species **3**, **4**, and **11**, complex **21** was formulated as $Cp_2Ti(\mu\text{-}SMe)_2NiPCy_3$, as shown in Figure 5.1

Two equivalents of $Cp_2Ti(SMe)_2$ were reacted with $(COD)_2Ni$ without added phosphine. The purple-red solution of $(COD)_2Ni$ and **10** gradually darkened over a 2 h period to a purple-black colour. Removal of the solvent and washing the residue with pentane yielded the black microcrystalline product **22**. The ^1H NMR spectrum of **22** shows resonances attributable to both cyclopentadienyl and methanethiolate fragments.

Table 5.1: Crystallographic Parameters for $(Cp_2Ti(\mu\text{-}SMe)_2)_2Ni$ and $(Ni(\mu\text{-}SMe)_2)_6$

	22	23
Formula	$C_{24}H_{32}NiTi_2S_4$	$C_{12}H_{36}S_{12}Ni_6$
Crystal colour, form	black blocks	black blocks
Crystal system	tetragonal	monoclinic
a (Å)	8.100(2)	11.393(3)
b (Å)		11.483(3)
c (Å)	20.021(6)	11.821(4)
β (deg)		90.08(2)
Space group	$I\bar{4}$	$P2_1/n$
Volume ($Å^3$)	1317(1)	1547(1)
Density (gcm^{-3}) calcd	1.53	0.98
Z	2	2
Crystal dimens (mm)	0.46 x 0.15 x 0.19	0.31 x 0.15 x 0.23
Abs coeff, μ (cm^{-1})	15.42	42.44
Radiation, λ (Å)	Mo Kα (0.71069)	Mo Kα (0.71069)
Temperature (°C)	24	24
Scan speed (deg/min)	2.0-5.0(θ/2θ scan)	2.0-5.0(θ/2θ scan)
Scan range (deg)	1.0 below Kα1	1.0 below Kα1
	1.0 above Kα2	1.0 above Kα2
Bkgd/scan time ratio	0.5	0.5
Data collected	1133	2285
No. of unique data		
$Fo^2>3\sigma(Fo^2)$	760	1500
No. of variables	71	136

R (%)	3.50	2.85
Rw (%)	3.93	3.05
Largest Δ/σ in the final least squares cycle	0.004	0.002
Maximum residual electron density ($e/Å^3$)	0.69	0.58
Atom associated	Ni	Ni2

Table 5.2: **Positional Parameters for $(Cp_2Ti(\mu\text{-}SMe)_2)_2Ni$ and $(Ni(\mu\text{-}SMe)_2)_6$[1]**

$(Cp_2Ti(\mu\text{-}SMe)_2)_2Ni$ (22)

Atom	x	y	z	Atom	x	y	z
Ti	0	0	1391(1)	Ni	0	0	0
S	-1147(2)	-2039(2)	10576(1)	C1	7201(8)	97(10)	1753(3)
C2	7403(8)	1398(9)	1297(3)	C3	8477(8)	2549(9)	1550(4)
C4	8977(9)	1966(11)	2182(4)	C5	8171(9)	466(12)	2310(4)
C6	-3376(7)	-2101(8)	10444(3)				

$(Ni(\mu\text{-}SMe)_2)_6$ (23)

Atom	x	y	z	Atom	x	y	z
Ni1	4459(1)	6111(1)	6906(1)	Ni2	2917(1)	4117(1)	5744(1)
Ni3	6577(1)	7074(1)	6238(1)	S1	4193(1)	4231(1)	7145(1)
S2	2766(1)	5993(1)	6036(1)	S3	1924(1)	4077(1)	4122(1)
S4	2972(1)	2230(1)	5443(1)	S5	4858(1)	7936(1)	6410(1)
S6	6089(1)	6316(1)	7884(1)	C1	3364(6)	4131(6)	8450(5)
C2	2853(6)	6751(5)	4702(5)	C3	631(5)	3172(6)	4264(6)
C4	4183(6)	1494(5)	6150(5)	C5	4856(6)	8798(5)	7701(5)
C6	6829(6)	4958(5)	8240(6)				

[1]Positions multiplied by 10^4

Table 5.3: Selected Bond Distances and Angles for $(Cp_2Ti(\mu\text{-}SMe)_2)_2Ni$ and $(Ni(\mu\text{-}SMe)_2)_6$

$(Cp_2Ti(\mu\text{-}SMe)_2)_2Ni$ (22)

Distances (Å)

Ti-S	2.503(2)	Ni-S	2.220(1)	S-C6	1.828(6)
Ti-C1	2.384(6)	Ti-C2	2.400(6)	Ti-C3	2.429(6)
Ti-C4	2.396(7)	Ti-C5	2.392(7)	C1-C2	1.41(1)
C2-C3	1.37(1)	C3-C4	1.41(1)	C4-C5	1.40(1)
C1-C5	1.40(1)	Ti..Ni	2.786(1)		

Angles (Degrees)

Ti-S-Ni	72.0(1)	S-Ti-S'	98.6(1)	S-Ni-S'	117.4(1)
S-Ni-S	105.6(1)	C6-S-Ti	118.7(2)	C6-S-Ni	111.1(2)
Cp-Ti-Cp'	129.3(1)				

$(Ni(\mu\text{-}SMe)_2)_6$ (23)

Distances (Å)

Ni1-S1	2.198(2)	Ni1-S2	2.188(2)	Ni1-S5	2.224(2)
Ni1-S6	2.199(1)	Ni2-S1	2.206(2)	Ni2-S2	2.188(2)
Ni2-S3	2.225(2)	Ni2-S4	2.197(2)	Ni3-S3	2.201(1)
Ni3-S4	2.203(1)	Ni3-S5	2.204(2)	Ni3-S6	2.204(2)
S1-C1	1.814(7)	S2-C2	1.805(6)	S3-C3	1.812(7)
S4-C4	1.821(6)	S5-C5	1.819(6)	S6-C6	1.822(6)
Ni1..Ni2	3.195(1)	Ni1..Ni3	2.771(1)	Ni2..Ni3	2.774(1)

Angles (Degrees)

Ni1-S1-Ni2	93.0(1)	Ni1-S2-Ni2	93.8(1)	Ni1-S5-Ni3	77.5(1)
Ni1-S6-Ni3	78.0(1)	Ni1-S3-Ni3	77.6(1)	Ni2-S4-Ni3	78.2(1)
S1-Ni1-S2	83.0(1)	S1-Ni2-S2	82.8(1)	S1-Ni1-S5	171.0(1)
S1-Ni1-S6	98.9(1)	S2-Ni1-S5	96.9(1)	S2-Ni1-S6	175.4(1)
S5-Ni1-S6	82.2(1)	S1-Ni2-S3	169.0(1)	S1-Ni2-S4	99.3(1)
S2-Ni2-S3	96.7(1)	S2-Ni2-S4	177.1(1)	S3-Ni2-S4	81.6(1)
S5-Ni3-S6	82.6(1)	C1-S1-Ni1	104.1(2)	C1-S1-Ni2	107.0(2)
C2-S2-Ni1	109.4(2)	C2-S2-Ni2	109.4(2)	C3-S3-Ni2	110.2(2)
C4-S4-Ni2	113.9(2)	C5-S5-Ni1	106.9(2)	C5-S5-Ni3	108.9(2)
C6-S6-Ni1	114.8(2)	C6-S6-Ni3	115.1(2)		

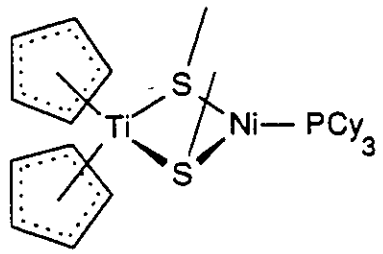

Figure 5.1: Schematic Drawing of $Cp_2Ti(\mu\text{-}SMe)_2NiPCy_3$

The differences between the chemical shifts of compounds **22** and **10** were consistent with coordination of the methanethiolate groups of **10** to Ni, thus bridging the two metal centres. The absence of COD resonances in the ^1H NMR spectrum of **22** and the reaction stoichiometry suggest the formulation of **22** as $(Cp_2Ti(\mu\text{-}SMe)_2)_2Ni$, shown in Figure 5.2.

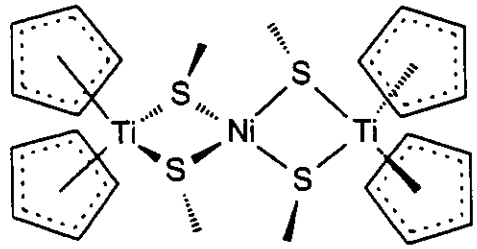

Figure 5.2: Schematic Drawing of $(Cp_2Ti(\mu\text{-}SMe)_2)_2Ni$

This complex is analogous to **14** and the formulation was confirmed by a crystallographic study (*vide infra*).

The complex $Cp_2Ti(\mu\text{-}SMe)_2Ni(COD)$ may be postulated as an intermediate in the formation of **22**. Attempts to spectroscopically observe and/or isolate this species directly from reactions of one equivalent of $Cp_2Ti(SMe)_2$ with $(COD)_2Ni$ were unsuccessful. In all cases, resonances attributable only to compound **22** were observed and diminished yields of **22** were obtained. These results suggest that the rate determining step in the formation of **22** is probably initial replacement of a COD on Ni with the chelating metalloligand **10** and that subsequent replacement of the remaining COD is rapid. Thus,

the equilibrium lies toward the trimetallic species (Scheme 5.1). The position of this equilibrium is shifted by the addition of PCy_3 to reaction mixtures of $Ni(COD)_2$ and one equivalent of $Cp_2Ti(SMe)_2$.

An X-ray crystallographic study of **22** showed that the complex crystallizes in a tetragonal space group with two discrete molecules in the unit cell. The closest approach between the two molecules is 2.526 Å (H4...H5). The symmetry of the unit cell requires that the Ni atom occupies a special position with $\bar{4}$ symmetry and that the Ti atoms sit directly on a two-fold axis of symmetry. Thus, the asymmetric unit is only one fourth of the trimetallic molecule. An ORTEP drawing of the trimetallic species is shown in Figure 5.3. The geometry about both the Ti and Ni centres is best described as pseudo-tetrahedral. The coordination sphere of the Ti atoms is comprised of two π bonded cyclopentadienyl groups and the two methanethiolato moieties, while the four symmetry related sulfur atoms of the methanethiolate groups complete the coordination sphere of the Ni.

The TiS_2NiS_2Ti core of **22** is shown in Figure 5.4. The Ti-S bond length of 2.503(2) Å is substantially longer than the corresponding distance found in **10**, as expected as a result of the thiolate bridging to Ni. The Ni-S distance of 2.220(1) Å is comparable to that found in $Cp_2Ti(\mu\text{-}SCH_2CH_2CH_2PPh_2)_2Ni$[112] and yet it is also considerably longer than the Ni-S bond lengths found in other Ni(II) thiolate species (2.141(2)-2.228(2) Å).[138] These data, as well as, the pseudo-tetrahedral geometry are consistent with the formulation of **22** as a Ti(IV)-Ni(0) species. The Ti-S-Ni angle in **22** is 72.0(1)°, which is the smallest Ti-S-M value reported for thiolato-bridged heterobimetallic species. The S-Ti-S in **22** is 98.6(1)°, substantially greater than the corresponding S-Ti-S angle in **10** of 93.7(1)°. The S-Ni-S angle of 117.4(1)° is greater than expected for a tetrahedral Ni centre. It is also substantially larger than the S-M-S angles found in complexes containing simple dithioligands. These data are also consistent with core distortions to accommodate metal-metal bonding.

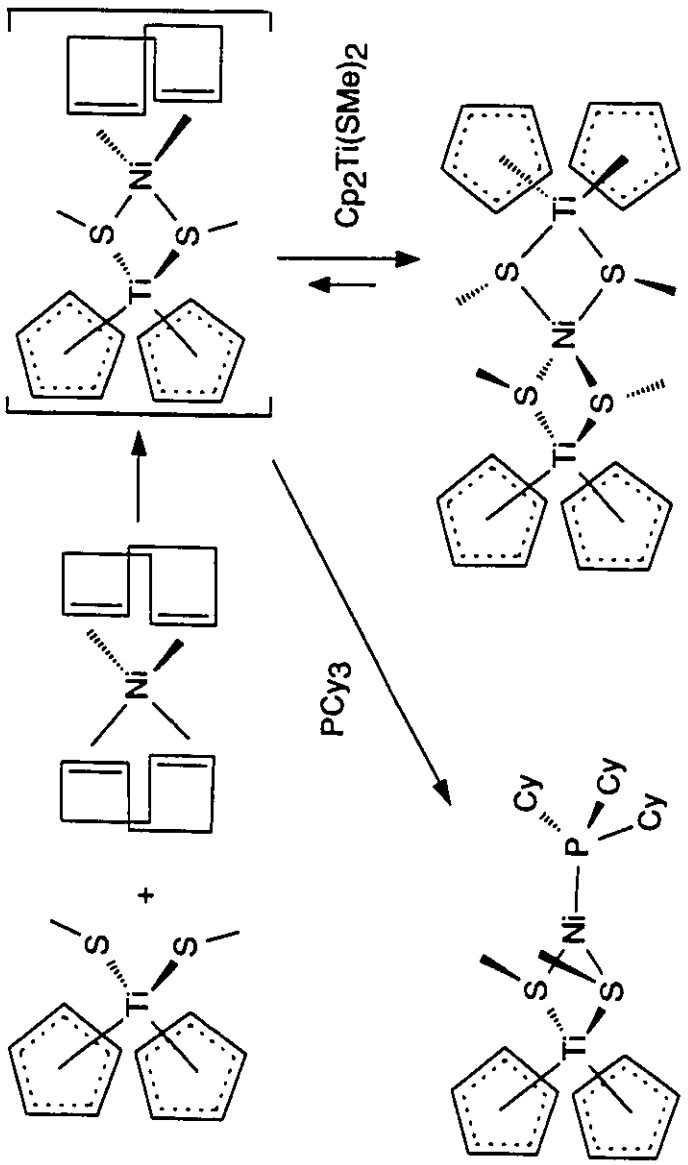

Scheme 5.1: Reaction Scheme for Preparation of **21** and **22**

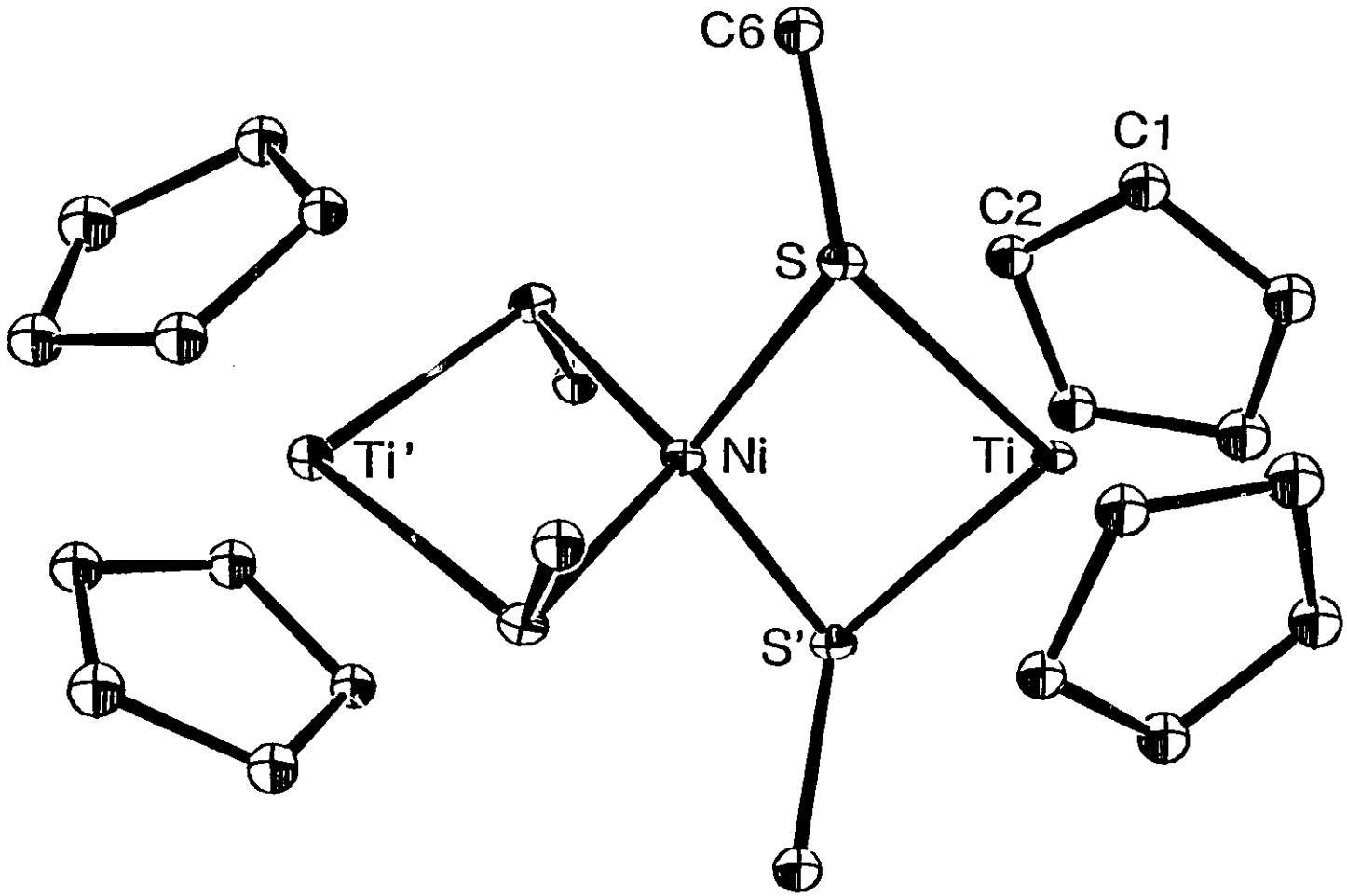

Figure 5.3: ORTEP Drawing of $(Cp_2Ti(\mu\text{-}SMe)_2)_2Ni$; 20% thermal ellipsoids are shown, hydrogen atoms are omitted for clarity

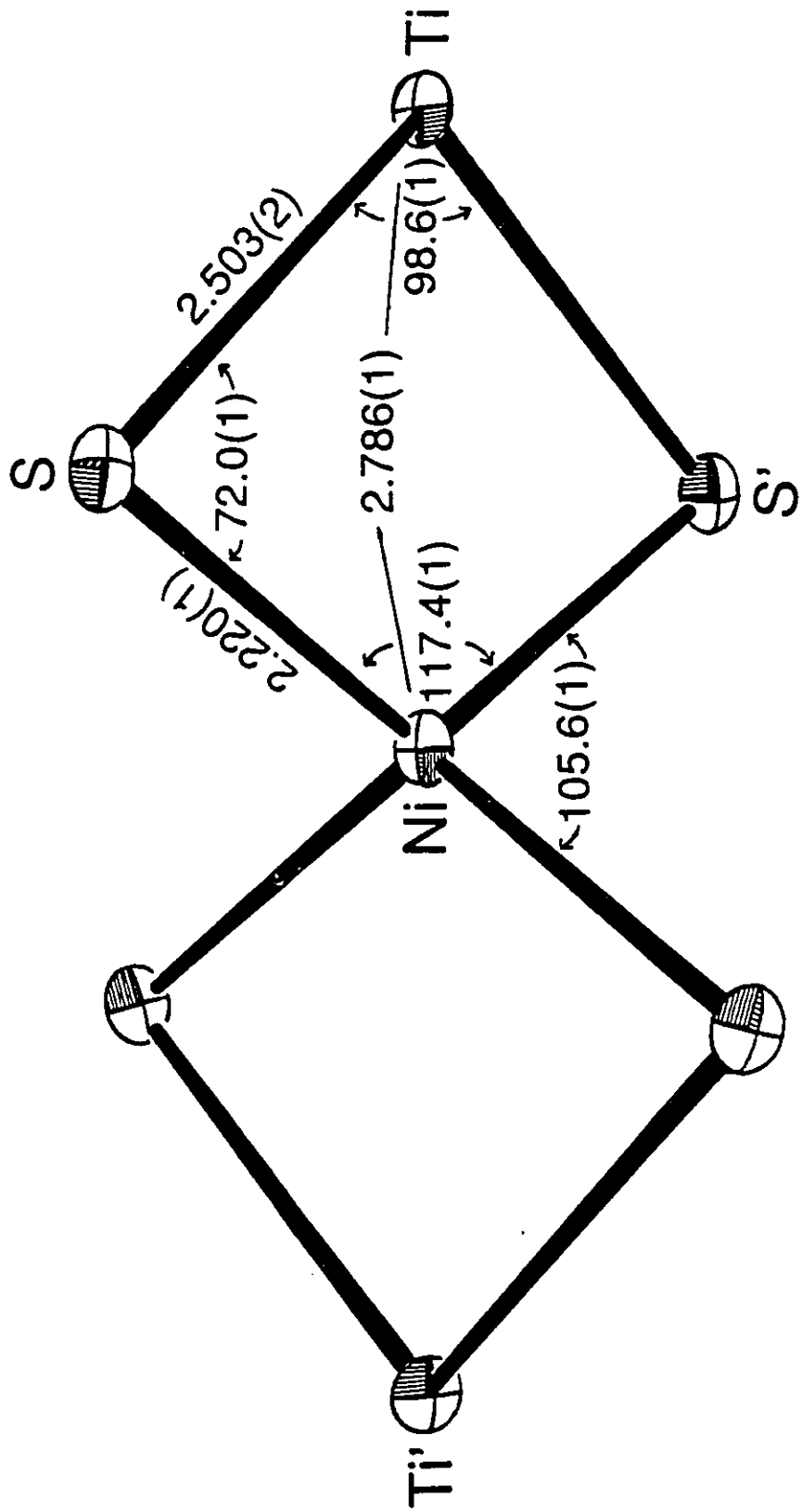

Figure 5.4: ORTEP Drawing of of the TiS_2NiS_2Ti Core of $(Cp_2Ti(\mu\text{-}SMe)_2)_2Ni$; distances in Å, angles in degrees

In other early/late heterobimetallics where metal-metal bonding has been implicated, core distortions from planarity have allowed a closer approach of the metal centres.[111-113,133-135] In the present compound, presumably steric interactions between the two $Cp_2Ti(SMe)_2$ fragments precludes a puckering of the TiS_2Ni cores. Consequently, the angular distortions about the TiS_2Ni cores accommodate the close approach of the metal centres. The Ni-Ti distance of 2.786(1) Å is slightly larger than the sum of the covalent radii (2.47 Å) thus, the metal-metal interactions are formulated as dative interactions between the electron-rich, d^{10} Ni(0) centre and the Lewis acidic, d^0 Ti(IV) centres. The Ti-Ni distance in **22** is shorter than the corresponding distance found in the isoelectronic Ti(IV)-Cu(I) complexes **3**, **4**, **11**, and $[Cp_2Ti(\mu\text{-}SCH_2CH_2PPh_2)_2Cu]BF_4$. This is consistent with the notion of a dative metal-metal bond, as the absence of the positive charge on the late metal in **22** enhances donation of electron density from the Ni to Ti. Similarly, the M-Ti distance increases if the number of valence electrons on the late metal is reduced. Thus, the metal-metal separation in the related Ti-Rh complex,[113] $[Cp_2Ti(\mu\text{-}SCH_2CH_2CH_2PPh_2)_2Rh]^+$, is larger than that seen in either the Ti-Cu or Ti-Ni species. In the case of the only other Ti-Ni thiolato-bridged species reported $[Cp_2Ti(\mu\text{-}SCH_2CH_2CH_2PPh_2)_2Ni]$,[112] the Ti-Ni separation is 2.825(3) Å. Initially, the larger separation in this species seems contrary to the notion of dative bonding. The presence of phosphine ligands on the Ni(0) centre should make the metal centre more electron rich compared to a Ni(0) centre with four sulfur ligands. However, we believe that the geometric constraints of the chelating phosphinothiolate ligands are responsible for holding the Ni atom in place, thus inhibiting a greater core distortion and a closer Ni-Ti approach.

Compound **22** is isoelectronic with the d^0-d^{10}-d^0 complexes $[(Cp_2Nb(\mu\text{-}SMe)_2)_2Ni]^{2+}$ and $[(Cp_2Ta(\mu\text{-}SMe)_2)_2Pt]^{2+}$.[116,118] These cationic species have molecular geometries very similar to that of **22**, although strict crystallographic symmetry is not seen for the Nb/Ni or Ta/Pt species. The metal-metal separations seen in the Nb-Ni

species are 2.776(5) and 2.765(5) Å, while in the Ta-Pt complex, the Ta-Pt distances are 2.788(7) and 2.809(7) Å. These metal-metal separations are closer to the sum of the respective covalent radii (Nb/Ni 2.49 Å, Ta/Pt 2.64 Å) than that seen for **22**. These data are consistent with an increased strength of the dative metal-metal bonding arising from the presence of a formal positive charge on the early metal centres of the Nb-Ni and Ta-Pt species.

The notion of dative metal-metal bonding in these early/late heterobimetallic complexes is supported by theoretical calculations. For related phosphido-bridged Th-Ni and Th-Pt complexes, calculations reported by Ortiz are consistent with the presence of substantial dative metal-metal bonding.[136] Although only preliminary results are available for models of thiolato-bridged systems, Extended Hückel, as well as, Xα calculations for such systems do suggest the presence of dative bonding.[137] In the absence of detailed treatment of models for the present system, one can consider a very simplistic argument based on the frontier orbitals of Cp_2M.[131] Of the two frontier orbitals which will not be involved in bonding to the sulfur bridges, the $2a_1$ orbital is the only orbital oriented spatially between the sulfur bridges directed towards the late metal centre. This vacant frontier orbital is thus capable of accepting electron density from a donor, just as is postulated for complexes of the form Cp_2MH_3.[131] Thus, one might view the present heterobimetallic complexes as perturbations of these simple metallocene systems in which the central donor is a late metal centre.

The possibility of redox chemistry at one of the metal centres of **22** offers the potential for a direct spectroscopic handle on metal-metal interactions. To investigate this possibility, a cyclic-voltammetric study of **22** was conducted. The cyclic voltammogram appears in Figure 5.5. Features attributable to the sequential oxidation of Ni(0) to Ni(I) and Ni(II) were observed at +0.2 V and +0.4 V vs Ag/AgCl; however, these waves were not reversible. Thus, in contrast to related thiolato-bridged early/late heterobimetallics, (i.e., $[Cp_2Ti(\mu\text{-}SCH_2CH_2PPh_2)_2Cu]^+$, $[Cp_2Ti(\mu\text{-}SCH_2CH_2CH_2PPh_2)_2Rh]^+$ and

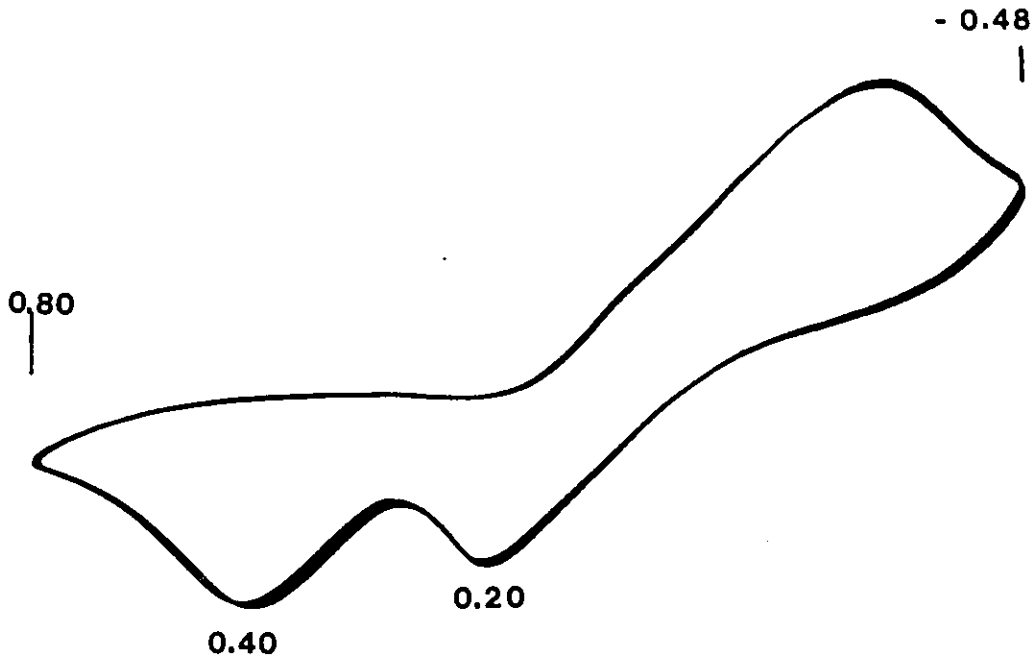

Figure 5.5: Cyclic Voltammogram of $(Cp_2Ti(\mu\text{-}SMe)_2)_2Ni$; potentials in mV vs. Ag/AgCl

$[Cp_2Ti(\mu\text{-}SCH_2CH_2CH_2PPh_2)_2Ni]^0$)[111-113] no other oxidation states of **22** appear to be readily accessible. A similar result was observed for the thiolato-bridged complexes $[Cp_2Ti(\mu\text{-}SEt)_2CuL]^+$. It may be that the stability to redox chemistry of the phosphinoethanethiolate linked heterobimetallics is associated with the chelating nature of the metalloligands.

In attempts to prepare a vanadium/nickel complex analogous to **22**, the reaction of **15** with $(COD)_2Ni$ was investigated. The reaction was monitored by EPR spectroscopy, employing a variety of reaction conditions, solvents and stoichiometries. In all cases, a signal attributable to **15** was seen to rapidly diminish in intensity with time. Typically, within 1 h of reagent mixing, the solutions showed no EPR signal. On standing, black blocks of compound **23** crystallized from the reaction mixture.

A crystallographic study of **23** was undertaken. The empirical formula units aggregate to give the hexamer $(Ni(\mu\text{-}SMe)_2)_6$ in a monoclinic space group. The closest approach between the molecules is 2.37 Å (H5B..H2A). The coordination sphere of each Ni atom is comprised of four sulfur atoms each of which bridges to another Ni centre (Figure 5.6 and 5.7). The Ni-S distances range from 2.188(2) to 2.224(2) Å, which are typical of Ni(II)-thiolate species.[112,138] The S-C distance are also typical. The S-Ni-S angles where both sulfurs bridge the same two Ni atoms are about 81-83°, while the S-Ni-S angles between adjacent sulfur bridges are 96-99°. Thus, the coordination geometry at Ni is best described as pseudo-square planar. The Ni-S-Ni angles at S1 and S2 are 93.0(1)° and 93.8(1)°, respectively, with a Ni1...Ni2 separation of 3.195(1) Å. In contrast, the Ni-S-Ni angles at S3, S4, S5 and S6 range from 77-78° giving rise to Ni...Ni separations of 2.771(1) Å and 2.774(1) Å. These data demonstrate the range of angles that can be accommodated by a bridging-thiolate sulfur atom. This tolerance of such geometric variations at sulfur results in the cyclization of the present compound; that is the two asymmetric units each containing a $Ni_3(SMe)_6$ fragment pair up, giving the hexameric structure. The geometry of the total molecule can be likened to that of a 'basketball net'

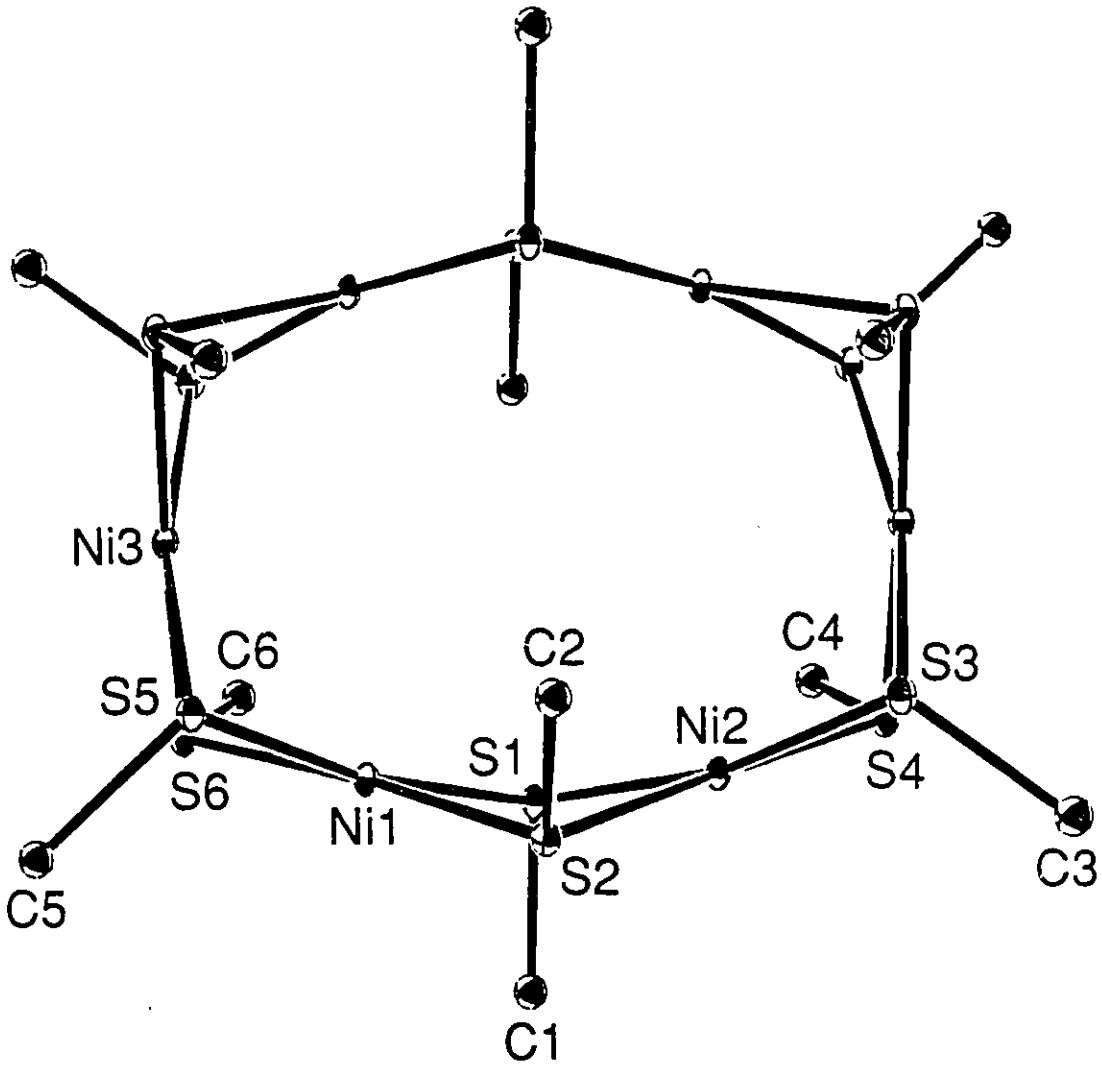

Figure 5.6: ORTEP Drawing of $(Ni(\mu\text{-}SMe)_2)_6$; 20% thermal ellipsoids are shown, hydrogen atoms are omitted for clarity

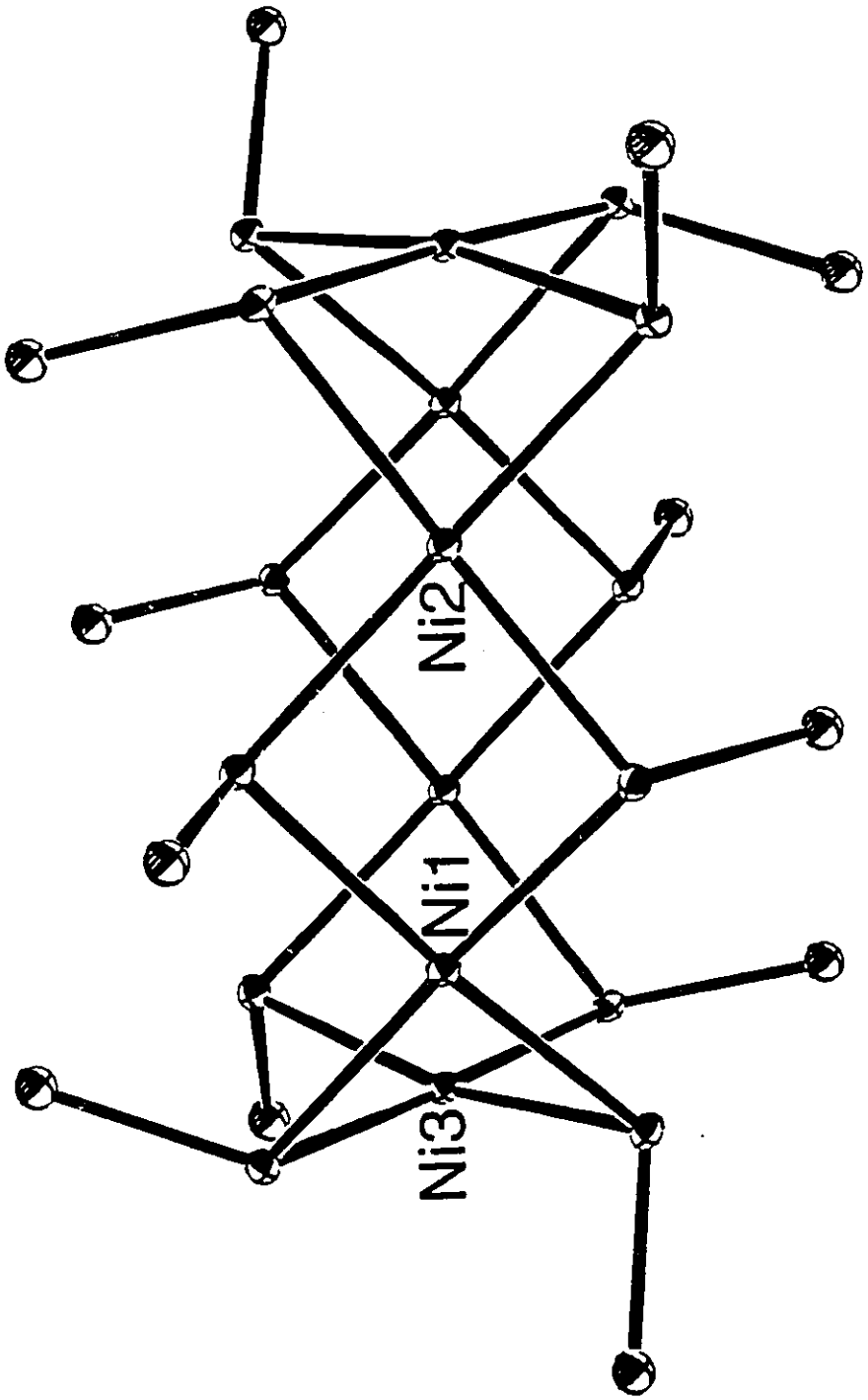

Figure 5.7: ORTEP Drawing of $(Ni(\mu\text{-}SMe)_2)_6$; 20% thermal, ellipsoids are shown, hydrogen atoms are omitted for clarity

in which the 'hoop' is oval with cross 'hoop' Ni...Ni distances of 5.325 Å (Ni1...Ni1'), 5.455 Å (Ni2...N2') and 6.644 Å (Ni3...Ni3'). The 'net' is comprised of the pseudo-square planar coordination spheres of the Ni atoms, each containing four sulfur atoms. The 'net' is woven together by two methanethiolate groups bridging the Ni centres. Related Ni thiolate oligomers have been reported by the research groups of Dahl,[139] Dance,[140] and others.[141,142]

The mechanism of formation of **23** from the reaction of **15** with $(COD)_2Ni$ is not known. However, it is noteworthy that in the related reaction involving of $Cp_2V(SPh)_2$ and $[Cp_3Ni_2][BF_4]$, redox chemistry is accompanied by ligand transfer, yielding $[Cp_2V][BF_4]$ and $[CpNi(\mu\text{-}SPh)]_2$.[90] Isolation of **22** suggests that the initial step in the reaction may be coordination of **15** to Ni. Although the V by-product is not isolated or characterized in this reaction, the stoichiometry of the reaction is consistent with the V(IV) dithiolate **15** being reduced to a V(III) species. These data suggest that the formation of the Ni(II) product **23**, may proceed via two inner sphere, one electron transfers from Ni to V, which are accommodated by the formation of a V_2Ni intermediate analogous to **22**. The molecular orbital containing the unpaired electron for V(IV) has anti-bonding V-S character.[129] This causes a lengthening of the vanadium-sulfur bond relative to that seen for the analogous Ti(IV) species. The weakening of the V-S bond makes the thiolate more susceptible to abstraction upon reaction with late metal centres.

5.4 Summary

The titanium methanethiolate metalloligand can be used to prepare Ti(IV)/Ni(0), mixed-metal complexes analogous to the three-coordinate copper complexes **3**, **4**, and **11** containing one ancillary ligand. Also, a trimetallic complex analogous to **14** is also obtained from the reaction of two equivalents of $Cp_2Ti(SMe)_2$ and $(COD)_2Ni$. These results are in contrast to the product of the reaction of $Cp_2V(SMe)_2$ with $(COD)_2Ni$ which yields the Ni(II) hexamer. The mechanism in the formation of $(Ni(\mu\text{-}SMe)_2)_6$ may involve

initial coordination of the thiolate on vanadium to nickel, followed by thiolate abstraction.

In the Ti/Ni trimetallic complex, the crystal structure shows a close approach of the metals. The metal-metal separation is shorter in the Ti/Ni complex compared to the isoelectronic Ti/Cu species. This close approach is due to the neutral, electron-rich nickel being a better electron donor relative to Cu(I). Again, the angles at the bridging sulfurs are consistent with closing down of the angles to accommodate a M-M interaction. Assignment of the type of electronic communication for the Ti/Ni trimetallic species is d^{10}—d^{0} dative donation, as it is for the related Ti/Cu complexes.

CHAPTER SIX

USE OF TITANIUM AND VANADIUM METALLOLIGANDS FOR THE PREPARATION OF RHODIUM COMPLEXES

6.1 Introduction

Copper and nickel heterobimetallic complexes have been prepared employing titanium alkylthiolates. The use of Cu(I) and Ni(0) as the late metal centres provides structural models of heterogeneous systems; however, it is desirable to also mimic the reactivity of such systems. Having developed a synthetic route to heterobimetallic complexes using copper and nickel, this procedure was followed in order to prepare titanium/rhodium species as subsequent chemistry at rhodium could then be investigated. The reactions of the titanium(IV) metalloligand $Cp_2Ti(SMe)_2$ with rhodium species were investigated in efforts to prepare Ti/Rh complexes related to those reported in previous chapters. In attempts to model the oxidation states found in systems exhibiting SMSI, reactions of the Ti(III) species $(Cp_2Ti(\mu\text{-}SMe))_2$ with rhodium reagents were studied. Finally, attempts to synthesize V(IV)/Rh(I) heterobimetallic complexes were undertaken employing the metalloligand $Cp_2V(SCH_2CH_2CH_2PPh_2)_2$. Since ligand abstraction occurred in the reaction of $Cp_2V(SMe)_2$ with $(COD)_2Ni$, stabilization of a V(IV)/Rh(I) species by using this tetradentate metalloligand could be anticipated. In addition, the Ti(IV)/Rh(I) complex $[Cp_2Ti(\mu\text{-}SCH_2CH_2CH_2PPh_2)_2Rh]BF_4$, which exhibits reversible electrochemistry, has been previously reported.[132] The analogous vanadium complex would be isoelectronic with the reduced heterobimetallic species.

In all reactions of the metalloligands with rhodium species, thiolate abstraction was observed. In the reactions of the titanium containing ligands, the rhodium product was found to be the thiolato-bridged rhodium(I) dimer $((COD)Rh(\mu\text{-}SMe))_2$. The Ti/Rh reactions were monitored by EPR and NMR spectroscopy and the rhodium, thiolato-bridged complex was also characterized by X-ray crystallography. The reaction

of the vanadium metalloligand $Cp_2V(SCH_2CH_2CH_2PPh_2)_2$ with $[(COD)_2Rh]BF_4$ was monitored by EPR spectroscopy. Again, thiolate abstraction of one of the thiolates by the rhodium centre is observed.

6.2 Experimental Section

All preparations were done under an atmosphere of dry, O_2-free N_2. Solvents were reagent grade, distilled from the appropriate drying agents under N_2, and degassed by the freeze-thaw method at least three times prior to use. EPR experiments were performed using a Varian E-12 Spectrometer, using DPPH as the reference. PPh_3, Cp_2TiCl_2, and NEt_3 were purchased from the Aldrich Chemical Co. and Cp_2VCl_2 and PCy_3 from the Strem Chemical Co. $[(MeCN)_4Cu]PF_6$,[120] $(Cp_2Ti(\mu\text{-}Cl))_2$,[143] $HSCH_2CH_2CH_2PPh_2$,[113] $((COD)Rh(\mu\text{-}Cl))_2$,[144] and $[(COD)_2Rh]BF_4$[145] were prepared by the literature methods and the preparation of NaSMe is described in Chapter Three.

(i) Preparation of $(Cp_2Ti(\mu\text{-}SMe))_2$ (24) To a THF solution of $(Cp_2Ti(\mu\text{-}Cl))_2$ (100 mg, 0.24 mmoles) was added NaSMe (33 mg, 0.48 mmoles) and the mixture stirred overnight. The reaction mixture was filtered, the solvent removed *in vacuo* and the residue washed with 2 x 10 mL pentane. The mixture was filtered and the purple, microcrystalline solid dried under vacuum. (Yield: 74 mg, 80%) EPR (THF): g = 1.979, $a<^{47}Ti/^{49}Ti>$ = 12.5 G.

(ii) Preparation of $[(COD)Rh(sol)]PF_6$ (25) To a 20 mL THF solution of $((COD)Rh(\mu\text{-}Cl))_2$ (100 mg, 0.20 mmoles) was added $AgPF_6$ (103 mg, 0.40 mmoles) and the solution stirred for 10 min. The silver chloride was filtered off, leaving a clear, yellow solution of the solvated rhodium cation.

(iii) Preparation of $((COD)Rh(\mu\text{-}SMe))_2$ (26)

From $Cp_2Ti(SMe)_2$, PCy_3 and $[(COD)_2Rh]BF_4$ To a 30 mL THF suspension of

$[(COD)_2Rh]BF_4$ (149 mg, 0.37 mmoles) was added PCy_3 (208 mg, 0.74 mmoles) and the mixture stirred for 30 min. A 10 mL THF solution of $Cp_2Ti(SMe)_2$ (100 mg, 0.37 mmoles) was added to the reaction mixture , resulting in a colour change from purple to orange over 1 h of stirring. The solvent was removed *in vacuo* and the orange residue washed with 2 x 10 mL pentane. $^{31}P\{^1H\}$ NMR (THF): δ, 10.82 (s).

From $Cp_2Ti(SMe)_2$, PPh_3 and $[(COD)_2Rh]BF_4$ This reaction was performed in a manner analogous to that reported for the synthesis using PCy_3. ^{31}P NMR (THF): δ, -4.33 (s).

From $Cp_2Ti(SMe)_2$ and $[(COD)Rh(sol)]PF_6$ To a 20 mL THF solution of $[(COD)Rh(sol)]PF_6$ (0.40 mmoles) was added $Cp_2Ti(SMe)_2$ (109 mg, 0.40 mmoles) and the solution immediately changed from purple to orange-red. The mixture was stirred for 1 h and then stripped to dryness. The resulting oil was washed with pentane, giving an orange solution and an oil. The pentane solution was stripped to dryness. ^1H NMR (d_6-acetone): δ, 4.04 (br s, 4 H), 2.28 (br m, 8 H), 1.51 (s, 3 H).

From $(Cp_2Ti(\mu\text{-}SMe))_2$ and $((COD)Rh(\mu\text{-}Cl))_2$ To a 30 mL THF solution of $((COD)Rh(\mu\text{-}Cl))_2$ (100 mg, 0.20 mmoles) was added $(Cp_2Ti(\mu\text{-}SMe))_2$ (92 mg, 0.20 mmoles) and the mixture stirred for 1 h during which the colour changed from purple to yellow-green. The solvent was then removed under vacuum and the yellow-green residue washed with pentane. EPR (THF): g = 1.979, $a<^{47}Ti/^{49}Ti>$ = 10.0 G.

From NaSMe and $((COD)Rh(\mu\text{-}Cl))_2$ To a 20 mL THF solution of $(COD)Rh(\mu\text{-}Cl))_2$ (30 mg, 0.061 mmoles) was added NaSMe (8.5 mg, 0.12 mmoles) and the mixture was stirred for 1 h. The reaction mixture was filtered and then the yellow solution stripped to dryness. ^{1}NMR (d_6-benzene): δ, 4.04 (br s, 4 H), 2.29 (m, 8 H), 1.52 (s, 3 H).

(iv) Preparation of $Cp_2V(SCH_2CH_2CH_2PPh_2)_2$ (27) To a 30 mL THF suspension of Cp_2VCl_2 (100 mg, 0.040 mmoles) was added $HSCH_2CH_2CH_2PPh_2$ (217 g, 0.080 mmoles) and NEt_3 (80 mg, 0.080 mmoles) and the mixture stirred overnight. To the reaction mixture was added activated neutral, the mixture stirred for 10 min and then filtered. The alumina was washed with 4 x 10 mL portions of THF and the resulting solution stripped to dryness. The residue was washed with pentane and the blue-black solid isolated by filtration. (Yield: 190 mg, 68%). EPR (THF): g = 2.001, a<^{51}V> = 60.0 G.

(v) Reaction of $Cp_2V(SCH_2CH_2CH_2PPh_2)_2$ with $[(COD)_2Rh]BF_4$ To a 30 mL THF suspension of $[(COD)_2Rh]BF_4$ (100 mg, 0.027 mmoles) was added $Cp_2V(SCH_2CH_2CH_2PPh_2)_2$ (189 mg, 0.027 mmoles) and the mixture stirred for 10 min. EPR (THF): g = 2.001, a<^{51}V> = 57.5, a<^{31}P> = 25.0 G.

(vi) X-ray Data Collection and Reduction Diffraction experiments were performed on a four-circle Syntex $P2_1$ diffractometer with graphite-monochromatized Mo Kα radiation (λ = 0.71069 Å). The initial orientation matrix was obtained from 15 machine-centred reflections selected from a rotation photograph. These data were used to determine the crystal system. Partial rotation photographs around each axis were consistent with a monoclinic crystal system for **26**. The final lattice parameters and the orientation matrix were determined from 24 high-angle data ($20°<2\theta<25°$). The observed extinctions were consistent with the space group $P2_1/n$. $\pm h,+k,+l$ data were collected ($4.5°<2\theta<45.0°$), with three standard reflections recorded every 197 reflections. Their intensities showed no statistically significant change over the duration of the data collection. The data were processed using the SHELX-76 program package.

(vii) Structure Solution and Refinement Non-hydrogen atomic scattering factors were

taken from the literature tabulations.[121-123] The heavy atom positions were determined using direct methods. The remaining non-hydrogen atoms were located from successive difference Fourier map calculations. The refinement was carried out by using full-matrix least squares techniques on F, minimizing the function $w(|Fo|-|Fc|)^2$ where the weight, w, is defined as $4Fo^2/2\sigma(Fo^2)$ and Fo and Fc are the observed and calculated structure factor amplitudes. In the final cycles of refinement, the rhodium, sulfur, and methyl carbons were assigned anisotropic temperature factors. The methyl hydrogen atom positions were calculated and allowed to ride on the carbon to which they are bonded assuming a C-H bond length of 0.95 Å; however, the cyclooctadiene hydrogens were located from a difference map. Hydrogen atom temperature factors were fixed at 1.10 times the isotropic temperature factor of the carbon atom to which they are bonded. The hydrogen atom contributions were calculated, but not refined. The residual electron densities were of no chemical significance. Crystal data and data collection parameters are summarized in Table 6.1. Tables of Positional Parameters (Table 6.2) and Selected Bond Distances and Angles (Table 6.3) are reported in this chapter, and Thermal Parameters (Table A1.1) and Hydrogen Atom Parameters (Table A1.2) appear in Appendix One.

6.3 Results and Discussion

The reaction of $[(COD)_2Rh]BF_4$ with one and two equivalents of $Cp_2Ti(SMe)_2$ was performed. In the former case the object was to isolate a mixed-metal complex with bridging thiolate groups and one cyclooctadiene still bound to rhodium. Addition of two titanium metalloligands to $[(COD)_2Rh]BF_4$ was attempted in order to prepare a trimetallic complex analogous to **14** and **22**. Upon addition of the purple thiolate to the late-metal reagent, the solution changed immediately from yellow to orange. Isolation of an orange solid was achieved by removal of the solvent under vacuum and washing the residue with pentane. The resulting yellow-orange, pentane solution was cooled to -10 °C which caused precipitation of orange crystals. Since the crystals were soluble in pentane, the

Table 6.1: Crystallographic Parameters for $((COD)Rh(\mu\text{-}SMe))_2$

	26
Formula	$C_{18}H_{30}Rh_2S_2$
Crystal colour, form	orange blocks
Crystal system	monoclinic
a (Å)	8.551(2)
b (Å)	10.058(3)
c (Å)	22.187(4)
β (deg)	92.54(1)
Space group	$P2_1/n$
Volume ($Å^3$)	1906(1)
Density (gcm^{-3}) calcd	1.80
Z	4
Crystal dimens (mm)	0.43 x 0.32 x 0.34
Abs coeff, μ (cm^{-})	17.72
Radiation, λ (Å)	Mo Kα (0.71069)
Temperature (°C)	24
Scan speed (deg/min)	2.0-5.0(θ/2θ scan)
Scan range (deg)	1.0 below Kα1
	1.0 above Kα2
Bkgd/scan time ratio	0.5
Data collected	2762
No. of unique data	
$Fo^2>3\sigma(Fo^2)$	1666
No. of variables	199
R (%)	3.82

Rw (%)	4.14
Largest Δ/σ in the final least squares cycle	0.002
Maximum residual electron density (e/Å^3)	0.59
Atom associated	Rh1, Rh2

Table 6.2: Positional Parameters for $((COD)Rh(\mu\text{-}SMe))_2$[1]

$((COD)Rh(\mu\text{-}SMe))_2$

Atom	x	y	z	Atom	x	y	z
Rh1	687(1)	2678(1)	6889(1)	Rh2	2692(1)	2480(1)	5846(1)
S1	2545(3)	1059(2)	6676(1)	S2	2945(3)	3910(2)	6689(1)
C1	1839(13)	-625(9)	6554(5)	C2	2633(11)	5667(9)	6540(4)
C11	-1005(10)	4231(8)	6763(4)	C12	-544(10)	4175(8)	7368(4)
C13	-1380(13)	3547(10)	7867(5)	C14	-1827(13)	2152(10)	7777(5)
C15	-964(11)	1424(9)	7315(5)	C16	-1331(11)	1471(9)	6716(4)
C17	-2622(15)	2277(11)	6411(6)	C18	-2576(12)	3725(10)	6523(5)
C21	2467(11)	3984(9)	5159(4)	C22	3977(12)	3513(9)	5207(5)
C23	4686(16)	2535(11)	4759(6)	C24	3656(13)	1368(11)	4617(5)
C25	2683(12)	989(10)	5163(5)	C26	1207(11)	1435(9)	5235(4)
C27	288(13)	2439(9)	4845(5)	C28	1233(12)	3600(10)	4672(5)

[1]Positions multiplied by 10^4

Table 6.3: Selected Bond Distances and Angles for $((COD)Rh(\mu\text{-}SMe))_2$

$((COD)Rh(\mu\text{-}SMe))_2$

Distances (Å)

Rh1..Rh2	2.948(1)	Rh1-S1	2.338(2)	Rh1-S2	2.353(2)
Rh2-S1	2.340(2)	Rh2-S2	2.363(2)	S1-C1	1.815(10)
S2-C2	1.815(9)	Rh1-C11	2.138(8)	Rh1-C12	2.145(9)
Rh1-C15	2.144(10)	Rh1-C16	2.131(9)	Rh2-C21	2.149(9)
Rh2-C22	2.104(10)	Rh2-C25	2.132(10)	Rh2-C26	2.098(10)
C11-C12	1.381(12)	C12-C13	1.486(13)	C13-C14	1.466(13)
C14-C15	1.483(13)	C15-C16	1.353(12)	C16-C17	1.506(14)
C17-C18	1.478(13)	C11-C18	1.512(12)	C21-C22	1.375(12)
C22-C23	1.542(14)	C23-C24	1.493(14)	C24-C25	1.548(13)
C25-C26	1.356(12)	C26-C27	1.525(13)	C27-C28	1.480(13)
C21-C28	1.526(13)	S1..S2	2.888		

Angles (Degrees)

S1-Rh1-S2	76.0(1)	S1-Rh2-S2	75.8(1)	Rh1-S1-Rh2	78.1(1)
Rh1-S2-Rh2	77.4(1)	C1-S1-Rh1	117.1(4)	C1-S1-Rh2	118.8(3)
C2-S2-Rh1	115.6(3)	C2-S2-Rh2	116.1(3)		

product was proposed to be a neutral species. The proton NMR spectrum of the pentane-soluble species shows a methyl peak and resonances attributable to cyclooctadiene. Based on NMR data and solubility, the complex was proposed to be $((COD)_2Rh(\mu\text{-}SMe))_2$ (**26**) and confirmed by an X-ray crystallographic study (*vide infra*). This compound has been previously prepared by heating together $((CO)_2Rh(\mu\text{-}SMe))_2$ and cyclooctadiene.[146] Complex **26** is formed by abstraction of a thiolate from the titanium metalloligand by the Rh(I) centre, followed by dimerization. The titanium product in this reaction is not known; however, it is presumably a titanium(IV) cation possessing one thiolate moiety. The orange solid is similar in colour to that observed for the monosubstitution product $Cp_2Ti(SMe)Cl$, which is a by-product in the preparation of the Ti(IV) metalloligand.

In order to reduce the tendency of the late metal to abstract thiolate, preparation of a mixed-metal species incorporating a trisubstituted phosphine was attempted. This would reduce the Lewis acidity of the Rh(I) centre. In these reactions the intention was to preform Rh-P bonds by displacing one COD, and then displace the second COD with the thiolates of the metalloligand. Preforming the late metal-phosphine bonds is the approach used in the preparation of **3**, **4**, and **11**. Two equivalents of tricyclohexylphosphine were added to a THF suspension of $[(COD)_2Rh]BF_4$. Upon addition of the titanium species there was a gradual colour change from purple to orange. After stripping the reaction mixture to dryness, the residue was washed with pentane. As was found in the reaction of **10** and $[(COD)_2Rh]BF_4$, the orange pentane washings yielded orange crystals when cooled to -10 °C. In the ^{31}P NMR there is only one broad single due to uncoordinated tricyclohexylphosphine. If a Rh-P complex had been isolated, one would expect a doublet in the NMR spectrum due to coupling of rhodium to phosphorus. The titanium product in this reaction is presumably a Ti(IV) cation which does not have the phosphine bound to the early-metal centre.

Reaction of $[(COD)_2Rh]BF_4$ with $Cp_2Ti(SMe)_2$ and triphenylphosphine was also

performed. The $^{31}P\{^1H\}$ NMR spectrum of $[(COD)_2Rh]BF_4$ and PPh_3 shows a doublet corresponding to phosphine coordinated to rhodium. When $Cp_2Ti(SMe)_2$ is added to the rhodium-phosphine complex, there is a gradual colour change from purple to orange. The $^{31}P\{^1H\}$ NMR spectrum of the orange solution shows only a single resonance corresponding to free triphenylphosphine. The NMR results suggest that the phosphine is displaced by the thiolate of the metalloligand and then the thiolate is abstracted by the rhodium centre giving **26**. This hypothesis is supported by the ability of allylic aryl sulfides to displace triphenylphosphine from $RhH(PPh_3)_4$ to give rhodium-thiolate dimers and olefins.[147]

Since displacement of cyclooctadiene may be a difficulty in obtaining mixed-metal complexes, a rhodium solvated species $[(COD)Rh(sol)]PF_6$ (**25**) was used as the late metal reagent. The thiolates on the metalloligands should be able to displace the coordinated solvents more easily than they would displace a cyclooctadiene. This would give a species related to $[(C_5H_4CH_2CH_2S\text{-}n\text{-}Pr)_2Mo(\mu\text{-}S\text{-}n\text{-}Pr)_2Rh(COD)]^+$ which was reported by Green and coworkers.[92] The solvated rhodium cation was prepared by reaction of $((COD)Rh(\mu\text{-}Cl))_2$ with two equivalents of silver hexafluorophosphate. A clear, yellow solution containing **25** is obtained after the reaction mixture is filtered in order to remove silver chloride. To the THF solution of the rhodium cation was added $Cp_2Ti(SMe)_2$ causing an immediate colour change from yellow to orange. The proton NMR data shows resonances consistent with those expected for the rhodium thiolato-bridged dimer.

The titanium(III) chloro-bridged dimer was prepared using a synthesis reported by Manzer involving the reaction of TlCp with $TiCl_3$.[143] It was not find it necessary to reflux the reaction mixture in order to obtain good yields. The EPR spectrum of the Ti(III) chloro-bridged dimer shows a singlet with a g value of 1.980 with hyperfine coupling to the titanium centres of 10.0 G, consistent with the reported literature values.[148,149] This olive-green species was reacted with two equivalents of NaSMe in THF and the mixture was stirred for 4 h; however, the solution became purple after approximately 10 min.

After stirring, the reaction mixture was filtered to remove sodium chloride and the solvent was removed *in vacuo*. After work-up, a purple solid was obtained and was formulated as $(Cp_2Ti(\mu\text{-}SMe))_2$ (**24**) (Figure 6.1). The EPR spectrum of **24** shows a singlet with a *g*

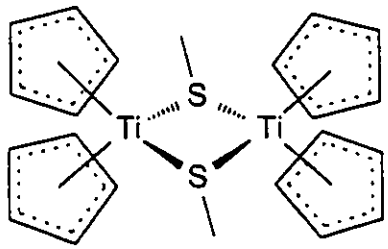

Figure 6.1: Schematic Drawing of $(Cp_2Ti(\mu\text{-}SMe))_2$

value of 1.979 and hyperfine coupling to the two isotopes of titanium of 12.5 G. The EPR results support the formulation of **24** as a Ti(III) species.

Two approaches were used in order to incorporate Ti(III) and Rh(I) in a heterobimetallic complex. The first of these methods was the reaction of the titanium(III) thiolato-bridged dimer (**24**) with $((COD)Rh(\mu\text{-}Cl))_2$ in order to prepare a mixed-metal dimer with one chloro- and one thiolato-bridge. This target complex would give a bridging chloride which could be exchanged with a different bridging ligand. As the purple THF solution of the metalloligand was added to the yellow THF solution of the Rh reagent, the colour changed to yellow-green. The EPR spectrum which was run on the reaction mixture showed a singlet with a *g* value of 1.980. This *g* value is the same as that obtained from the EPR spectrum of $(Cp_2Ti(\mu\text{-}Cl))_2$. Results obtained from the EPR experiment imply that there is bridging ligand exchange between the titanium and rhodium dimers as shown in Scheme 6.1. The rhodium containing product from this reaction was formulated as $((COD)Rh(\mu\text{-}SMe))_2$.

The second approach used to prepare mixed-metal species containing Ti(III) and Rh(I) was the reaction of the two homometallic, chloro-bridged dimers in an attempt to prepare mixed-metal, dimers with chloride bridges. By addition of the sodium thiolate salt to the bimetallic dimers it was hoped that the thiolate-bridged, mixed-metal species could

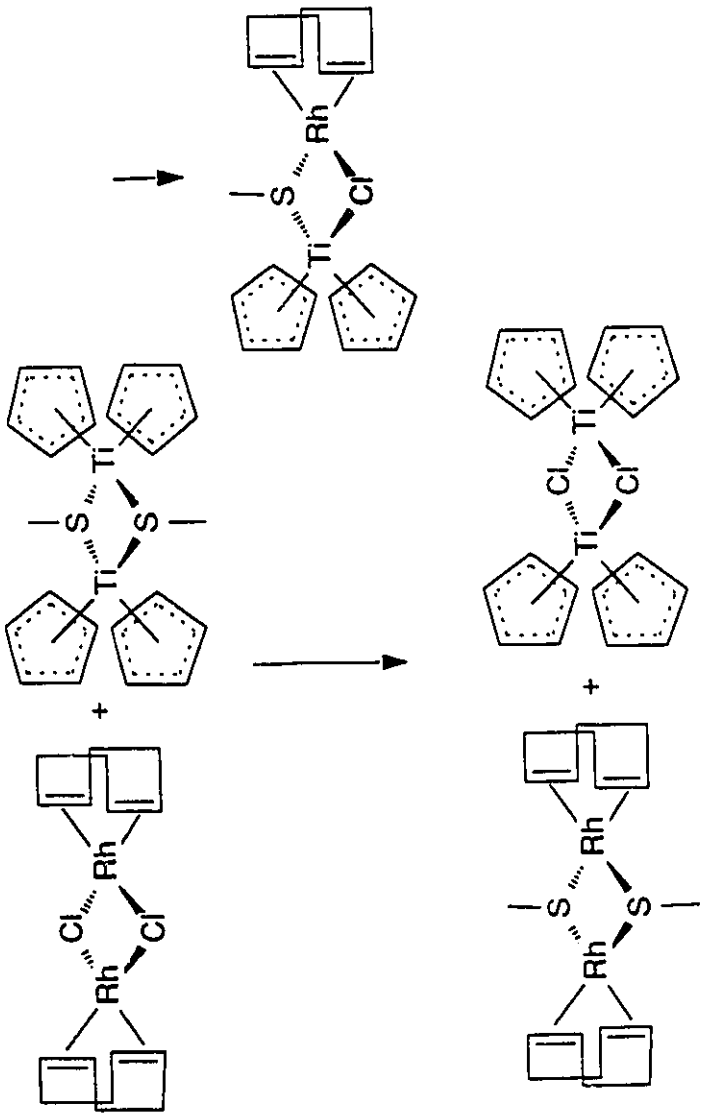

Scheme 6.1: Bridging Ligand Exchange Between $(Cp_2Ti(\mu\text{-}SMe)_2$ and $((COD)Rh(\mu\text{-}Cl))_2$

be isolated. However, addition of two equivalents of thiolate to the reaction mixture gave only **26** and $(Cp_2Ti(\mu\text{-}Cl))_2$, while addition of more thiolate gave the purple titanium species $(Cp_2Ti(\mu\text{-}SMe))_2$. The EPR of the reaction mixture shows no Ti-Rh coupling, implying that the mixed-metal complex does not form.

X-ray quality crystals of $((COD)Rh(\mu\text{-}SMe))_2$ (**26**) were obtained by cooling a pentane solution of **26** to -10 °C. These crystals are made up of monoclinic unit cells containing four formula units per cell. The closest approach between any of these molecules is 2.252 Å (H1B-H27B). An ORTEP drawing of the dimer appears in Figure 6.2 and in Figure 6.3 appears an ORTEP drawing in which the molecule is rotated 90°. Each square-planar rhodium is π-bonded to the double bonds of a cyclooctadiene molecule and to two bridging methanethiolates. The cyclooctadiene rings each have a boat configuration, with a mean carbon-carbon double bond length of 1.366 Å, which is less than that of 1.425 found for $((COD)Rh(\mu\text{-}Cl))_2$.[150] In the crystal structure of the chloro-bridged dimer, the authors reported that the double and single bonds of the olefin could not be distinguished. In **26**, there is a significant difference between the single and double bond lengths as expected. The average Rh-S distance of 2.349 Å is smaller than that found for $(Rh(SPh)(CO)(PMe_3))_2$(2.388 Å),[151] but larger than 2.306 Å found in $(CpRh(\mu\text{-}SPh))_2$.[152] There is an exo arrangement of the methyl groups on the sulfur atoms with respect to the RhS_2Rh core. A smaller Rh-Rh separation is found in **26** (2.948 Å), compared 3.061 Å found in $(Rh(\mu\text{-}SPh)(CO)(PMe_3))_2$[151] or a distance of 3.12 Å for $(CO)_2Rh(\mu\text{-}SPh)_2Rh(COT)$.[148] In $(Rh(\mu\text{-}SPh)(CO)(PMe_3))_2$, a metal-metal interaction has been proposed.[151]

The S-Rh-S angles found in **26** (76.0(1)° and 75.8(1)°) are smaller than those found for $(Rh(SPh)(CO)(PMe_3))_2$ (81.0(1)° and 80.9(1)°), as are the Rh1-S-Rh2 angles of 78.1(1)° and 77.4(1)° compared to 80.2(1)° and 79.2(1)°.[151] The metal-metal separation found in **26** is considerably less than that found in $((COD)Rh(\mu\text{-}Cl))_2$ (3.498 Å).[150] The small angle at the rhodium centres and the shorter than expected S-S separation of 2.888 Å

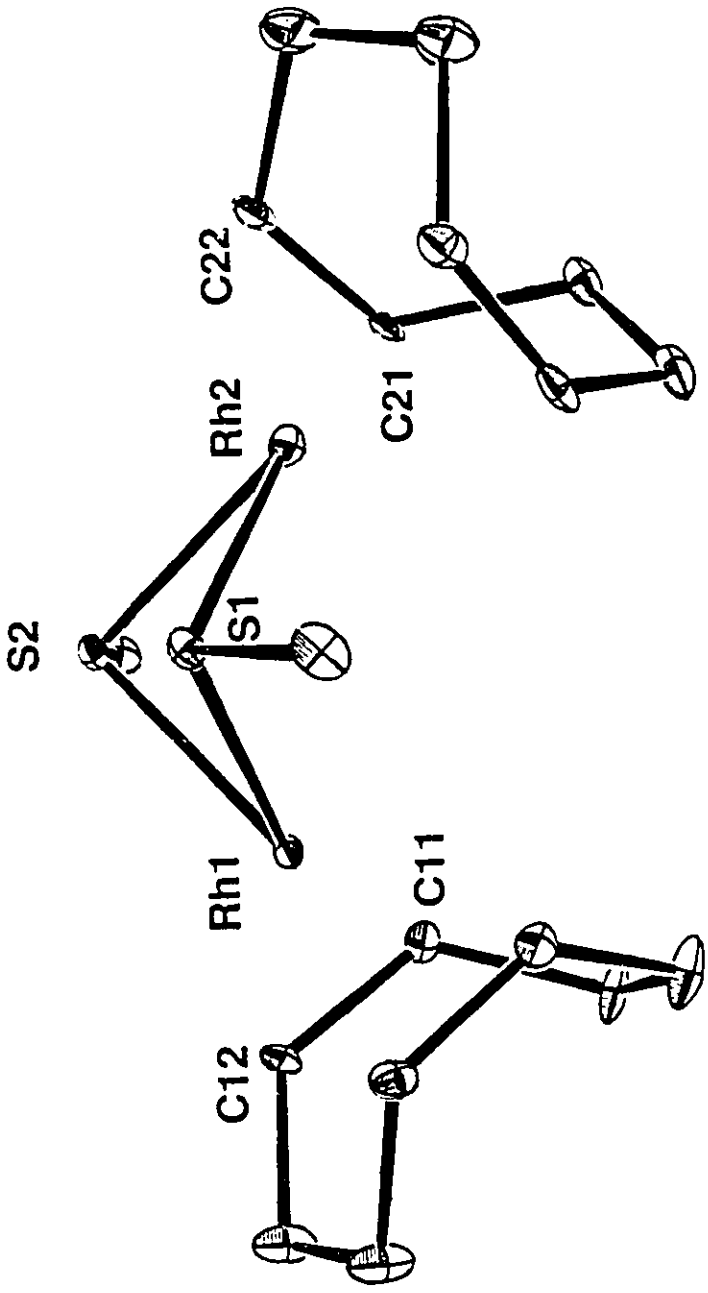

Figure 6.2: ORTEP Drawing of ((COD)Rh(μ-SMe))$_2$; 20% thermal, ellipsoids are shown, hydrogen atoms are omitted for clarity

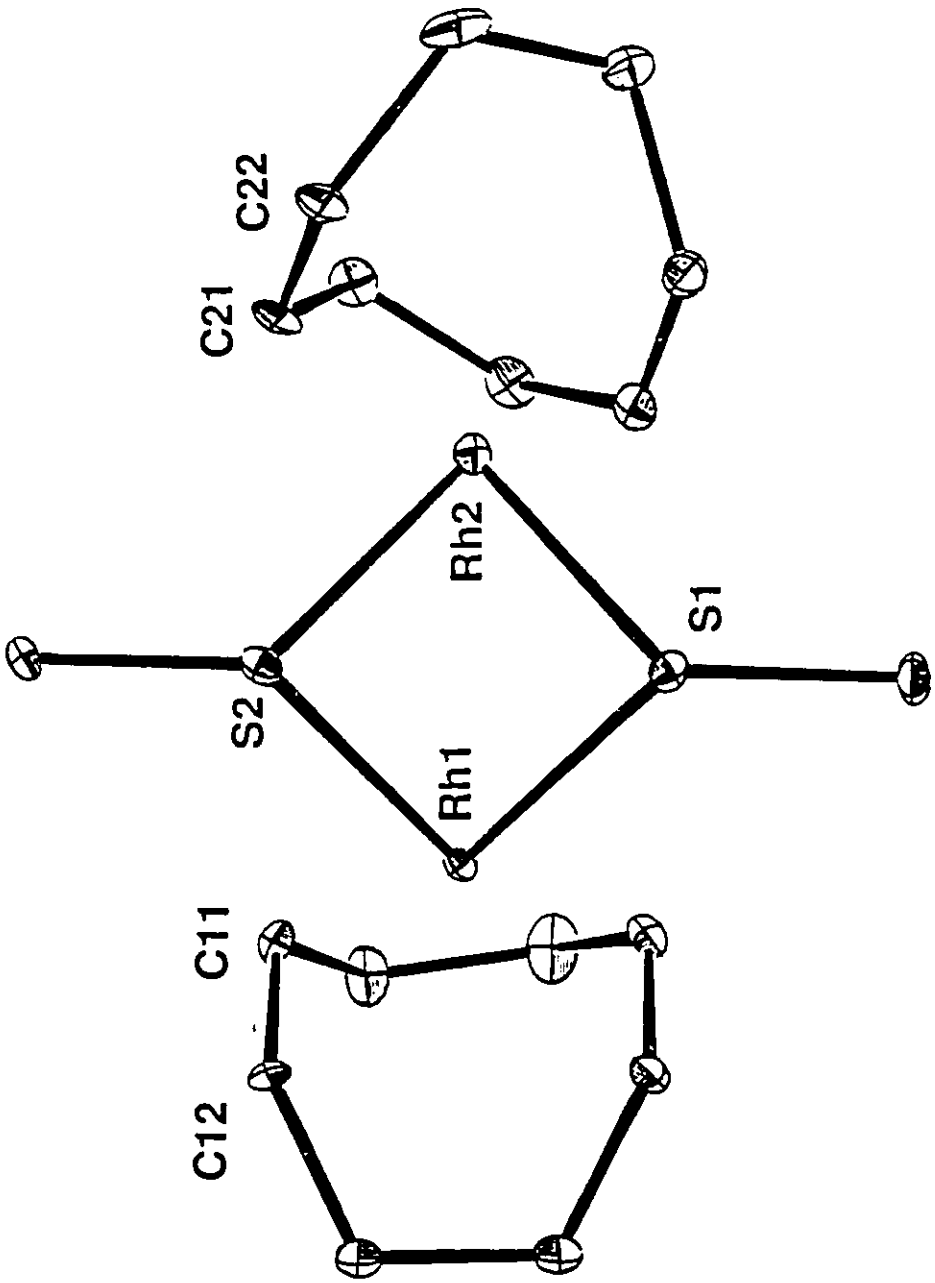

Figure 6.3: ORTEP Drawing of $((COD)Rh(\mu\text{-}SMe))_2$; 20% thermal, ellipsoids are shown, hydrogen atoms are omitted for clarity

in 26 are evidence for disulfide bonding character. In $Cp_2Nb(SPh)_2$, at a S-S distance of 3.08 Å, there is also indication of interaction between the sulfur centres.[117] The existence of disulfide bonding character would also explain the short Rh-Rh separation, since the metals would interact.

Previously, our group has reported the synthesis and crystal structure of $[Cp_2Ti(\mu\text{-}SCH_2CH_2CH_2PPh_2)_2Rh]BF_4$.[113] This complex exhibits reversible, one-electron reduction giving a stable Ti(III)/Rh(I) species. Preparation of the vanadium metalloligand $Cp_2V(SCH_2CH_2CH_2PPh_2)_2$ and subsequent reaction with $[(COD_2)Rh]BF_4$ would give a species isoelectronic with the Ti(III)/Rh(I) compound. Also, it was thought that the tetradentate vanadium metalloligand would stabilize the V(IV) centre against thiolate abstraction. The metalloligand $Cp_2V(SCH_2CH_2CH_2PPh_2)_2$ (27) was prepared by reaction of vanadocene dichloride and 3-diphenylphosphinopropanethiol in the presence of base.

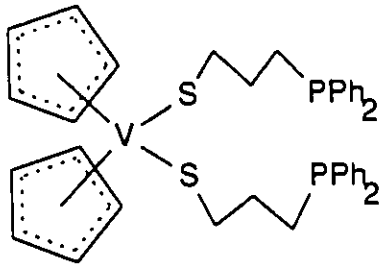

Figure 6.4: Schematic Drawing of $Cp_2V(SCH_2CH_2CH_2PPh_2)_2$

After treatment with alumina and work-up, a dark, blue-black solid is obtained in 68% yield. A schematic drawing of the metalloligand is shown in Figure 6.4. The EPR spectrum of 27 (Figure 6.5) shows an eight line pattern due to coupling of the unpaired electron on vanadium to the vanadium nucleus.

The vanadium metalloligand was reacted with $[(COD)_2Rh]BF_4$ in THF. The yellow THF suspension of $[(COD)_2Rh]BF_4$ changed to brown-green during addition of the dark, blue-black vanadium metalloligand. An EPR study was performed on the reaction mixture and the spectrum is shown in Figure 6.6. The spectrum is a 16 line pattern due to

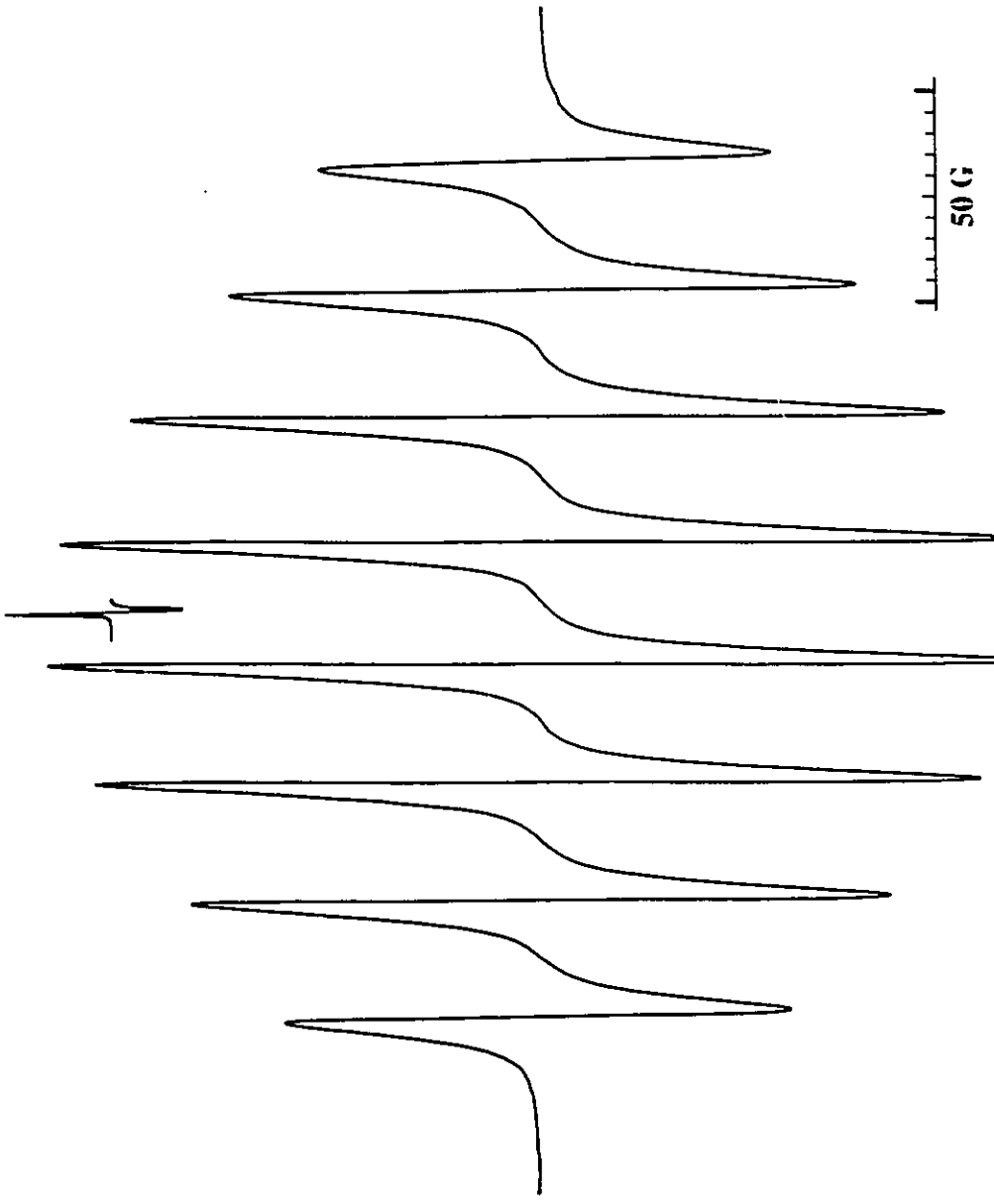

Figure 6.5: EPR Spectrum of $Cp_2V(SCH_2CH_2CH_2PPh_2)_2$

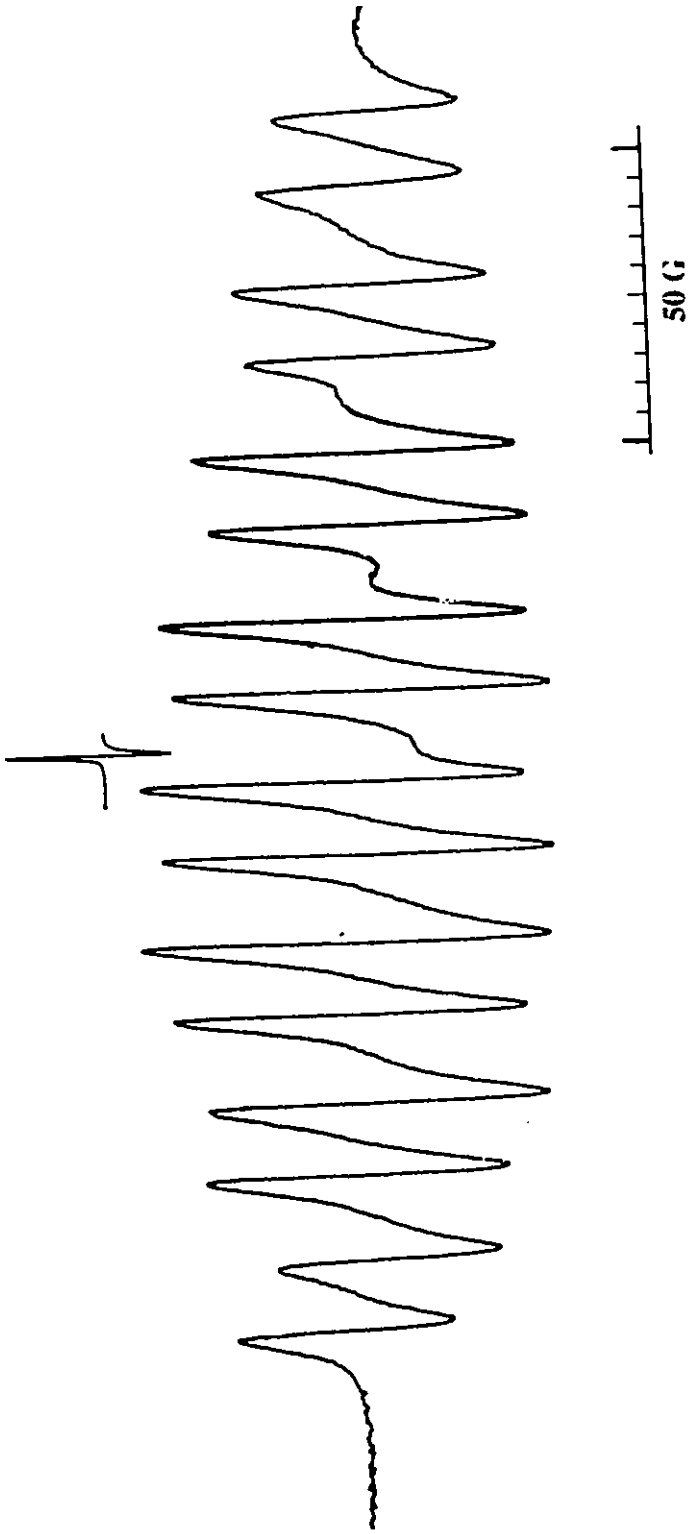

Figure 6.6: EPR Spectrum of $Cp_2V(SCH_2CH_2CH_2PPh_2)$

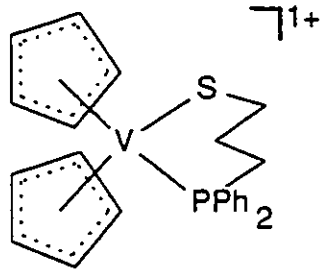

Figure 6.7: Schematic Drawing of $Cp_2V(SCH_2CH_2CH_2PPh_2)$

coupling of the unpaired electron on vanadium coupling to the vanadium nucleus and to one phosphorus centre with no evidence of coupling to rhodium. The coupling was found to be 57.5 G to vanadium and 25.0 G to phosphorus. In other reports of a phosphine bound to a d^1, early metal centre, coupling to phosphorus of 19.3 G and 30.0 G has been reported.[149] This spectrum is consistent with the formulation of the vanadium species as shown in Figure 6.7. As was found in the reactions of $Cp_2V(SMe)_2$ with $(COD)_2Ni$, the late metal abstracts thiolate from the early-metal species. The rhodium product from this reaction has not been characterized, although the complexes $[(Ph_2PCH_2CH_2SPh)_2Rh]BPh_4$ and $(H_2PCH_2CH_2S)_3Rh$ have been reported.[153,154] Thus, a possible rhodium product is $(COD)Rh(SCH_2CH_2CH_2PPh_2)$.

6.4 Summary

The reactions of the titanium and vanadium metalloligands with rhodium complexes have provided information about thiolate abstraction. Reaction of rhodium species with Ti(III) and Ti(IV) led to the thiolato-bridged rhodium dimer $((COD)Rh(\mu\text{-}SMe))_2$. Initial formation of a heterobimetallic species is thought to be an intermediate in the preparation of the thiolato-bridged rhodium dimer, as was proposed for the preparation of $(Ni(\mu\text{-}SMe)_2)_6$. In the reaction of $Cp_2V(SCH_2CH_2CH_2PPh_2)_2$ with $[(COD)_2Rh]BF_4$, evidence for thiolate abstraction by the late metal has again been observed.

CHAPTER SEVEN

SUMMARY

The focus of this work has been to develop a synthetic method which would incorporate two widely divergent transition metals in a discrete molecule. Study of these complexes, both spectroscopically and crystallographically, was hoped to lead to a better understanding of the type of electronic communication occurring in heterogeneous catalytic systems exhibiting strong metal-support interactions. The use of titanium and vanadium metalloligands for the preparation of early/late, heterobimetallic complexes was very limited until this work was undertaken. Previously, thiolates had been explored as bridging ligands for similar or closely related metal centres.

The metalloligand approach has proven useful for synthesizing several mixed-metal complexes which are shown in Figure 7.1. With the d^{10} late metals, Cu(I) and Ni(0), complexes with three- and four-coordinate late metals have been prepared. This is in contrast to the reactions of Ti(III) or Ti(IV) metalloligands with rhodium species which resulted in thiolate abstraction reactions affording the thiolato-bridged rhodium dimer $((COD)Rh(\mu\text{-}SMe))_2$. In the case of the vanadium metalloligands $Cp_2V(SEt)_2$ and $Cp_2V(SMe)_2$, four-coordinate copper(I) complexes were prepared, as well as, three-coordinate copper species using $Cp_2V(SEt)_2$. However, thiolate abstraction was seen when nickel(0) was reacted with $Cp_2V(SMe)_2$ giving the Ni(II) hexamer $(Ni(\mu\text{-}SMe)_2)_6$. Similar thiolate abstraction was seen for the reaction of rhodium(I) and $Cp_2V(SCH_2CH_2CH_2PPh_2)_2$.

X-ray crystallography provides a method to investigate the geometric perturbations seen in the heterobimetallic species caused by electronic communication between the constituent metals. The Ti(IV)/Cu(I) and Ti(IV)/Ni(0) species show structural features which are attributed to metal-metal interaction. At the bridging sulfur atoms there is a

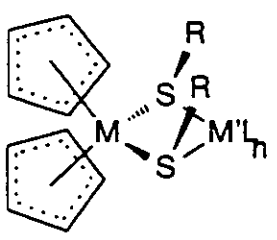

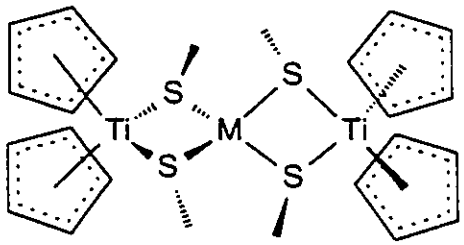

M = Ti or V, M' = Cu, n = 1, L = PCy_3
n = 2, L = NCMe
M = Ti, M' = Ni, n = 1, L = PCy_3

M = Cu or Ni

Figure 7.1: Schematic Drawings of Early/Late Heterobimetallic Complexes Synthesized

closing down of the M-S-M' angles to less than 80° which has been used as evidence for interaction between the metals. The angles at the late metal of 111-114° in $[Cp_2Ti(\mu\text{-}SEt)_2CuPR_3]PF_6$ are larger than observed for four-atom cores in which no metal-metal interaction is proposed. Also, the angles at the late metal in $[Cp_2Ti(\mu\text{-}SMe)_2Cu(NCMe)_2]PF_6$ (112.1°) and $((Cp_2Ti(\mu\text{-}SMe)_2)_2Ni$ (117.4°) are larger than those normally found for tetrahedral metals. In the Ti complexes prepared using the methanethiolate metalloligand direct comparison between the metalloligand and the complexes shows the angles at titanium to be 5-6° larger in the mixed-metal species than in the free metalloligand. This opening of the metal angle would facilitate metal-metal interaction. The Ti/Cu complexes show puckering of the TiS_2Cu cores ranging from 11-17° which is considered to be an indication of interaction between the metals.

Another parameter to consider when evaluating metal-metal interaction is the separation of the metals. In complexes prepared using alkylthiolate metalloligands, shorter M-M separations have been achieved than in related bimetallic complexes using bidentate, phosphinoethane- and phosphinopropanethiolate metalloligands. The M-M separation for the Ti(IV)/Ni(0) complex $((Cp_2Ti(\mu\text{-}SMe)_2)_2Ni$ is shorter than those found for the Ti(IV)/Cu(I) complexes. Since the nickel centre in the bimetallic complex is neutral, it is a better electron donor than the isoelectronic Cu(I) centre. Listed in Table 7.1

are all of the thiolato-bridged, early/late, heterobimetallic complexes which have been structurally characterized. The features of the core previously discussed which are pertinent to M-M interaction are included in this table.

The EPR studies of the heterobimetallic complexes containing vanadium and copper provide insight into metal-metal communication. Coupling between vanadium, copper and phosphorus is seen in the EPR spectra of $[Cp_2V(\mu\text{-}SEt)_2CuPR_3]PF_6$ which is consistent with a transannular interaction between the magnetic nuclei. This through space coupling supports the idea that in heterogeneous systems, electronic communication can occur between the metal of the support and the dispersed metal. It would be of considerable interest to obtain crystallographic data on a V(IV)/Cu(I) species, since the spectroscopic data could be compared directly to the structure, rather than using related compounds. Also, a crystal structure of a V/Cu species would provide information regarding the change in the metal-metal separation due to reduction of the early metal.

The observation of thiolate abstraction precludes a study of the chemistry of Ti/Rh thiolato-bridged complexes. This combination of metals is of particular interest since it would both model SMSI and lead directly into the next phase of the long-term goal of this research, namely the development of discrete, homogeneous catalysts. The limitations of our model are demonstrated by our inability to isolate a Ti/Rh thiolato-bridged complex. Since the thiolate metalloligand approach has not proven general for all early/late metal combinations attempted, modification of the model is warranted. Employing different bridging ligands which better mimic the oxides found in heterogeneous catalytic systems would be one improvement which would lead to a deeper understanding of SMSI.

In summary, a number of early/late heterobimetallic complexes containing titanium and vanadium metalloligands have been prepared and characterized. The EPR and crystallographic data are consistent with $d^{10} \rightarrow d^0$ dative donation of electron density from the electron-rich late metal to the Lewis acidic, early metal. A through space interaction could be the mechanism by which the dispersed metal and the metal of the

Table 7.1: Thiolato-Bridged Early/Late Heterobimetallics[1]

Compound	M-M'	M-S-M'	S-M-S'	S-M'-S'	Ref
$Cp_2Ti(\mu\text{-}SMe)_2Mo(CO)_4$	3.321(2)	82.4(1)	99.9(1)	94.6(1)	
		83.2(1)			
$[Cp_2Ti(\mu\text{-}SCH_2CH_2CH_2PPh_2)_2Rh]^+$	3.127(2)	81.5(1)	96.8(1)	100.1(1)	113
		81.6(1)			
$Cp_2Ti(\mu\text{-}SCH_2CH_2CH_2PPh_2)_2Ni$	2.825(2)	74.1(2)	96.2(2)	115.5(2)	112
		74.2(1)			
$[(Cp_2Ti(\mu\text{-}SMe)_2)_2Ni]$	2.786(1)	72.0(1)	98.6(1)	117.4(1)	
$[Cp_2Ti(\mu\text{-}SMe)_2Cu(NCMe)_2]^+$	2.846(2)	73.5(1)	99.4(1)	112.2(1)	
		74.1(1)			
$[Cp_2Ti(\mu\text{-}SCH_2CH_2PPh_2)_2Cu]^+$	3.024(1)	78.1(1)	97.5(1)	106.4(1)	111
		78.0(1)			

$[Cp_2Ti(\mu\text{-}SEt)_2CuPPh_3]^+$	2.803(1)	72.9(1)	99.1(2)	114.1(2)	
		72.9(2)			
$[Cp_2Ti(\mu\text{-}SEt)_2CuPCy_3]^+$	2.840(1)	74.1(1)	99.1(1)	110.9(1)	
		73.8(1)			
$[Cp_2Nb(\mu\text{-}SPh)_2Mo(CO)_4]^+$	3.116(2)	77.7(1)	101.8(1)	103.1(1)	117
		77.4(1)			
$[(Cp_2Nb(\mu\text{-}SMe)_2)_2Ni]^{2+}$	2.765(5)	72.3(3)	98.0(3)	106.0(3)	116
	2.776(5)	72.6(3)	97.8(3)	104.4(3)	
		72.7(3)			
		72.3(3)			
$[(Cp_2Ta(\mu\text{-}SMe)_2)_2Pt]^{2+}$	2.788(1)	70(1)	104(1)	115(1)	118
	2.809(1)	71(1)	105(1)	109(1)	
		70(1)			
		69(1)			

[1]Distance are given Å, Angles in degrees, M and M' refer to the early and late metals, respectively.

oxide support interact. It may be that this communication is responsible for the perturbation of the adsorption behaviour observed in heterogeneous systems which exhibit strong metal-support interactions.

APPENDIX ONE

SUPPLEMENTARY DATA FOR CRYSTALLOGRAPHIC STUDIES

Table A3.1: Thermal Parameters[1]

$[Cp_2Ti(\mu\text{-}SEt)_2CuPPh_3]PF_6 \cdot 1.62$ THF (3·1.62 THF)

Atom	U11	U22	U33	U12	U13	U23
Cu	46(1)	48(1)	43(1)	-5(1)	6(1)	3(1)
Ti	42(2)	38(2)	41(2)	0(1)	1(1)	4(1)
S1	52(3)	55(3)	33(2)	2(2)	6(2)	-2(2)
S2	51(3)	60(3)	34(2)	3(2)	6(2)	-1(2)
P1	46(3)	50(3)	42(3)	-10(2)	11(2)	-3(2)
P2	64(4)	72(4)	63(4)	6(3)	10(3)	-10(3)
F1	135(14)	327(31)	169(17)	-118(18)	25(12)	27(19)
F2	234(27)	310(37)	442(51)	-44(26)	76(31)	256(38)
F3	103(11)	204(18)	140(13)	-58(11)	5(9)	53(12)
F4	218(24)	322(36)	274(29)	-108(24)	-107(23)	218(29)
F5	184(20)	346(35)	228(25)	-83(23)	-44(19)	192(27)
F6	188(21)	244(26)	355(37)	7(20)	24(24)	-185(29)
C1	28(11)	68(14)	83(16)	-8(9)	3(10)	-2(14)
C2	28(10)	72(17)	100(20)	-21(10)	30(11)	-19(13)
C3	42(12)	122(23)	75(17)	-38(14)	-3(10)	35(16)
C4	56(12)	74(15)	78(16)	-10(11)	-6(11)	-26(14)
C5	64(13)	86(16)	43(11)	-6(11)	-6(10)	11(14)
C6	163(31)	11(13)	218(41)	-8(16)	-79(34)	16(18)

C7	104(20)	112(24)	76(17)	58(20)	4(16)	30(18)
C8	80(23)	38(14)	259(44)	7(15)	-107(26)	34(23)
C9	64(16)	100(24)	120(27)	-23(15)	25(17)	25(21)
C10	211(46)	131(38)	87(24)	118(36)	-56(26)	-48(23)
C11	41(4)					
C12	48(4)					
C13	58(5)					
C14	83(6)					
C15	107(8)					
C16	90(7)					
C21	42(4)					
C22	59(5)					
C23	79(6)					
C24	89(7)					
C25	93(7)					
C26	61(5)					
C31	52(4)					
C32	78(6)					
C33	92(7)					
C34	87(6)					
C35	84(6)					
C36	81(6)					
C41	75(6)					
C42	76(6)					
C51	77(6)					
C52	11[illegible]					
O1	[illegible]	257(42)	160(29)	144(37)	14(28)	64(29)

C61	150(15)					
C62	164(17)					
C63	160(17)					
C64	175(19)					
O2	134(25)	155(28)	215(103)	51(20)	149(42)	141(43)
C71	412(64)					
C72	251(27)					
C73	301(34)					
C74	227(23)					

$[Cp_2Ti(\mu\text{-}SEt)_2CuPCy_3]PF_6$ (4)

Atom	U11	U22	U33	U12	U13	U23
Cu	48(1)	46(1)	49(1)	-7(0)	5(0)	-6(0)
Ti	40(1)	46(1)	45(1)	-7(1)	2(1)	1(1)
S1	44(1)	43(1)	52(1)	-1(1)	8(1)	2(1)
S2	56(1)	47(1)	55(1)	3(1)	4(1)	4(1)
P1	50(1)	39(1)	58(1)	-3(1)	-1(1)	-9(1)
P2	112(2)	94(2)	84(2)	11(2)	56(2)	15(2)
F1	341(16)	145(9)	336(15)	-149(10)	238(13)	-102(9)
F2	152(8)	195(11)	270(13)	25(7)	60(9)	-70(9)
F3	237(14)	206(13)	573(30)	22(10)	257(18)	-127(16)
F4	256(11)	139(8)	175(8)	-95(7)	112(8)	-23(6)
F5	291(15)	271(15)	95(6)	-55(11)	-27(8)	-4(8)
F6	400(20)	223(14)	107(7)	-46(13)	65(10)	11(7)
C11	64(5)	59(6)	74(6)	-3(5)	14(5)	-18(5)
C12	76(6)	67(7)	99(8)	13(5)	15(6)	-15(6)

C13	89(8)	85(9)	184(14)	31(7)	24(9)	-44(9)
C14	114(12)	148(15)	245(21)	-36(11)	101(14)	-125(15)
C15	125(12)	160(15)	134(13)	-16(11)	66(11)	-49(11)
C16	89(8)	112(10)	88(8)	-13(7)	33(6)	-18(7)
C21	82(6)	58(6)	92(7)	-17(5)	34(6)	-18(5)
C22	87(7)	57(7)	112(9)	-24(5)	24(6)	-6(6)
C23	190(17)	110(13)	203(18)	-70(11)	109(15)	-9(12)
C24	147(13)	122(13)	147(14)	-26(11)	63(11)	37(10)
C25	127(10)	104(10)	105(9)	4(8)	56(8)	14(8)
C26	158(12)	74(8)	102(9)	-26(8)	62(8)	4(7)
C31	112(9)	76(9)	112(9)	6(7)	-66(7)	-27(7)
C32	95(8)	71(8)	87(7)	-5(6)	-35(6)	-10(6)
C33	157(14)	151(16)	174(16)	16(12)	-125(12)	-50(13)
C34	108(10)	142(13)	109(10)	-39(9)	-48(8)	23(9)
C35	75(6)	84(8)	74(7)	14(6)	-5(5)	18(6)
C36	133(11)	90(10)	140(12)	23(8)	-84(9)	-5(8)
C1	85(7)	63(7)	53(5)	-10(5)	8(5)	-15(5)
C2	75(6)	61(7)	68(6)	-2(5)	1(5)	-18(5)
C3	99(8)	55(7)	64(6)	-24(6)	-14(6)	-3(5)
C4	56(5)	84(8)	76(7)	-23(5)	-9(5)	-4(6)
C5	62(6)	66(7)	59(6)	0(5)	-12(5)	0(5)
C6	96(8)	95(9)	76(7)	19(7)	48(6)	41(6)
C7	64(6)	80(8)	114(9)	-14(5)	42(6)	12(6)
C8	53(6)	84(8)	102(8)	4(5)	28(5)	13(6)
C9	87(8)	88(8)	79(7)	-19(6)	51(6)	-23(6)
C10	53(6)	162(13)	52(6)	-22(7)	19(5)	-8(7)
C41	57(5)	67(6)	70(6)	-11(4)	28(4)	3(5)

C42	67(6)	80(8)	115(8)	11(5)	47(6)	4(6)
C51	192(13)	73(8)	47(6)	-12(8)	27(7)	21(5)
C52	241(17)	77(9)	95(9)	-46(10)	28(10)	21(7)

$Cp_2Ti(SMe)_2$ (10)

Atom	U11	U22	U33	U23	U13	U12
Ti	29.2(4)	29.2(4)	24.1(6)	0	0	0(1)
S1	38.4(6)	46.5(7)	38.6(7)	6.1(5)	7.5(4)	2.9(5)
C1	56(3)	53(3)	31(2)	-10(2)	-8(2)	-3(2)
C2	48(3)	47(3)	34(2)	2(2)	-12(2)	3(2)
C3	40(3)	68(3)	41(3)	-15(3)	-12(2)	24(3)
C4	31(2)	98(4)	46(3)	-2(3)	-1(2)	-10(3)
C5	54(3)	60(3)	53(3)	-11(3)	-18(3)	-16(3)
C6	37(2)	64(3)	73(3)	10(3)	-1(2)	-5(3)

$[Cp_2Ti(\mu\text{-}SMe)_2Cu(NCMe)_2]PF_6$ (12)

Atom	U11	U22	U33	U23	U13	U12
Ti	40.2(9)	32.0(9)	33.0(9)	3.2(7)	14.2(7)	-2.4(7)
Cu	56.6(8)	44.0(7)	49.0(7)	11.1(6)	20.8(6)	-2.0(6)
S1	37(1)	55(2)	51(2)	10(1)	8(1)	-4(1)
S2	43(1)	49(1)	49(1)	11(1)	14(1)	10(1)
N1	88(7)	48(5)	57(6)	15(4)	32(5)	-2(5)
N2	74(6)	48(5)	59(6)	10(5)	22(5)	-6(5)
P	92(2)	52(2)	84(2)	26(2)	45(2)	9(2)
F1	177(9)	180(9)	124(8)	78(7)	67(7)	37(8)

F2	239(11)	142(8)	135(8)	-17(7)	81(8)	-103(9)
F3	143(9)	156(9)	271(15)	-35(10)	90(10)	-76(8)
F4	152(8)	129(7)	132(7)	28(6)	71(6)	58(6)
F5	238(12)	311(16)	200(12)	208(12)	110(10)	107(12)
F6	147(8)	129(8)	200(10)	49(7)	107(7)	57(6)
C1	71(7)	30(5)	52(6)	-6(5)	29(6)	-3(5)
C2	64(7)	31(5)	71(7)	3(5)	23(6)	8(5)
C3	104(10)	38(6)	70(7)	25(5)	28(7)	2(6)
C4	75(8)	39(6)	79(8)	-2(6)	38(7)	-21(6)
C5	59(7)	34(5)	54(6)	-7(5)	21(5)	-4(5)
C6	98(11)	98(12)	51(8)	-14(8)	24(7)	-42(10)
C7	92(11)	100(11)	59(8)	33(7)	24(7)	10(9)
C8	107(11)	78(9)	48(7)	15(6)	34(7)	-20(9)
C9	57(8)	159(15)	30(6)	-2(8)	26(6)	15(9)
C10	199(17)	45(7)	53(8)	6(6)	76(10)	22(10)
C11	76(8)	48(6)	66(8)	19(6)	24(6)	-1(5)
C12	94(8)	60(7)	54(6)	20(5)	40(6)	17(6)
C21	74(8)	47(7)	62(7)	3(6)	25(6)	-19(6)
C22	108(10)	56(7)	116(11)	-7(7)	57(9)	-2(7)
C31	49(6)	77(8)	87(8)	11(7)	34(6)	7(6)
C41	70(7)	88(8)	50(6	27(6)	1(6)	6(6)

$Cp_2V(SMe)_2$ (15)

Atom	U11	U22	U33	U23	U13	U12
V	26.7(4)	26.7(4)	20.2(6)	0	0	0(1)
S	34.9(7)	42.5(7)	32.9(7)	3.7(5)	6.9(5)	1.7(5)

C1	52(3)	57(3)	28(3)	-12(2)	-14(3)	4(2)
C2	43(3)	36(2)	30(3)	3(2)	-13(2)	1(2)
C3	39(3)	47(3)	36(3)	-7(3)	-6(2)	14(3)
C4	29(2)	96(5)	37(3)	-6(3)	2(2)	-7(3)
C5	42(3)	59(3)	51(3)	1(3)	-16(3)	-17(3)
C6	32(3)	69(4)	53(3)	5(3)	-2(2)	-6(3)

$(Cp_2Ti(\mu\text{-}SMe)_2)_2Ni$ (22)

Atom	U11	U22	U33	U23	U13	U12
Ti	26.9(8)	46.6(10)	47.0(8)	0	0	1.8(6)
Ni	30.4(5)	30.4(5)	45.6(7)	0	0	0
S	33(1)	38(1)	56(1)	5(1)	1(1)	-3(1)
C1	33(4)	82(5)	74(4)	-5(4)	25(3)	-4(3)
C2	34(3)	76(5)	52(4)	-3(4)	5(3)	12(3)
C3	49(4)	52(4)	81(5)	-14(4)	13(4)	9(3)
C4	50(4)	106(7)	73(5)	-47(5)	5(4)	10(4)
C5	58(4)	101(7)	58(5)	-1(4)	16(4)	22(5)
C6	37(3)	59(4)	80(5)	-3(4)	0(3)	-9(3)

$(Ni(\mu\text{-}SMe)_2)_6$ (23)

Atom	U11	U22	U33	U23	U13	U12
Ni1	31.4(4)	23.1(4)	32.9(4)	1.7(3)	-6.1(3)	-2.2(3)
Ni2	29.7(4)	22.8(4)	36.8(4)	-1.0(3)	-5.0(3)	-1.0(3)
Ni3	33.7(4)	23.3(4)	34.3(4)	1.1(3)	-4.5(3)	-1.6(3)
S1	34(1)	25(1)	39(1)	-1(1)	-7(1)	-1(1)

S2	30(1)	26(1)	39(1)	-2(1)	-5(1)	4(1)
S3	35(1)	35(1)	42(1)	-1(1)	-8(1)	3(1)
S4	44(1)	23(1)	38(1)	1(1)	-3(1)	-5(1)
S5	37(1)	24(1)	38(1)	2(1)	-5(1)	1(1)
S6	38(1)	31(1)	34(1)	2(1)	-10(1)	-3(1)
C1	56(4)	49(4)	42(4)	5(3)	5(3)	-13(3)
C2	59(4)	36(4)	42(4)	4(3)	-18(3)	-2(3)
C3	34(4)	66(5)	65(5)	-14(4)	-13(3)	-2(3)
C4	51(4)	38(4)	49(4)	7(3)	5(3)	9(3)
C5	45(4)	39(4)	48(4)	-9(3)	-1(3)	1(3)
C6	52(4)	36(4)	57(4)	12(3)	-12(4)	-3(3)

$((COD)Rh(\mu\text{-}SMe))_2$ (26)

Atom	U11	U22	U33	U23	U13	U12
Rh1	31.8(4)	32.6(4)	29.1(4)	2.1(3)	-2.4(3)	-2.8(3)
Rh2	40.0(4)	43.3(5)	26.3(4)	1.6(3)	-1(1)	1(1)
S1	50(2)	40(1)	34(2)	5(1)	-5(1)	8(1)
S2	36(1)	48(1)	32(2)	-1(1)	-4(1)	-11(1)
C1	92(9)	44(6)	54(7)	1(5)	-1(6)	7(6)
C2	64(7)	55(6)	45(7)	1(7)	12(5)	-15(5)
C11	43(2)					
C12	43(2)					
C13	73(3)					
C14	70(3)					
C15	52(3)					
C16	48(2)					

C17	84(4)
C18	66(3)
C21	47(2)
C22	57(3)
C23	87(4)
C24	78(4)
C25	59(3)
C26	51(3)
C27	69(3)
C28	61(3)

[1]Thermal parameters multiplied by 10 and are given in $Å^2$

Table A1.2: Hydrogen Positions and Thermal Parameters[1]

$[Cp_2Ti(\mu\text{-}SEt)_2CuPPh_3]PF_6 \cdot 1.62$ THF (3·1.62 THF)

Atom	x	y	z	U	Atom	x	y	z	U
H1	4571	4408	3989	53	H2	4693	4761	2749	77
H3	4442	6308	2541	77	H4	4182	6928	3757	61
H5	4311	5750	4668	64	H6	3091	7056	2506	101
H7	2381	5923	1701	95	H8	1239	5199	2407	104
H9	1305	5974	3553	93	H10	2327	7075	3581	89
H12	831	3979	4643	52	H13	-522	4361	4995	74
H14	-1870	3709	4440	92	H15	-1864	2676	3533	149
H16	-512	2294	3181	92	H22	895	1889	4869	62
H23	1725	1078	5820	83	H24	3275	894	5891	91
H25	3994	1523	5012	107	H26	3164	2334	4061	74
H32	1164	1002	3439	80	H33	894	88	2425	103
H34	653	640	1229	88	H35	682	2107	1048	110
H36	952	3022	2062	110	H41A	3706	3872	2397	91
H41B	3828	3451	3166	91	H42A	3993	2413	2283	97
H42B	3022	2429	1831	97	H42C	3193	2165	2652	97
H51A	3928	4413	5126	88	H51B	3025	4503	4576	88
H52A	3223	3851	6032	129	H52B	2267	3862	5550	129
H52C	2731	4704	5834	129	H61	4065	8422	2578	85
H61B	3647	8332	3276	85	H62	3339	9623	2248	116
H62B	2675	9289	2725	116	H63	3102	10297	3530	89
H63B	3765	10632	3052	89	H64	4160	9542	4240	95
H64B	4810	10180	3977	95	H71	-113	9452	4729	148

H71B	-46	8504	4529	148	H72	1330	9523	5250	143
H72B	1237	8553	5339	143	H73	2109	8343	4535	160
H73B	2201	9313	4446	160	H74	1000	8250	3566	132
H74B	1405	908	3	3328					

$[Cp_2Ti(\mu\text{-}SEt)_2CuPCy_3]PF_6$ (4)

Atom	x	y	z	U	Atom	x	y	z	U
H11	4902	4585	9021	73	H12A	3403	4765	7169	93
H12B	2190	4482	7235	93	H13A	3013	5102	8740	124
H13B	1478	5054	7753	124	H14A	824	4588	8877	148
H14B	1274	4931	9706	148	H15A	2384	4406	10723	133
H15B	3591	4683	10612	133	H16A	4173	4107	10114	107
H16B	2639	4083	9112	107	H21	4840	4441	6351	84
H22A	6298	4782	7711	95	H22B	7637	4517	7866	95
H23A	8053	4971	6710	135	H23B	6392	4980	5912	135
H24A	7577	4755	4767	136	H24B	8540	4501	5785	136
H25A	5649	4381	4354	113	H25B	7006	4119	4540	113
H26A	6851	3917	6309	110	H26B	5194	3933	5503	113
H31	7163	3935	8505	126	H32A	6915	4184	10563	929
H32B	7646	4364	9670	93	H33A	9334	4129	11482	193
H33B	9661	4017	10296	193	H34A	10043	3503	11341	134
H34B	8684	3567	11812	134	H35A	7824	3126	10537	84
H35B	8704	3254	9673	84	H36A	5859	3418	9576	142
H36B	6509	3359	8510	142	H1	1637	3141	3929	80
H2	2091	2532	4974	89	H3	-194	2356	5543	91
H4	-2122	2854	4691	92	H5	-1037	3327	3726	78

H6	1534	2644	8379	90	H7	-1142	2627	7028	88
H8	-2009	3288	6601	87	H9	47	3693	7748	86
H10	2237	3305	8851	85	H41A	5349	3113	6142	73
H41B	3972	2925	5239	73	H42A	5785	2512	5680	89
H42B	4737	2365	6382	89	H42C	6231	2556	7077	89
H51A	1125	3742	3703	102	H51B	1445	3801	5085	102
H52A	1529	4371	3449	134	H52B	1865	4432	4832	134
H52C	260	4330	4039	134					

$Cp_2Ti(SMe)_2$ (10)

Atom	x	y	z	U	Atom	x	y	z	U
H1	-801	-971	8008	60	H2	-839	1682	8427	10
H3	-2540	1973	9762	40	H4	-3487	-444	10203	45
H5	-2522	-2249	9088	60	H6A	4023	472	9304	40
H6B	3655	-716	10019	40	H6C	3148	855	10182	40

$[Cp_2Ti(\mu\text{-}SMe)_2Cu(NCMe)_2]PF_6$ (12)

Atom	x	y	z	U	Atom	x	y	z	U
H1	3239	8484	10045	54	H2	1219	9060	8359	62
H3	2963	9424	7035	71	H4	6048	9070	7925	69
H5	6228	8533	9787	58	H6	1182	5732	5135	82
H7	1554	7482	5027	96	H8	4611	8061	5654	78
H9	6322	6646	6405	82	H10	4086	5116	6025	82
H12A	3082	6232	12625	76	H12B	1657	5309	12285	76
H12C	1138	6416	12165	76	H22A	2163	1787	5138	98

H22B	1888	1566	6294	98	H22C	3726	1939	6323	98
H31A	-1310	7080	8702	76	H31B	-860	8009	8388	76
H31C	471	7679	9415	76	H41A	6029	6218	10648	76
H41B	5128	7280	10749	76	H41C	6938	7190	10517	76

$Cp_2V(SMe)_2$ (15)

Atom	x	y	z	U	Atom	x	y	z	U
H1	-802	-1042	8009	60	H2	-760	1611	8460	10
H3	-2488	1979	9802	40	H4	-3514	-356	10258	60
H5	-2580	-2275	9133	60	H6A	3892	611	9329	40
H6B	3622	-608	10058	40	H6C	3263	978	10315	40

$(Cp_2Ti(\mu\text{-}SMe)_2)_2Ni$ (22)

Atom	x	y	z	U	Atom	x	y	z	U
H1	6331	-853	1694	65	H2	6874	1472	874	10
H3	8818	3544	1340	72	H4	9731	2501	2474	83
H5	8270	-181	2703	75	H6A	-3802	-2639	10809	65
H6B	-3505	-2752	10052	65	H6C	-3856	-1051	10377	65

$(Ni(\mu\text{-}SMe)_2)_6$ (23)

Atom	x	y	z	U	Atom	x	y	z	U
H1A	3101	3342	8431	51	H1B	2699	4628	8531	51
H1C	3864	4231	9091	51	H2A	2160	6583	4284	48
H2B	3521	6534	4265	48	H2C	2887	7557	4866	48

H3A	2	3610	4558	57	H3B	741	2485	4701	57
H3C	471	2961	3500	57	H4A	4297	752	5808	49
H4B	3917	1392	6903	49	H4C	4896	1914	6146	49
H5A	5138	9526	7439	48	H5B	5375	8500	8261	48
H5C	4097	8893	8017	48	H6A	7606	5161	8447	52
H6B	6847	4448	7606	52	H6C	6454	4578	8856	52

$((COD)Rh(\mu\text{-}SMe))_2$ (26)

Atom	x	y	z	U	Atom	x	y	z	U
H1A	2517	-1311	6688	62	H1B	1568	-712	6141	62
H1C	904	-652	6780	62	H2A	2500	6000	6938	52
H2B	1784	5966	6284	52	H2C	3588	5966	6397	52
H11	-525	4889	6531	50	H12	433	4570	7439	58
H13A	-2308	4043	7923	76	H13B	-719	3597	8222	76
H14A	-1659	1702	8151	77	H14B	-2909	2127	7660	77
H15	-276	755	7478	53	H16	-835	836	6467	53
H17A	-3591	1950	6544	87	H17B	-2575	2143	5988	87
H18A	-2834	4170	6154	66	H18B	-3335	3931	6809	66
H21	2211	4795	5348	48	H22	4747	4108	5366	60
H23A	5655	2220	4930	91	H23B	4863	2996	4395	91
H24A	2965	1583	4284	81	H24B	4289	633	4515	81
H25	2993	109	5300	58	H26	429	1135	5507	52
H27A	-571	2749	5063	71	H27B	-92	2004	4488	71
H28A	1746	3390	4313	65	H28B	553	4335	4600	65

[1]Positional parameters multiplied by 10^4; thermal parameters multiplied by 10^3 and given in $Å^2$.

Table A1.3: **Bond Distances and Angles Associated with the Cyclohexyl and Cyclopentadienyl Rings and the PF_6 Anion**

$[Cp_2Ti(\mu\text{-}SEt)_2CuPPh_3]PF_6 \cdot 1.62$ THF (3·1.62 THF)

Distances (Å)

C1-C2	1.31(4)	C2-C3	1.38(4)	C3-C4	1.42(3)
C4-C5	1.37(3)	C5-C1	1.42(3)	C6-C7	1.30(5)
C7-C8	1.48(6)	C8-C9	1.31(6)	C9-C10	1.25(6)
C10-C6	1.39(7)	P2-F1	1.51(3)	P2-F2	1.48(3)
P2-F3	1.55(2)	P2-F4	1.46(3)	P2-F5	1.48(2)
P2-F6	1.54(4)				

Angles (Degrees)

Ti-C1-C2	75(1)	Ti-C1-C5	73(1)	Ti-C2-C3	73(1)
Ti-C2-C1	73(1)	Ti-C3-C4	71(1)	Ti-C3-C2	73(1)
Ti-C4-C5	74(1)	Ti-C4-C3	73(1)	Ti-C5-C1	72(1)
Ti-C5-C4	72(1)	Ti-C6-C7	76(2)	Ti-C6-C10	73(2)
Ti-C7-C8	73(2)	Ti-C7-C6	73(2)	Ti-C8-C9	75(2)
Ti-C8-C7	71(2)	Ti-C9-C10	72(2)	Ti-C9-C8	73(2)
Ti-C10-C6	72(2)	Ti-C10-C9	77(3)	F1-P2-F2	93(2)
F1-P2-F3	177(1)	F2-P2-F3	84(2)	F1-P2-F4	92(1)
F2-P2-F4	91(2)	F3-P2-F4	89(1)	F1-P2-F5	88(1)
F2-P2-F5	92(2)	F3-P2-F5	92(1)	F4-P2-F5	177(2)
F1-P2-F6	90(2)	F2-P2-F6	175(2)	F3-P2-F6	93(2)
F4-P2-F6	93(2)	F5-P2-F6	84(2)		

$[Cp_2Ti(\mu\text{-}SEt)_2CuPCy_3]PF_6$ (4)

Distances (Å)

C1-C2	1.38(1)	C2-C3	1.39(2)	C3-C4	1.42(1)
C4-C5	1.34(2)	C5-C1	1.42(1)	C6-C7	1.40(1)
C7-C8	1.41(2)	C8-C9	1.36(1)	C9-C10	1.39(2)
C10-C6	1.39(2)	C11-C12	1.50(1)	C12-C13	1.54(2)
C13-C14	1.55(3)	C14-C15	1.50(2)	C15-C16	1.48(2)
C16-C11	1.56(2)	C21-C22	1.50(1)	C22-C23	1.53(2)
C23-C24	1.44(3)	C24-C25	1.50(2)	C25-C26	1.53(2)
C26-C21	1.46(2)	P2-F1	1.53(1)	P2-F2	1.55(1)
P2-F3	1.46(2)	P2-F4	1.54(1)	P2-F5	1.48(1)
P2-F6	1.53(1)				

Angles (Degrees)

Ti-C1-C2	73.8(6)	Ti-C1-C5	72.8(6)	Ti-C2-C3	72.7(6)
Ti-C2-C1	72.3(6)	Ti-C3-C4	72.2(5)	Ti-C3-C2	73.3(6)
Ti-C4-C5	73.8(5)	Ti-C4-C3	72.9(5)	Ti-C5-C1	72.2(5)
Ti-C5-C4	73.3(5)	Ti-C6-C7	71.9(7)	Ti-C6-C10	74.9(7)
Ti-C7-C8	72.4(7)	Ti-C7-C6	73.9(7)	Ti-C8-C9	75.4(7)
Ti-C8-C7	72.8(7)	Ti-C9-C10	74.3(7)	Ti-C9-C8	71.5(7)
Ti-C10-C6	71.6(6)	Ti-C10-C9	72.4(6)	C11-C12-C13	110.0(9)
C12-C13-C14	111(1)	C13-C14-C15	111(1)	C14-C15-C16	110(1)
C15-C16-C11	112(1)	C16-C11-C12	109.8(8)	C21-C22-C23	113(1)
C22-C23-C24	116(1)	C23-C24-C25	116(2)	C24-C25-C26	114(1)
C25-C26-C21	115(1)	C26-C21-C22	116(1)	C31-C32-C33	115.9(9)
C32-C33-C34	116.4(9)	C33-C34-C35	114.3(9)	C34-C35-C36	119.0(8)

C35-C36-C31	117.8(8)	C36-C31-C32	116.4(8)	F1-P2-F2	8.2(7)
F1-P2-F3	89.2(8)	F2-P2-F3	169.7(9)	F1-P2-F4	178.3(8)
F2-P2-F4	90.3(6)	F3-P2-F4	92.4(7)	F1-P2-F5	88.6(7)
F2-P2-F5	83.8(7)	F3-P2-F5	106.1(9)	F4-P2-F5	90.5(7)
F1-P2-F6	93.0(8)	F2-P2-F6	87.0(8)	F3-P2-F6	83.2(9)
F4-P2-F6	87.7(7)	F5-P2-F6	170.6(9)		

APPENDIX TWO

CRYSTALLOGRAPHIC STUDIES OF TWO SYNTHETIC MODELS FOR METALLOBLEOMYCINS

A2.1 Introduction

Bleomycins are a family of anti-tumor drugs which cause DNA strand cleavage in the presence of transition metal ions and molecular oxygen. However, the precise nature of the metal binding site is not known and has been the subject of many studies.[155] In this chapter, the crystallographic study of two synthetic models for metallobleomycin $[CuCl(C_3H_3N_2CH_2CH_2)N(COC_6H_4N)]_2$(**28**) and $[CuBr(C_3H_3N_2CH_2CH_2)N(COC_5H_4BrN_2)]_2$ (**29**) is reported.

A2.2 Experimental Section

(i) X-ray Data Collection and Reduction Green crystals of **28** or **29** were obtained by crystallization from methanol and supplied by Dr. P. K. Mascharak (University of California, Santa Cruz). Diffraction experiments were performed on a four-circle Syntex $P2_1$ diffractometer with graphite-monochromatized Mo Kα radiation. The initial orientation matrices were obtained from 15 machine-centred reflections selected from rotation photographs. These data were used to determine the crystal systems. Partial rotation photographs around each axis were consistent with monoclinic crystal systems. For **28**, 30 high-angle reflections ($22°<2\theta<25°$) were used to obtain the final lattice parameters and the orientation matrix while for **29**, the initial 15 reflections were employed. Machine parameters, crystal data, and data collection parameters are summarized in Table A2.1. The observed extinctions were consistent with the space groups $P2_1/n$ and $P2_1/c$ for **28** and **29**, respectively. $\pm h,+k,+l$ data were collected over the range $4.5°<2\theta<45.0°$ for both **28** and **29**. Three standard reflections were recorded every

197 reflections in both cases. Their intensities showed no statistically significant change over the duration of data collection. The data were processed using the SHELX-76 program package. Analytical absorption corrections were applied to both data sets employing the program ABSORB.

(ii) Structure Solutions and Refinements Non-hydrogen atomic scattering factors were taken from the literature tabulation.[121-123] The Cu atom position for **28** was determined using the heavy atom (Patterson) method. The Cu and Br atom positions for **29** were obtained employing direct methods. The remaining non-hydrogen atoms in both cases were located from successive difference Fourier map calculations. Refinement was carried out by using full-matrix least squares techniques on F, minimizing the function $w((|Fo|-|Fc|)^2$ where the weight, w, is defined as $4Fo^2/\sigma^2(Fo)^2$ and Fo and Fc are the observed and calculated structure factor amplitudes. In the final cycles of refinement all non-hydrogen atoms were assigned anisotropic temperature factors. Hydrogen atom positions were allowed to ride on the carbon to which they are bonded assuming a C-H bond length of 0.95 Å. Hydrogen atom temperature factors were fixed at 1.10 times the isotropic temperature factor of the C atom to which they are bonded. In all cases the hydrogen atom contributions were calculated, but not refined. The maximum Δ/σ values on any of the parameters in the final cycles of refinement are also given in Table A2.1. Final difference Fourier map calculations showed no peaks of chemical significance; the magnitudes of the largest peaks in the final difference maps and the location of these residuals are given in Table A2.1. Tables of Crystallographic Parameters (Table A2.1), Positional Parameters (Table A2.2), Selected Bond Distances and Angles (Table A2.3), Thermal Parameters (Table A2.4) and Hydrogen Atom Parameters (Table A2.5) appear in this Appendix.

A2.3 Results and Discussion

Single crystals of **28** were obtained by slow addition of methanol to an aqueous solution of **28**. An X-ray crystallographic study of this species revealed that the crystals were made up of unit cells each containing four CuLCl:H_2O units. These units pair up to result in centrosymmetric chloro-bridged dimers. The closest non-bonded contact between dimers is 2.335 Å (O-H2). Hydrogen bonding between the water molecule in the asymmetric unit and the amide oxygen atom is evidenced by the close contact (1.727 Å, O-HO2A). Selected interatomic dimensions are given in Table A2.3. An ORTEP drawing of the dimeric molecule is shown in Figure A2.1. The geometry about the copper atom can be described essentially as a distorted square-based pyramid. The three nitrogens of the peptide ligand are in the axial plane with the pyridine and the imidazole nitrogen atoms being trans. The peptide nitrogen is trans to a bridging chlorine atom. The second bridging chlorine is in the axial position. It is clear both from charge balance and molecular geometry that the peptide nitrogen is not protonated, thus ligand is both tridentate and anionic. This type of binding for a peptide linkage to a metal atom has been previously observed. Cu-N bond distances are typical of those found in other related compounds.[156] The Cu-Cl distances are within the range observed in other chloro-bridged dimers. The axial Cu-Cl' bond is considerably longer than the Cu-Cl bond in the equatorial plane (i.e., 2.831(1) vs 2.319(1) Å). The Cu-Cu' distance of 3.693 Å is very similar to that found in other μ-dichloro-copper species.

Single crystals of **29** were obtained by slow evaporation of methanol solution of **29**. An X-ray crystallographic study of this species revealed that the crystals were made up of unit cells, each containing four CuLBr units. These units are bridged through Br, resulting in chain-type structures through the lattice. Selected interatomic dimensions are given in Table A1.3. An ORTEP drawing of the repeating unit is shown in Figure A1.2. The chain-like structure within the lattice is shown in an ORTEP drawing in Figure A1.3. The donor atoms comprising the coordination sphere of copper are in a distorted, square-pyramidal geometry. Three nitrogens of the deprotonated peptide ligand occupy

Table A2.1: Crystallographic Parameters $[CuCl(C_3H_3N_2CH_2CH_2)N(COC_6H_4N)]_2 \cdot H_2O$ and $[CuBr(C_3H_3N_2H_2CH_2)N(COC_5H_4BrN_2)]_2$

	28	29
Formula	$C_{11}H_{13}ClCuN_4O_2$	$C_{11}H_{11}Br_2CuN_5O$
Crystal colour, form	blue prisms	green blocks
Crystal system	monoclinic	monoclinic
Space group	$P2_1/n$	$P2_1/c$
a (Å)	10.134(2)	18.002(7)
b (Å)	14.141(4)	9.951(4)
c (Å)	9.198(4)	22.79(1)
β (deg)	95.01(3)	112.27(3)
Volume ($Å^3$)	1313.1(7)	3778(3)
Density (gcm^{-1})	1.68	1.36
Z	4	4
Crystal dimens (mm)	0.35 x 0.29 x 0.33	0.46 x 0.46 x 0.77
Crystal faces	$(1\bar{1}0)$ $(\bar{1}10)$ (110)	(100) $(\bar{1}00)$ (010)
	$(\bar{1}\bar{1}0)$ (101) $(10\bar{1})$	$(0\bar{1}0)$ (001) $(00\bar{1})$
Abs coeff, (cm^{-1})	17.88	69.14
Radiation λ, (Å)	Mo Kα (0.71069)	Mo Kα (0.71069)
Temp.(°C)	24	24
Scan speed (deg/min)	2.0-5.0 (θ/2θ scan)	2.0-5.0 (θ/2θ scan)
Scan range (deg)	1.0 below Kα1	1.0 below Kα1
	1.1 above Kα2	1.0 above Kα2
Bkgd/scan time ratio	0.5	0.5
No. of unique data	1929	2087

Data $F\sigma^2>3\sigma(F\sigma^2)$	1581	2565
No. of variables	172	261
R (%)	2.99	4.66
Rw (%)	3.96	5.15
Largest Δ/σ in the final least squares cycle	0.008	0.002
Maximum residual electron density ($e/Å^3$)	0.5	0.39
Atom associated	Cu	C45

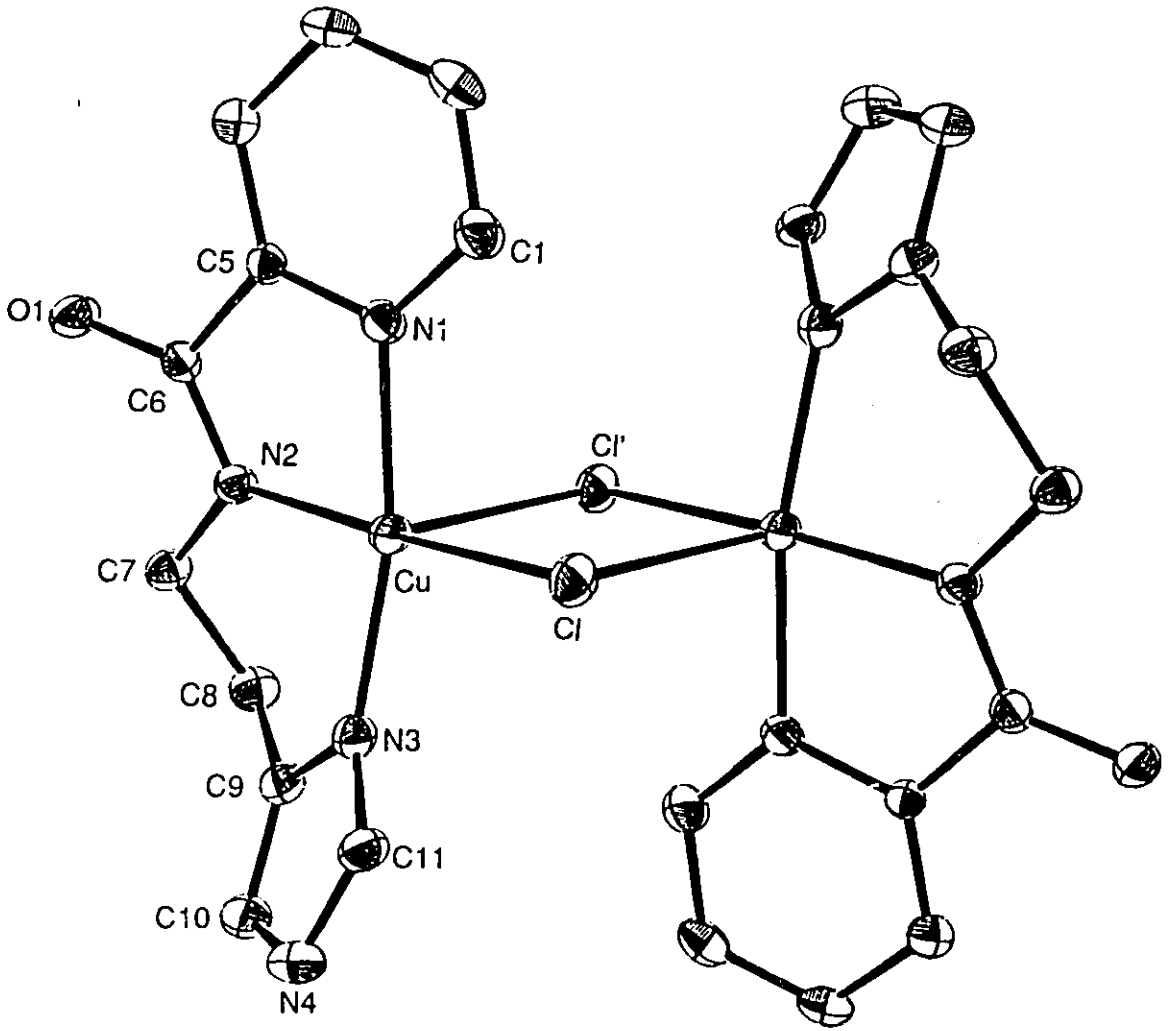

Figure A2.1: ORTEP Drawing of $[CuCl(C_3H_3N_2CH_2CH_2)N(COC_6H_4N)].H_2O$

the basal sites and the bromine which bridges to the next repeating unit occupies the apical position.

A2.4 Summary

The crystal structures reported in this Appendix are part of a continuing investigation into elucidation of the binding site in bleomycin. In addition to the structural studies on these compounds, they have been studied by Dr. Mascharak using EPR spectroscopy, magnetic susceptibility and absorption spectroscopy. For a bioinorganic model to be appropriate, it must mimic both the structural and spectroscopic properties of the biological molecule. The X-ray studies of **28** and **29** are an important part of this study since the biological molecule has not been crystallized.

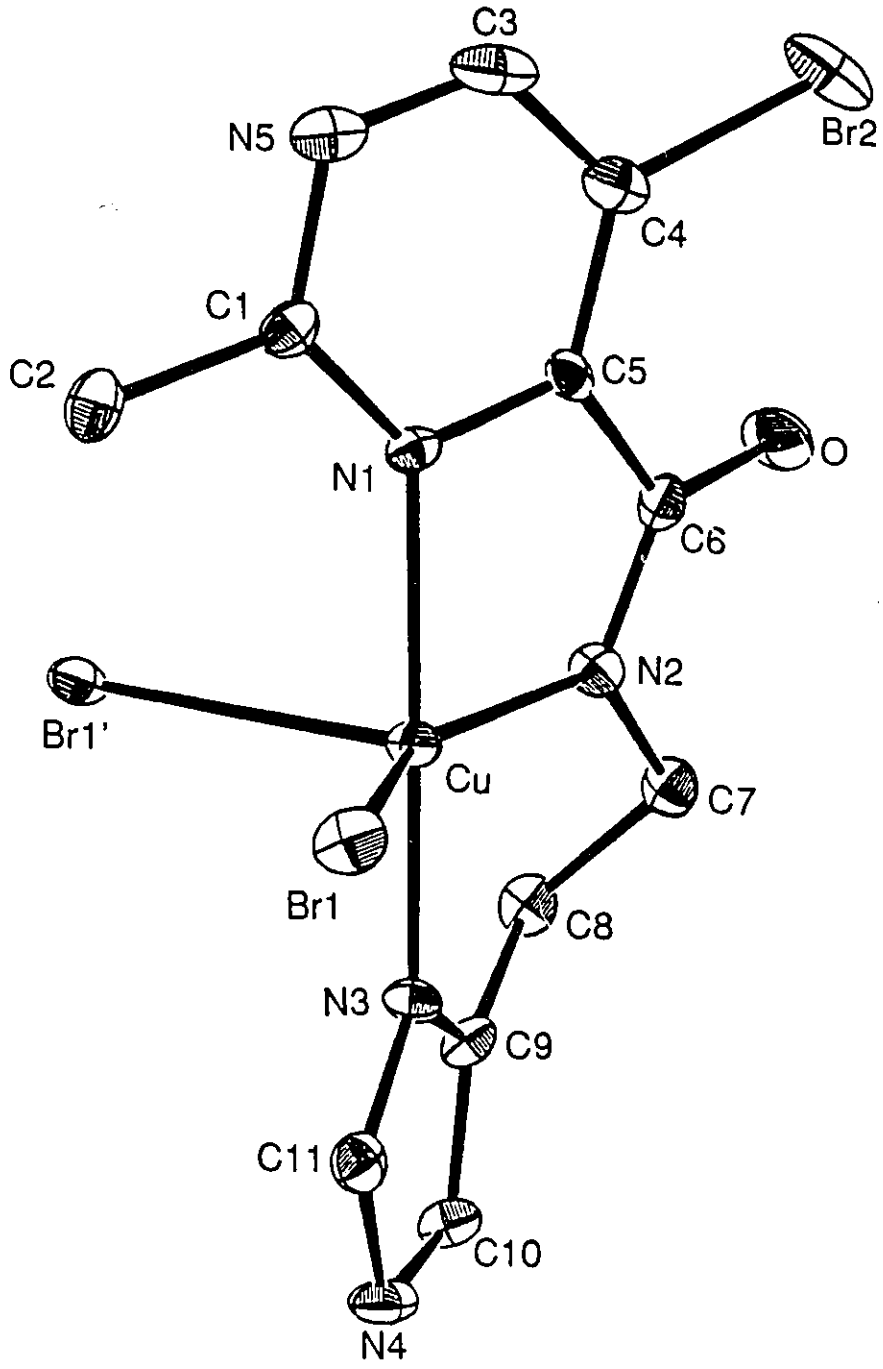

Figure A2.2: ORTEP Drawing of the Monomer of $[[CuBr(C_3H_3N_2CH_2CH_2)N(COC_5H_4BrN_2)]$

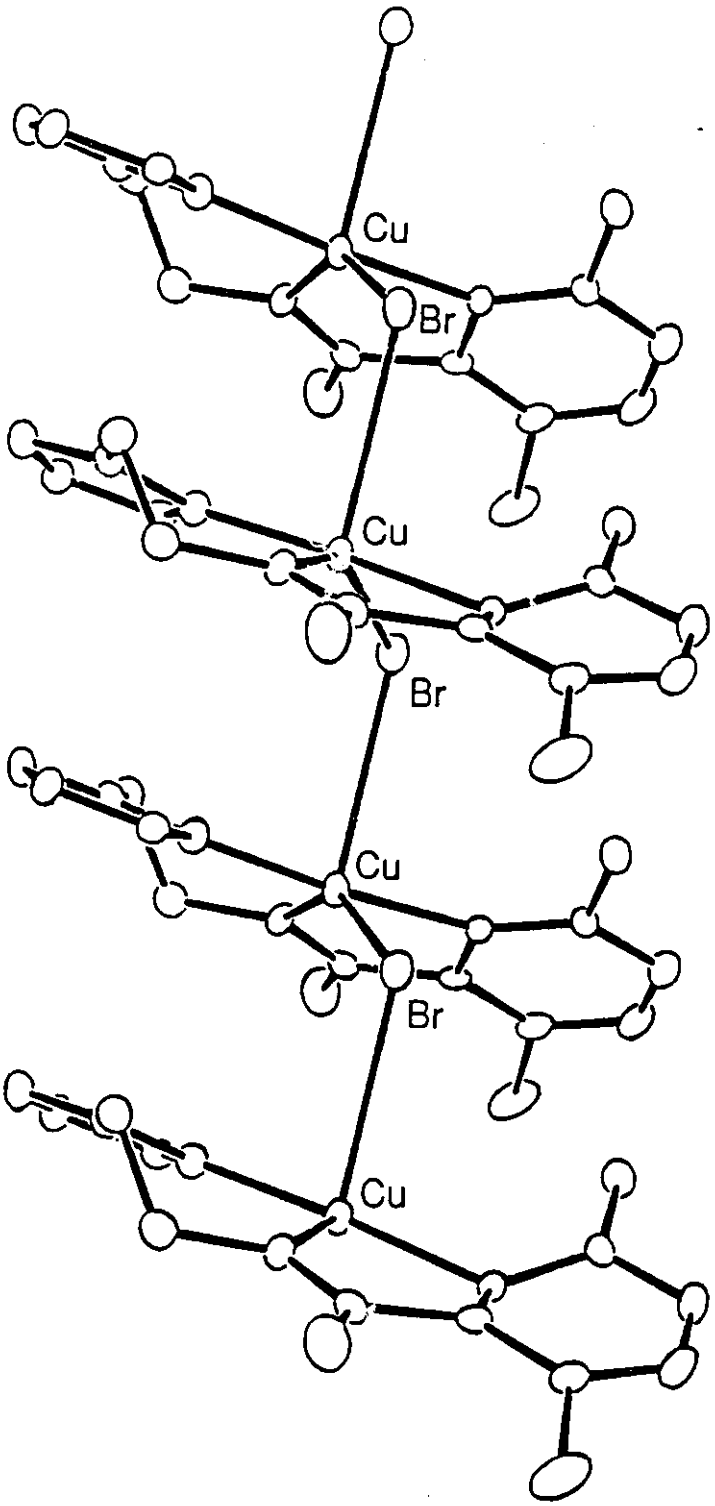

Figure A2.3: ORTEP Drawing of the Chain Structure of $[[CuBr(C_3H_3N_2CH_2CH_2)N(COC_5H_4BrN_2)]$

Table A2.2: Positional Parameters for $[CuCl(C_3H_3N_2CH_2CH_2)N(COC_6H_4N)]_2 \cdot H_2O$ and $[CuBr(C_3H_3N_2CH_2CH_2)N(COC_5H_4BrN_2)]_2$[1]

$[CuCl(C_3H_3N_2CH_2CH_2)N(COC_6H_4N)]_2:H_2O$ (28)

Atom	x	y	z	Atom	x	y	z
Cu	4888(1)	5289(1)	3035(1)	Cl	6680(1)	5377(1)	4779(1)
N1	5308(3)	3958(2)	2444(3)	N2	3515(3)	5145(2)	1395(3)
N3	4522(3)	6655(2)	3175(3)	N4	4827(3)	8188(2)	3110(3)
O1	3030(2)	4240(2)	-682(3)	C1	6144(3)	3326(2)	3130(4)
C2	6336(3)	2448(2)	2572(4)	C3	5709(3)	2205(2)	1246(4)
C4	4841(3)	2848(2)	533(4)	C5	4653(3)	3711(2)	1164(3)
C6	3658(3)	4415(2)	538(3)	C7	2435(3)	5804(2)	916(4)
C8	2174(3)	6501(2)	2141(4)	C9	3346(3)	7084(2)	2614(4)
C10	3541(4)	8023(2)	2557(4)	C11	5375(4)	7354(2)	3467(4)
O2	6102(3)	9872(2)	2602(3)				

$[CuBr(C_3H_3N_2CH_2CH_2)N(COC_5H_4BrN_2)]_2$ (29)

Atom	x	y	z	Atom	x	y	z
Cu	3106(1)	3039(1)	1484(1)	Br1	2474(1)	1774(1)	2481(1)
Br2	911(1)	5680(1)	3838(2)	O	3255(7)	5311(4)	3126(10)
N1	1471(6)	3618(4)	1285(9)	N2	3742(6)	4095(4)	2201(10)
N3	4706(6)	2648(4)	1441(9)	N4	6286(7)	1886(5)	1505(11)
N5	-687(7)	3741(5)	900(11)	C1	275(8)	3366(5)	619(11)
C2	-10(9)	2638(6)	-521(13)	C3	-435(10)	4406(7)	1846(15)

C4	735(10)	4727(6)	2504(12)	C5	1706(8)	4322(5)	2177(11)
C6	3000(8)	4619(6)	2578(12)	C7	5016(9)	4363(6)	2464(13)
C8	5499(9)	3993(6)	1049(13)	C9	5649(8)	3128(6)	1261(12)
C10	6624(8)	2648(6)	1290(12)	C11	5117(8)	1906(6)	1570(12)

[1]Parameters multiplied by 10^4

Table A2.3: Selected Bond Distances and Angles $[CuCl(C_3H_3N_2CH_2CH_2)N(COC_6H_4N)]_2 \cdot H_2O$ and $[CuBr(C_3H_3N_2CH_2CH_2)N(COC_5H_4BrN_2)]_2$

$[CuCl(C_3H_3N_2CH_2CH_2)N(COC_6H_4N)]_2 \cdot H_2O$ (28)

Distances (Å)

Cu-Cl	2.319(1)	Cu-Cl'	2.831(1)	Cu-N1	2.014(3)
Cu-N2	1.972(3)	Cu-N3	1.973(3)	N1-C1	1.350(4)
N1-C5	1.346(5)	C1-C2	1.365(5)	C2-C3	1.369(6)
C3-C4	1.390(5)	C4-C5	1.372(5)	C5-C6	1.496(5)
C6-O1	1.265(4)	N2-C6	1.315(5)	N2-C7	1.475(4)
C7-C8	1.537(5)	C8-C9	1.479(5)	N3-C9	1.396(5)
N3-C11	1.325(5)	N4-C11	1.332(5)	N4-C10	1.377(5)
C9-C10	1.345(5)	Cu..Cu'	3.693(1)		

Angles (Degrees)

Cl-Cu-N1	93.8(1)	Cl-Cu-N2	173.0(1)	Cl-Cu-N3	92.4(1)
Cl'-Cu-N1	91.5(1)	Cl'-Cu-N2	96.1(1)	Cl'-Cu-N3	99.2(1)
N1-Cu-N2	81.3(1)	N1-Cu-N3	167.8(1)	Cl-Cu-Cl'	88.9(1)
Cu-Cl-Cu'	91.1(1)	N2-Cu-N3	91.5(1)	Cu-N1-C1	129.1(3)
Cu-N1-C5	112.3(2)	C1-N1-C5	118.6(3)	N1-C1-C2	122.1(4)
C1-C2-C3	119.6(3)	C2-C3-C4	118.8(3)	C3-C4-C5	119.2(4)
C4-C5-C6	122.9(3)	C4-C5-N1	121.7(3)	N1-C5-C6	115.4(3)
C5-C6-O1	118.8(3)	O1-C6-N2	127.7(3)	C5-C6-N2	113.4(3)
C6-N2-Cu	115.6(2)	C6-N2-C7	115.8(3)	Cu-N2-C7	128.2(2)
N2-C7-C8	110.9(3)	C7-C8-C9	112.8(3)	C8-C9-C10	131.0(4)

C8-C9-N3	120.3(3)	N3-C9-C10	108.6(3)	C9-C10-N4	106.9(3)
C10-N4-C11	107.6(3)	N4-C11-N3	111.1(3)	C11-N3-C9	105.7(3)
C11-N3-Cu	128.4(3)	C9-N3-Cu	124.1(2)		

$[CuBr(C_3H_3N_2CH_2CH_2)N(COC_5H_4BrN_2)]_2$ (29)

Distances (Å)

Cu-Br1	2.452(1)	Cu-Br1'	3.027(1)	Cu-N1	2.066(7)
Cu-N2	1.936(7)	Cu-N3	1.950(7)	N1-C1	1.368(10)
N1-C5	1.360(11)	C1-C2	1.494(13)	C1-N5	1.341(11)
N5-C3	1.326(14)	C3-C4	1.383(15)	C4-Br2	1.892(10)
C4-C5	1.391(12)	C5-C6	1.496(13)	C6-O	1.245(11)
N2-C6	1.318(12)	N2-C7	1.473(11)	C7-C8	1.522(13)
C8-C9	1.469(12)	N3-C9	1.386(11)	N3-C11	1.326(11)
N4-C11	1.350(11)	N4-C10	1.364(12)	C9-C10	1.369(12)
Cu..Cu'	4.338(1)				

Angles (Degrees)

Br1-Cu-N1	94.2(2)	Br1-Cu-N2	145.4(2)	Br1-Cu-N3	94.7(2)
Br1'-Cu-N1	87.4(2)	Br1'-Cu-N2	99.0(2)	Br1'-Cu-N3	86.5(2)
N1-Cu-N2	80.6(3)	N1-Cu-N3	170.1(3)	Br1-Cu-Br1'	115.2(2)
Cu-Br1-Cu'	104.2(2)	N2-Cu-N3	92.6(3)	Cu-N1-C1	130.7(6)
Cu-N1-C5	110.0(5)	C1-N1-C5	118.8(7)	N1-C1-C2	119.3(8)
C2-C1-N5	116.6(8)	N1-C1-N5	124.1(8)	C1-N5-C3	116.3(9)
C3-C4-C5	118.0(9)	C3-C4-Br2	117.6(8)	Br2-C4-C5	124.4(8)
C4-C5-C6	125.9(8)	C4-C5-N1	118.8(8)	N1-C5-C6	115.1(7)
C5-C6-O1	119.7(9)	O1-C6-N2	127.3(9)	C5-C6-N2	112.9(8)

C6-N2-Cu	118.0(6)	C6-N2-C7	116.0(7)	Cu-N2-C7	125.9(6)
N2-C7-C8	109.7(7)	C7-C8-C9	112.2(8)	C8-C9-C10	130.6(9)
C8-C9-N3	121.5(8)	N3-C9-C10	107.9(8)	C9-C10-N4	107.3(8)
C10-N4-C11	107.6(3)	N4-C11-N3	110.5(9)	C11-N3-C9	106.8(7)
C11-N3-Cu	128.8(6)	C9-N3-Cu	124.4(5)		

Table A2.4: **Thermal Parameters for $[CuCl(C_3H_3N_2CH_2CH_2)N(COC_6H_4N)]_2 \cdot H_2O$ and $[CuBr(C_3H_3N_2CH_2CH_2)N(COC_5H_4BrN_2)]_2$[1]**

$[CuCl(C_3H_3N_2CH_2CH_2)N(COC_6H_4N)]_2 \cdot H_2O$ (28)

Atom	U11	U22	U33	U23	U13	U12
Cu	33.2(4)	27.3(4)	30.0(4)	-2.1(2)	-8.1(2)	1.5(2)
Cl	34.8(6)	41.8(6)	33.5(6)	-0.5(4)	-8.0(4)	-4.5(3)
O1	54(2)	34(1)	40(2)	-9(1)	-17(1)	10(1)
N1	33(2)	27(2)	33(2)	3(1)	-3(1)	0(1)
N2	30(2)	26(1)	32(2)	-2(1)	-3(1)	2(1)
N3	34(2)	33(2)	32(2)	-1(1)	-2(1)	2(1)
N4	56(2)	29(2)	54(2)	-5(1)	3(2)	-4(1)
C1	38(2)	38(2)	39(2)	3(2)	-4(2)	4(2)
C2	35(2)	33(2)	53(2)	12(2)	2(2)	8(2)
C3	43(2)	22(2)	53(2)	0(2)	7(2)	6(2)
C4	41(2)	32(2)	34(2)	0(2)	4(2)	1(2)
C5	31(2)	26(2)	26(2)	2(1)	0(1)	-4(1)
C6	30(2)	28(2)	29(2)	3(2)	0(2)	-2(1)
C7	31(2)	33(2)	36(2)	-4(1)	0(1)	1(1)
C8	31(2)	36(2)	45(2)	-2(2)	2(2)	8(2)
C9	39(2)	34(2)	31(2)	-3(2)	4(2)	4(2)
C10	49(2)	31(2)	44(2)	-2(2)	2(2)	12(2)
C11	39(2)	32(2)	38(2)	-6(2)	-2(2)	-2(2)
O2	72(2)	50(2)	54(2)	8(1)	-15(2)	-24(2)

$[CuBr(C_3H_3N_2CH_2CH_2)N(CO)C_5H_4BrN_2)]_2$ (29)

Atom	U11	U22	U33	U23	U13	U12
Cu	26.2(6)	25.5(6)	46.4(7)	-1.3(5)	11.0(5)	-2.3(5)
Br1	39.5(6)	38.6(6)	59.4(7)	-7.1(5)	14.6(5)	8.7(5)
Br2	117(1)	45.8(8)	94(1)	16.4(7)	71.7(9)	-2.9(7)
O	65(5)	34(5)	101(6)	2(4)	16(4)	-26(4)
N1	26(4)	36(4)	29(4)	5(3)	9(3)	7(4)
N2	33(4)	37(5)	46(5)	-7(4)	18(4)	-4(4)
N3	38(4)	19(4)	44(5)	7(3)	14(4)	7(3)
N4	40(5)	57(6)	52(5)	22(4)	19(4)	10(4)
N5	39(5)	55(6)	59(6)	12(5)	18(4)	10(5)
C1	32(5)	40(6)	32(5)	-1(4)	7(4)	9(4)
C2	40(5)	49(6)	47(6)	-16(5)	8(5)	-4(5)
C3	54(7)	66(8)	65(8)	29(6)	37(6)	27(7)
C4	58(7)	46(6)	39(6)	19(5)	26(5)	17(5)
C5	44(6)	32(5)	24(5)	9(4)	13(4)	3(4)
C6	38(5)	35(6)	32(5)	-2(5)	3(4)	1(5)
C7	48(6)	36(6)	49(6)	-6(5)	12(5)	-1(5)
C8	44(6)	44(6)	48(6)	-9(5)	15(5)	6(5)
C9	29(5)	43(6)	37(6)	0(5)	4(4)	12(5)
C10	32(5)	44(6)	53(6)	4(5)	10(5)	10(5)
C11	43(6)	51(7)	35(5)	1(5)	15(4)	0(5)

[1]Thermal parameters multiplied by 10^3 and given in $Å^2$

Table A2.5: **Hydrogen Atom Parameters for $[CuCl(C_3H_3N_2CH_2CH_2)N(COC_6H_4N)]_2 \cdot H_2O$ and $[CuBr(C_3H_3N_2CH_2CH_2)N(COC_5H_4BrN_2)]_2$[1]**

$[CuCl(C_3H_3N_2CH_2CH_2)N(COC_6H_4N)]_2 \cdot H_2O$ (28)

Atom	x	y	z	U	Atom	x	y	z	U
H1	614	3499	4030	43	H2	6901	2008	3100	35
H3	5865	1607	821	29	H4	4382	2692	-381	32
H7A	2676	6149	93	36	H7B	1651	5453	654	36
H8A	1924	6152	2955	37	H8B	1470	6910	1798	37
H10	2912	8485	2203	35	H11	6261	7272	3877	32
HO2A	6775	10140	3348	49	HO2B	6454	9967	1661	49
HN4	5271	8808	3130	43					

$[CuBr(C_3H_3N_2CH_2CH_2)N(COC_5H_4BrN_2)]_2$ (29)

Atom	x	y	z	U	Atom	x	y	z	U
H21	643	2457	-932	47	H22	-680	2809	-1510	47
H23	-274	2219	79	47	H3	-1096	4678	2086	47
H7A	5029	4926	2369	47	H7B	5525	4206	3614	47
H8A	6277	4223	1136	46	H8B	4934	4103	-95	46
H10	7393	2815	1181	46	H11	4654	1452	1692	44
HN4	6664	1532	1210	50					

[1]Positional parameters multiplied by 10^4, thermal parameters multiplied by 10^3 and given in $Å^2$

REFERENCES

(1) Collman, J. P.; Hegedus, L. S.; Norton, J, R.; Finke, R. G. Principles and Applications of Organotransition Metal Chemistry, University Science Books, California: 1987.

(2) Lukehart, C. M. Fundamental Transition Organometallic Chemistry, Brooks/Cole Publishing Company, California: 1985.

(3) Tauster, S. J.; Fung, S. C.; Garten, R. L. *J. Am. Chem. Soc.*, **1978**, *100*, 170.

(4) Baker, R. T. K.; Tauster S. J.; Dumesic, J. A. Eds. Strong Metal-Support Interactions, Am. Chem. Soc., Washington, DC: **1986**.

(5) Stevenson, S. A.; Dumesic, J. A.; Baker, R. T. K.; Ruckenstein, E. Metal-Support Interactions in Catalysis, Sintering, and Redispersion, Van Nostrand Reinhold, New York: **1987**.

(6) Masters, C. in Advances in Organometallic Chemistry, Academic Press, New York: **1979**.

(7) Herrmann, W. A. *Angew. Chem. Int. Ed. Engl.*, **1982**, *21*, 117.

(8) Rofer-DePoorter, C. K. *Chem. Rev.*, **1981**, *81*, 447.

(9) Sleight, A. *Science*, **1980**, *208*, 895.

(10) Brady, R. C.; Pettit, R. *J. Am. Chem. Soc.*, **1980**, *102*, 6181.

(11) Cole, T.; Ramage, R.; Cann, K.; Pettit, R. *J. Am. Chem. Soc.*, **1980**, *102*, 6184.

(12) Tauster, S. J.; Fung, S. C.; Baker, R. T. K.; Horsley, J. A. *Science*, **1981**, *211*, 1121.

(13) Tauster, S. J. *Acc. Chem. Res.*, **1987**, *20*, 389.

(14) Tauster, S. J.; Fung, S. C. *J. Catal.*, **1978**, *55*, 29.

(15) Koningsberger, D. C.; Martens, J. H. A.; Prins, R.; Short, D. R.; Sayers, D. E. *J. Phys. Chem.*, **1986**, *90*, 3047.

(16) Sakellson, S.; McMillan, M.; Haller, G. L. *J. Chem. Phys.*, **1986**, *90*, 1733.

(17) Sadeghi, H. R.; Henrich, V. E. *J. Catal.*, **1984**, *87*, 279.

(18) Sheng, T.; Guoxing, X.; Hongli, W. *J. Catal.*, **1988**, *111*, 136.

(19) Sadeghi, H. R.; Henrich, V. E. *J. Catal.*, **1988**, *109*, 1.

(20) Bonneviot, L.; Haller, G. L. *J. Catal.*, **1988**, *113*, 96.

(21) Badyal, J. P. S.; Gellman, A. J.; Lambert, R. M. *J. Catal.*, **1988**, *111*, 383.

(22) Belton, D. N.; Sun, Y. M.; White, J. M. *J. Phys. Chem.*, **1984**, *88*, 5172.

(23) Shpiro, E. S.; Dysenbina, B. B.; Tkachenko, O. P.; Antoshin, G. V.; Minachev, Kh. M. *J. Catal.*, **1988**, *110*, 262.

(24) Hoflund, G. B.; Grogan, Jr., A. L.; Asbury, D. A. *J. Catal.*, **1988**, *109*, 226.

(25) Baker, R. T. K.; Prestridge, E. B.; Garten, R. L. *J. Catal.*, **1979**, *56*, 293.

(26) Horsley, J. A. *J. Am. Chem. Soc.*, **1979**, *101*, 2870.

(27) Levin, M. E.; Salmeron, M.; Bell, A. T.; Somorjai, G. A. *J. Chem. Soc., Faraday Trans. 1*, **1987**, *83*, 2061.

(28) Gambarotta, S.; Floriaani, C.; Chiesi-Villa, A.; Guastini, C. *Organometallics*, **1986**, *5*, 2425.

(29) Belmonte, P. A.; Cloke, F. G. N.; Schrock, R. R. *J. Am. Chem. Soc.*, **1983**, *105*, 2643.

(30) Barger, P. T.; Santarsiero, B. D.; Armantrout, J.; Bercaw, J. E. *J. Am. Chem. Soc.*, **1984**, *106*, 5178.

(31) Mayer, J. M.; Curtis, C. J.; Bercaw, J. E. *J. Am. Chem. Soc.*, **1983**, *105*, 2651.

(32) Choukroun, R.; Gervais, D.; Kalck, P.; Senocq, F. *J. Organomet. Chem.*, **1987**, *335*, C9

(33) Ferguson, G. S.; Wolczanski, P. T.; Párkányi, L.; Zonnevylle, M. C. *Organometallics*, **1988**, *7*, 1967.

(34) Erker, G.; Dorf, U.; Atwood, J. L.; Hunter, W. E. *J. Am. Chem. Soc.*, **1986**, *108*, 2251.

(35) Moloy, K. G.; Marks, T. J. *J. Am. Chem. Soc.*, **1984**, *106*, 7051.

(36) Chatt, J.; Hart, F. A. *J. Chem. Soc.*, **1960**, 2807.

(37) McCleverty, J. A.; Seddon, D. *J. Chem. Soc. Dalton*, **1972**, 2588

(38) Bonnet, J. J.; Galy, J.; De Montauzon, D.; Poilblanc, R. *J. Soc. Chem. Commun.*, **1977**, 47.

(39) Poilblanc, R. *Inorg. Chim. Acta*, **1982**, *62*, 75.

(40) Thorez, A.; Maisonnat, A.; Poilblanc, R. *J. Chem. Soc. Chem. Commun.*, **1977**, 518.

(41) Bonnet, J. J.; Kalck, P.; Poilblanc, R. *Inorg. Chem.*, **1977**, *16*, 1514.

(42) Johnson, B. F. G.; Lewis, J.; Williams, I. G.; Wilson, J. M. *J. Chem. Soc. (A)*, **1967**, 338.

(43) Dev, S.; Imagawa, K.; Mizobe, Y.; Cheng, G.; Wakatsuki, *Organometallics*, **1989**, *8*, 1232.

(44) Harley-Mason, J. *J. Chem. Soc.*, **1952**, 146.

(45) Baker, D. J.; Goodall, D. C.; Moss, D. S. *J. Chem. Soc. Chem. Commun.*, **1969**, 325.

(46) Barclay, G. A.; McPartlin, E. M.; Stephenson, N. C. *Inorg. Nucl. Chem. Lett.*, **1967**, *3*, 397.

(47) McPartlin, E. M.; Stephenson, N. C. *Acta Cryst. B*, **1969**, 1659.

(48) Bayón, J. C.; Briansó, M. C.; Briansó, J. L.; Gonźalez, Duarte, P. *Inorg. Chem.*, **1979**, *18*, 3478.

(49) Briansó, M. C.; Briansó, J. L.; Gaete, W.; Ros, J.; Suñer, C. *J. Chem. Soc. Dalton*, **1981**, 852.

(50) Hagen, K. S.; Holm, R. H. *J. Am. Chem. Soc.*, **1982**, *104*, 5496.

(51) Henkel, G.; Tremel, W.; Krebs, B. *Angew. Chem. Int. Ed. Engl.*, **1983**, *22*, 319.

(52) Christou, G.; Huffman, J. C. *J. Chem. Soc. Chem. Commun.*, **1983**, 558.

(53) Rauchfuss, T. B.; Roundhill, D. M. *J. Am. Chem. Soc.*, **1975**, *97*, 3386.

(54) Herskovitz, T.; DePamphilis, B. V.; Gillum, W. O.; Holm, R. H. *Inorg. Chem.*, **1975**, *14*, 1426.

(55) Zhuang, B.; McDonald, J. W.; Schultz, F.A.; Newton, W. E. *Organometallics*, **1984**, *3*, 943.

(56) Smith, D. A.; Zhuang, B.; Newton, W. E.; McDonald, J. W.; Schultz, F. A. *Inorg. Chem.*, **1987**, *26*, 2524.

(57) Darensbourg, D. J.; Sanchez, K. M.; Reibenspies, J. *Inorg. Chem.*, **1988**, *27*, 3636.

(58) Treichel, P. M.; Nakagaki, P. C. *Organometallics*, **1986**, *5*, 711.

(59) Lyons, L. J.; Tegen, M. H.; Haller, K. J.; Evans, D. H.; Treichel, P. M. *Organometallics*, **1988**, *7*, 357.

(60) Osborne, A. G.; Stone, F. G. A. *J. Chem. Soc. (A)*, **1966**, 1143.

(61) McDonald, J. W. *Inorg. Chem.*, **1985**, *24*, 1734.

(62) Cotton, F. A.; Powell, G. L. *J. Am. Chem. Soc.*, **1984**, *106*, 3371.

(63) Canich, J. A. M.; Cotton, F. A.; Dunbar, K. R.; Falvello, L. R. *Inorg. Chem.*, **1988**, *27*, 804.

(64) Cotton, F. A.; Diebold, M. P.; O'Conner, C. J.; Powell, G. L. *J. Am. Chem. Soc.*, **1985**, *107*, 7438.

(65) Campbell, G. C.; Canich, J. A. M.; Cotton, F. A.; Duraj, S. A.; Haw, J. F. *Inorg. Chem.*, **1986**, *25*, 287.

(66) Alper, H.; Einstein, F. W. B.; Hartstock, F. W.; Willis, A. C. *J. Am. Chem. Soc.*, **1985**, *107*, 173.

(67) Alper, H.; Einstein, F. W. B.; Hartstock, F. W.; Willis, A. C. *Organometallics*, **1986**, *5*, 9.

(68) Alper, H.; Einstein, F. W. B.; Hartstock, F. W.; Willis, A. C. *Organometallics*, **1983**, *2*, 1291.

(69) Hagen, K. S.; Stephan, D. W.; Holm, R. H. *Inorg. Chem.*, **1982**, *21*, 3928.

(70) Stack, T. D. P.; Holm, R. H. *J. Am. Chem. Soc.*, **1988**, *110*, 2484.

(71) Kovacs, J. A.; Holm, R. H. *J. Am. Chem. Soc.*, **1986**, *108*, 340.

(72) Kovacs, J. A.; Holm, R. H. *J. Am. Chem. Soc.*, **1987**, *26*, 711.

(73) Costa, T.; Dorfman, J. R.; Hagen, K. S.; Holm, R. H. *Inorg. Chem.*, **1983**, *22*, 4091.

(74) Kanatzidis, M. G.; Salifoglou, A.; Coucouvanis, D. *Inorg. Chem.*, **1986**, *25*, 2460.

(75) Dance, I. G. *J. Am. Chem. Soc.*, **1979**, *101*, 6264.

(76) Henkel, G.; Tremel, W.; Krebs, B. *Angew. Chem. Int. Ed. Engl.*, **1983**, *22*, 318.

(77) Dance, I. G. *J. Am. Chem. Soc.*, **1980**, *102*, 3445.

(78) Dance, I. G. *Inorg. Chem.*, **1981**, *20*, 2155.

(79) Choy, A.; Craig, D.; Dance, I. G.; Scudder, M. *J. Chem. Soc., Chem. Commun.*, **1982**, 1246.

(80) Scattergood, C. D.; Bonney, P. G.; Salter, J. M.; Garner, C. D.; Clegg, W. *J. Chem. Soc., Chem. Commun.*, **1987**, 1749.

(81) Dance, I. G. *J. Chem. Soc. Chem. Commun.*, **1976**, 103.

(81) Blower, P. J.; Dilworth, J. R. *Coord. Chem. Rev.*, **1987**, *76*, 121.

(83) Wachter, J. *J. Coord. Chem.*, **1987**, *15*, 219.

(84) Dias, A. R.; Green, M. L. H. *J. Chem. Soc., Chem. Commun.*, **1969**, 962.

(85) Dias, A. R.; Green, M. L. H. *J. Chem. Soc., A*, **1971**, 2807.

(86) Dias, A. R.; Green, M. L. H. *J. Chem. Soc., A*, **1971**, 1951.

(87) Prout, K.; Rees, G. V. *Acta Cryst. B*, **1974**, *30*, 2717.

(88) Dahl, L. F.; Wei, C. H. *Inorg. Chem.*, **1963**, *2*, 328.

(89) Prout, K.; Critchley, S. R.; Rees, G. V. *Acta Cryst. B*, **1974**, *30*, 2305.

(90) Werner, H.; Ulrich, B.; Schubert, U.; Hofmann, P.; Zimmer-gasser, B. *J.*

Organomet. Chem., **1985**, *297*, 27.

(91) Prout, K.; Rees, G. V. *Acta Cryst. B*, **1974**, *30*, 2249.

(92) O'Hare, D.; Green, M. L. H.; Cloke, F. G. N. *J. Organomet. Chem.*, **1985**, *282*, 225.

(93) Otsuka, S.; Okura, N.; Payne, N. C. *J. Chem. Soc., Chem. Commun.*, **1982**, 531.

(94) Payne, N. C.; Okura, N.; Otsuka, S. *J. Am. Chem. Soc.*, **1983**, *105*, 245.

(95) Rosenhein, L. D.; McDonald, J. W.; Newton, W. E. *Inorg. Chim. Acta*, **1984**, *87*, L33.

(96) Lu, S. W.; Okura, N.; Yoshida, T.; Otsuka, S.; Hirotsu, K. Higuchi, T. *J. Am. Chem. Soc.*, **1983**, *105*, 7470.

(97) Rosenhein, L. D.; Newton, W. E.; McDonald, J. W. *Inorg. Chem.*, **1987**, *26*, 1695.

(98) Jicha, D. C.; Busch, D. H. *Inorg. Chem.*, **1962**, *4*, 872.

(99) Roundhill, D. M. *Inorg. Chem.*, **1980**, *19*, 557.

(100) Braterman, P. S.; Wilson, V. A.; Joshi, K. K. *J. Organomet. Chem.*, **1971**, *31*, 123.

(101) Zanella, R.; Ros, R.; Graziani, M. *Inorg. Chem.*, **1973**, *11*, 2739.

(102) Dance, I. G.; Guerney, P. J.; Rae, A. D.; Scudder, M. L. *Inorg. Chem.*, **1983**, *22*, 2883.

(103) Stephan, D. W. *Coord. Chem. Rev.*, **1989**, *95*, 41.

(104) Kopf H.; Rathlein, K. H. *Angew. Chem. Internat. Ed., Engl.*, **1969**, *8*, 980.

(105) Braterman, P. S.; Wilson, V. A.; Joshi, K. K. *J. Chem. Soc. (A)*, **1971**, 191.

(106) Cameron, T. S.; Prout, K. C.; Rees, G. V.; Green, M. L. H.; Joshi, K. K.; Davies, G. R.; Kilbourn, B. T. *J. Chem. Soc., Chem. Commun.*, **1971**, 14.

(107) Davies, G. R.; Kilbourn, B. T. *J. Chem. Soc. (A).*, **1971**, 87.

(108) Ruffing C. J.; Rauchfuss, T.B. *Organometallics*, **1985**, *4*, 524.

(109) Joshi, K. K.; Wardle, R.; Wilson, V. A. *Inorg. Nucl. Chem. Lett.*, **1970**, *6*, 49.

(110) Braterman, P. S.; Wilson, V. A. *J. Organomet. Chem.*, **1971**, *31*, 131.

(111) White, G. S.; Stephan, D. W. *Inorg. Chem.*, **1985**, *24*, 1499.

(112) White, G. S.; Stephan, D. W. *Organometallics*, **1987**, *6*, 2169.

(113) White, G. S.; Stephan, D. W. *Organometallics*, **1988**, *7*, 903.

(114) Douglas, W. E.; Green, M. L. H. *J. Chem. Soc., Dalton*, **1972**, 1796.

(115) Douglas, W. E.; Green, M. L. H.; Prout, C. K.; Rees, G. V. *J. Chem. Soc., Chem. Commun.*, **1971**, 896.

(116) Prout, K.; Critchley, S. R.; Rees, G. V. *Acta Cryst. B.*, **1974**, *30*, 2305.

(117) Darensbourg, M. Y.; Silva, R.;Reibensoies, J.; Prout, C. K. *Organometallics*, **1989**, *8*, 1315.

(118) Daran, J. C.; Meunier, B.; Prout, K. *Acta Cryst. B*, **1979**, *35*, 1709.

(119) Sato, M.; Yoshida, T. *J. Organomet. Chem.*, **1975**, *94*, 403.

(120) Kubas, G. J. *Inorg. Synth.*, **1979**, *19*, 90.

(121) Cromer, D. T.; Mann, J. B. *Acta Crystallogr. Sect. A: Cryst. Phys., Diffr., Theor. Gen. Crystallogr.*, **1968**, *A24*, 324.

(122) Cromer, D. T.; Mann, J. B. *Acta Crystallogr. Sect. A: Cryst. Phys., Diffr., Theor. Gen. Crystallogr.*, **1968**, *A24*, 390.

(123) Cromer, D. T.; Waber, J. T. International Tables for X-ray Crystallography, Kynoch Press: Birmingham, England, **1974**.

(124) Kopf, V.; Schmidt, M. Z. *Z. Anorg. Allg Chem.* **1965**, *340*, 139 and Coutts, R. S.; Surtees, J. R.; Swan, J. M.; Wailes, P. C. *Aust. J. Chem.*, **1966**, *19*, 1377.

(125) De C. T. Carrondo, M. A. A. F.; Jeffrey, G. A. *Acta Cryst. C.*, **1983**, *39*, 42.

(126) Muller, E. G.; Watkins, S. F.; Dahl, L. F. *J. Organomet. Chem.*, **1976**, *111*, 73.

(127) Bottomley, F.; Drummond, D. F.; Egharevba, G. O.; White, P. S. *Organometallics*, **1986**, *5*, 1620.

(128) Gelmini, L.; Stephan, D. W. *Organometallics*, **1988**, *7*, 1515.

(129) Petersen, J. L.; Dahl, L. F. *J. Am. Chem. Soc.*, **1974**, *96*, 2248.

(130) Benecke, J.; Drews, R.; Behrens, U.; Edelmann, F.; Keller, K.; Roesky, H. W. *J. Organomet. Chem.*, **1987**, *320*, C31.

(131) Lauher, J. W.; Hoffmann, R. *J. Am. Chem. Soc.*, **1976**, *98*, 1729.

(132) Lorenz, D. R.; Wasson, J.R. *J. Inorg. Nucl. Chem.*, **1975**, *37*, 2265.

(133) Gelmini, L.; Stephan, D. W. *Organometallics*, **1988**, *7*, 849.

(134) Zheng, P. Y.; Nadasdi, T. T.; Stephan, D. W. *Organometallics*, **1989**, *8*, 1393.

(135) Zheng, P. Y.; Stephan, D. W. *Can. J. Chem.*, **1989**, 0000.

(136) Ortiz, J. V. *J. Am. Chem. Soc.*, **1986**, *108*, 550.

(137) White, G. S.; Wark, T. A.; Tse, J. S.; Stephan, D. W. unpublished results.

(138) Rosenfield, S. G.; Wong, M. L. Y.; Stephan, D. W.; Marscharak, P. K. *Inorg. Chem.* **1987**, *26*, 4119.

(139) Woodward, P.; Dahl, L. F.; Abel, E. W.; Crosse, B. C. *J. Am. Chem. Soc.*, **1965**, *87*, 5251.

(140) Dance, I. G.; Scudder, M. L.; Secomb, R. *Inorg. Chem.*, **1985**, *24*, 1201.

(141) Gould, R. O.; Harding, M. M. *J. Chem. Soc. A.*, **1970**, 875.

(142) Gaete, W.; Ros, J.; Solans, X.; Font-Altaba, M.; Brianso, J. L. *Inorg. Chem.*, **1984**, *23*, 39.

(143) Manzer, L. E. *Orgnomet. Chem.*, **1976**, *110*, 291.

(144) Giordana, G.; Crabtree, R. H. *Inorg. Synth.*, **1979**, *9*, 218.

(145) Schrock, R. R.; Osborn, J. A. *J .Am. Chem. Soc.*, **1971**, *93*, 3089.

(146) Coutts, R. S. P.; Martin, R. L.; Wailes, P. C. *Aust. J. Chem.*, **1973**, *26*, 2101.

(147) Seewald, P. A.; White, G. S.; Stephan, D. W. *Can. J. Chem.*, **1988**, *66*, 1147.

(148) Hill, R.; Kelly, B. A.; Kennedy, F. G.; Knox, S. A. R.; Woodward, P. *J. Chem. Soc., Chem. Commun.*, **1977**, 434

(149) Osakada, K.; Matsumoto, K.; Yamamoto, T.; Yamamoto, A. *Organometallics*, **1985**, *4*, 857.

(150) Ibers, J. A.; Synder, R. G. *Acta Cryst.*, **1962**, *15*, 923

(151) Bonnet, J. J.; Kalck, P.; Poilblanc, R. *Inorg. Chem.*, **1977**, *16*, 1514.

(152) Connelly, N. G.; Johnson, G. A.; Kelly, B. A.; Woodward, P. *J. Chem. Soc., Chem Commun.*, **1977**, 436.(153) Sanger, A. R. *Can. J. Chem.*, **1983**, *61*, 2214.

(154) Issleib, V. K.; Gans, W. *Z. Anorg. Allg. Chem.*, **1982**, *491*, 163.

(155) Brown, S. J.; Mascharak, P. K.; Stephan, D. W. *J. Am. Chem. Soc.*, **1988**, *110*, 1996 and references
therein.

(156) Brown, S. J.; Tao, X.; Stephan, D. W.; Mascharak, P. K. *Inorg. Chem.*, **1986**, *25*, 3377.

CURRICULUM VITAE: TERESA ANNE WARK

Address: Department of Chemistry and Biochemistry
University of Windsor
Windsor, Ontario
N9B 3P4

Birthdate: January 1, 1962

Citizenship: Canadian

Education:

Ph.D. (1989), University of Windsor (Organometallic/Inorganic Chemistry)

B.Sc. (1984), McMaster University

Scholarships and Awards:

University of Windsor Summer Research Scholarship (1989)

University of Windsor Tuition Scholarship (1988-89)

University of Windsor Conference Travel Award (1988), 3rd Chemical Congress of North America/195th American Chemical Society National Meeting, Toronto, Ontario

University of Windsor Conference Travel Award (1987), 193rd American Chemical Society National Meeting, Denver, Colorado

Ontario Scholarship (1980)

Professional Experience:

Graduate Student (1984-present), Department of Chemistry and Biochemistry, University of Windsor, Windsor, Ontario

Teaching Assistant (1984-present), Department of Chemistry and Biochemistry, University of Windsor, Windsor, Ontario

Teaching Assistant (1983-1984), Department of Chemistry, McMaster University, Hamilton, Ontario

Metallurgical Analyst (Summer 1981 and 1982), Metallurgical Department, Dofasco Inc., Hamilton, Ontario

Full Papers:

4. T.A. Wark, D.W. Stephan, Early/Late Heterobimetallic Complexes: Synthesis, Spectral and Structural Study of Thiolato-Bridged Ti/Cu and V/Cu Complexes (manuscript in preparation)

3. T.A. Wark, D.W. Stephan, (1989) Early Metal Thiolato Species as Metalloligands in the Formation of Early/Late Heterobimetallic Complexes: Synthesis and Molecular Structure of $Cp_2Ti(SMe)_2$, $Cp_2V(SMe)_2$, $(Cp_2Ti(\mu\text{-}SMe)_2)_2Ni$ and $(Ni(\mu\text{-}SMe)_2)_6$ (accepted for publication in *Organometallics*).

2. S.J. Brown, X. Tao, T.A. Wark, D.W. Stephan, P.K. Mascharak, (1988) Synthetic Analogue Approach to Metallobleomycins 4. New Halobridged Dimeric and Polymeric (Infinite Zigzag Chain) Complexes of Copper (II) with Peptide Ligands Related to Bleomycins *Inorg. Chem.* 27, 1581-1587.

1. T.A. Wark, D.W. Stephan, (1987) Synthesis, Characterization and Structural Studies of Thiolato-Bridged Titanium(IV)-Copper(I) Species: Heterobimetallic Complexes Containing d^{10}-d^0 Dative Bonds *Inorg. Chem.* 363-369.

Talks/Posters:

7. T.A. Wark, L. Gelmini, G.S. White, D.G. Dick, P.Y. Zheng, T.T. Nadasdi, D.W. Stephan*, (1989) Heterobimetallic Complexes: Chemistry and Catalysis. Canadian Chemical Congress, Victoria, British Columbia.

6. T.A. Wark, L. Gelmini, G.S. White, P.Y. Zheng, T.T. Nadasdi, D.W. Stephan*, (1989) Early/Late Heterobimetallics. New York University, New York, New York.

5. T.A. Wark*, D.W. Stephan, (1988) Thiolato-Bridged Heterobimetallics. Third North American Chemical Congress, Toronto, Ontario.

4. T.A. Wark*, D.W. Stephan, (1987) Thiolato-Bridged Ti(IV)-Cu(I) Complexes, Heterobimetallics with d^{10}-d^0 Dative Bonds. ACS National Meeting, Denver, Colorado.

3. L. Gelmini, G.S. White, T.A. Wark, D.W. Stephan*, (1986) Metal-Metal Interactions in Early-Late Heterobimetallics. XIX Inorganic Discussion Weekend, McMaster University, Hamilton, Ontario.

2. T.A. Wark*, D.W. Stephan, (1986) Thiolato-Bridged Ti(IV)-Cu(I) Complexes, Heterobimetallics with d^{10}-d^0 Dative Bonds. XIX Inorganic Discussion Weekend, McMaster University, Hamilton, Ontario.

1. T.A. Wark, G.S. White, L. Gelmini, D.W. Stephan*, (1986) Metal-Metal Interactions in Early-Late Heterobimetallics. National Meeting of the American Chemical Society, Anaheim, California.